Stability Assessment of Slopes Along NH-44,

Jammu- Srinagar

MAJOR PROJECT –I REPORT

SUBMITTED IN PARTIAL FULFILLMENT OF THE REQUIREMENTS FOR THE AWARD OF DEGREE

OF

MASTER OF TECHNOLOGY

IN

GEOTECHNICAL ENGINEERING

Submitted by

SEHLA GOWHAR

2K20/GTE/16

Under the supervision of

Prof. A K Shrivastava

Dr. Majid Hussain

DEPARTMENT OF CIVIL ENGINEERING

DELHI TECHNOLOGICAL UNIVERSITY

(Formerly Delhi College of Engineering)

Bawana Road, Delhi-110042

MAY 2022

DELHI TECHNOLOGICAL UNIVERSITY

(Formerly Delhi College of Engineering)

Bawana Road, Delhi -110042

CANDIDATE'S DECLARATION

I, **Sehla Gowhar**, M. Tech Geotechnical Engineering, Roll No. 2K20/GTE/16, hereby declare that the Dissertation titled "**Stability Assessment of Slopes Along NH-44, Jammu- Srinagar**" that I submitted to the Department of Civil Engineering, Delhi Technological University, Delhi in partial fulfilment of the requirement for the award of Master of Technology is original and has not been copied from any source. In the past, this work has never been used to confer a degree, diploma associateship, fellowship or any other equivalent title or honour.

Place: Delhi **SEHLA GOWHAR**

Date: **2K20/GTE/16**

DEPARTMENT OF CIVIL ENGINEERING

DELHI TECHNOLOGICAL UNIVERSITY

(Formerly Delhi College of Engineering)

Bawana Road, Delhi-110042

CERTIFICATE

I hereby certify that the project Dissertation titled "Stability Assessment of Slopes Along NH-44, Jammu- Srinagar" submitted by Sehla Gowhar, roll no. 2K20/GTE/16 (Civil Engineering), Delhi Technological University, Delhi in partial fulfilment of the requirement for the award of Master of Technology degree, is a record of the project work completed by the student under my supervision. To the best of my knowledge, the matter embodied in the thesis has not been submitted to any other University/Institute for the award of any Degree or Diploma.

Prof. A K Shrivastava

Supervisor

Department of Civil Engineering

Delhi Technological University

Delhi-110042

Dr. Majid Hussain

Co-Supervisor

Department of Civil Engineering

NIT, Srinagar

Srinagar-190006

Abstract

To determine the effect of precipitation on the stability of slopes along NH-44, Jammu-Srinagar, a study was conducted to compare the stability of slopes under normal or no rainfall conditions and during conditions of intense rainfall. Both in terms of human deaths and economic damages, landslides have wreaked tremendous havoc. Identifying the hotspot locations for landslide occurrences is essential for mitigating the damage caused by landslides. Five slopes from an area prone to landslides are chosen for stability investigation. The research was undertaken in 3 parts: geotechnical soil assessment, ten-year rainfall data analysis, and numerical evaluation. For numerical analysis, GeoStudio 2018 R2's SEEP/W and SLOPE/W modules were utilized. In steady seepage analysis, annual average rainfall was utilized to determine the initial condition of pore water pressure within the slope, whereas in transient seepage analysis, maximum daily rainfall over the period of one day was used. The factor of safety of slopes was determined using the limit equilibrium-based Morgenstern and Price approach. It was determined that, under normal conditions, all slopes were stable with the exception of the slope at location S_1. A substantial decrease in FOS was seen during a one-day episode of intense rainfall in the selected slopes due to reduction in matric suction and subsequent rise of water table.

ACKNOWLEDGEMENT

First and foremost, praise to Almighty Allah for constantly showering me with blessings and guiding me through every phase of life.

I feel incredibly indebted to my guide Prof. A K Shrivastava, and my co-guide, Dr. Majid Hussain, for their constant guidance. Without their valuable suggestions, it would not have been possible for me to complete this project. I want to express my gratitude to the HOD Civil Department, Delhi Technological University, Prof. V K Minocha, for allowing me to conduct the experimental part of my project at NIT, Srinagar.

I am thankful to Dr. Riyaz Mir, Senior Geologist, and officer in charge, Geological Survey of India, for his invaluable advice on my project. I would also like to thank the technical staff at NIT Srinagar for constantly helping me in the laboratory work of my project.

I am grateful to Mr. Nadeem Gul, Ms. Rufaidah Shah, Mr. Abhishek Paswan, and Mr. Badal Mohanty for their guidance and assistance throughout my project. I would also like to thank my family and friends, without their support and encouragement, this project would not have happened.

Sehla Gowhar
2K20/GTE/16

Table of Contents

List of Tables

List of Figures

Chapter 1
Introduction

1.1 General

Landslides are hazardous as they are accompanied by massive losses both economically and human fatalities. As per a report of National Disaster Management Authority, almost 12.6% of land area of India fall under landslide hazard zone. Hilly and mountainous regions are mostly affected by landslides. One of the major impediments in the research field of landslide mitigation is the stability analysis of potential debris slopes (Kanungo et al., 2013). Slope failure usually occurs due to natural factors as well as anthropogenic factors. The natural factors causing instability in slopes include seismic activities, precipitation particularly rainfall, water level fluctuations etc. and anthropogenic factors include unplanned blasting for road widening, deforestation, rapid urbanization etc. Among the various factors inducing instability in slopes rainfall has been identified as main triggering factor.

The slope failures are primarily classified as deep seated and shallow. Generally, the landslides are shallow in nature and are triggered mainly due to rainfall infiltration within the slopes. Initially, the impact of rainfall on the stability of slopes was analysed by assuming slope in a state of saturation and neglecting the role of matric suction. The matric suction within the slope increases its stability by providing apparent cohesion within the soil particles. During rainfall event, rain water infiltrates within the slope and increases degree of saturation of soil. With the increase in degree of saturation of soil, the effective stress reduces which eventually decreases the shear strength of soil.

The stability analysis of slopes can be carried out using two methods: Total Stress Approach and Effect Stress Approach. The total stress approach is recommended only in case of under drained conditions while as effective stress approach is applicable on stability analysis of slope for long term. The latter method is highly useful for places where there is longer duration of high intensity rainfall events.

1.2 Methods of Analysis

1.2.1 Limit Equilibrium Method

In limit equilibrium method (LEM), the stability analysis of slopes is computed by dividing the sliding mass of soil over failure surface into a number of slices. The factor of safety is assumed to be constant along the slip surface. The factor of safety is computed by using equilibrium of force or moment. The analysis of slope stability is an indeterminate problem and assumption are required related to interslice forces to make it a determinate problem. The mobilized shear strength along the slip or failure surface in the LEM is given by :

$$s_m = \frac{s_f}{F} \quad (1)$$

where s_m is the mobilized shear strength, s_f is the ultimate shear strength computed using Mohr-Coulomb's equation and F is the factor of safety.

The limit equilibrium methods are classified into two types i.e., the simplified methods and rigorous methods . In simplified methods either force or moment equilibrium is satisfied but in rigorous methods both force and moment equilibrium are satisfied (Abramson et al., 2002). There are more than 10 LEMs based on whether they satisfy force or moment equilibrium or both and the assumptions related for the interslice forces. Some of the famous methods used are: The Ordinary Method of Slices or Fellinius Method (1936) satisfies moment equilibrium only and neglects the interslice forces. The Bishop's Simplified Method (1955) satisfies moment equilibrium and force equilibrium in horizontal direction but does not satisfy force equilibrium in vertical direction and it assumes zero interslice shear forces. Janbu's Simplified Method (1954) satisfies force equilibrium in both horizontal and vertical direction but does not satisfy moment equilibrium and it also assumes zero interslice shear forces. Spencer's Method (1973), satisfies all force and moment equilibrium and assumes a constant interslice force with an unknown inclination. Morgenstern-Price Method (1965) satisfies both force and moment equilibrium and assume an interslice force function.

1.2.2 Finite Element Method

In finite element analysis, no pre determination of failure or slip surface is required. Also, the soil mass above the slip surface is is not divided into slices, so the assumptions regarding the location of interslice shear forces are not needed. The finite element method can be used for monitoring of shear failure and progressive deformation (Griffith and Lane., 1999). Due to these advantages over limit equilibrium methods, finite element method is now widely used for the analysis of various geotechnical problems. The basic concept behind the working of finite element method is that a continuum is divided into small pieces and behavior of each piece is analysed. The behavior of the continuum is found by reconnecting each of these pieces. These individual pieces are known as finite elements and the entire process of dividing the continuum into finite elements is called meshing or discretization. Fig. 1.1 gives the schematic representation of steps involved in finite element method:

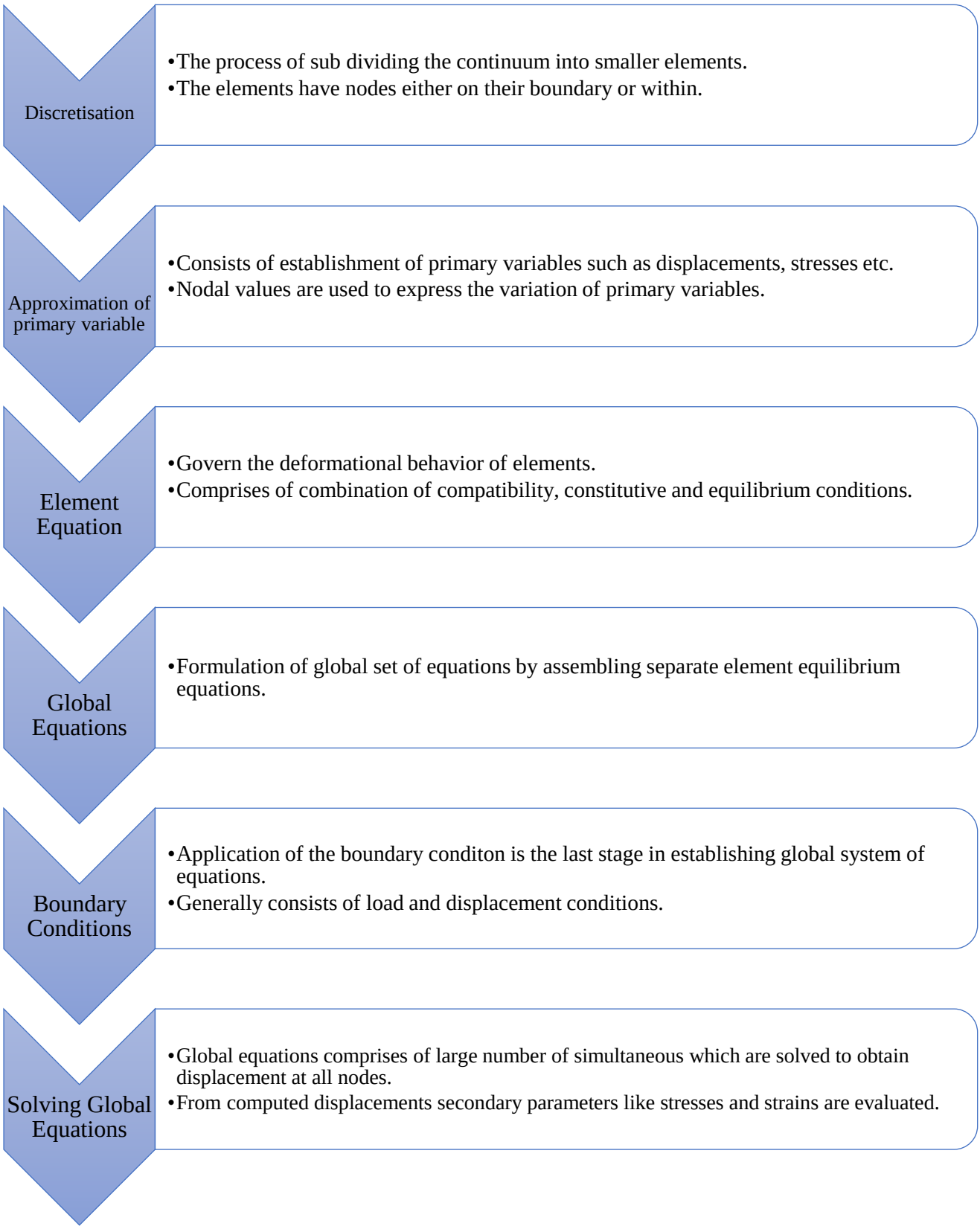

Fig. 1.1: Schematic representation of the steps involved in finite element analysis

1.3 Motivation of Present Study and Problem Statement

The UT of Jammu and Kashmir is the northern most part of India which lies in western Himalayas. It lies between Latitude 32°17'N and 37°05'N and longitude 72°31'E and 80°20'E. The UT shares it Northern borders with Afghanistan and China, Eastern border with Ladakh, Western borders with Pakistan and Southern borders with Punjab and Himachal Pradesh. 11% of the total area of the UT comes under seismic zone V and the rest of the part comes under Seismic Zone IV, as per a report Jammu and Kashmir State Disaster Management Policy, 2011. The Kashmir valley lies between Pir Panjal and Zanskar mountain ranges of Himalayas and the Jammu lowlands are a continuation of the great north Indian plains, which rise in Punjab and extend to the Shivalik hills (IMD, 2020). The Kashmir valley experiences temperate climatic conditions and Jammu region experiences a tropical climate (Patel et al., 2020).

National Highway (NH-44) is of prime importance to the union territory of Jammu and Kashmir as it connects the UT the rest of country. Every year this highway gets closed for days due to recurrent landslide occurrences. Fig. 1.2 shows the slopes which are either under progressive failure or already failed along national highway NH-44. The northwest Himalayan frontal fold–thrust belt is highly active in nature which exacerbated by precipitation due to high elevation, renders the area prone to landslides (Singh et al., 2018). Apart from natural factors such as earthquakes and precipitation, anthropogenic activities such as infrastructure construction, blasting and slope excavation for road widening, and deforestation have all contributed to new landslides and the activation of dormant landslides. The most sensitive landslides zones along the highway are: Ramban, Panthyal, Nashri, Samroli, Chenani, Peera, Ramsoo, Digdoul, and Anokhifal slide (Panday., 2018). The closure of highway is accompanied with heavy economic losses and human casualties. For a period of 30 years (1990 to 2020), Shah et al., 2021 observed 739 landslides reported in 506 days, resulting in 1000 deaths and 267 injuries. India suffers a monetary loss of Rs 150-200 crore every year from landslide as per an estimate of National Institute of Disaster Management in the year 2011.

The severity of the damages after a landslide event makes it necessary to understand the factors responsible for their occurrences and take proper measures for the mitigation of landslide hazards. Landslide early warning system (LEWS) can be developed in the areas which are prone to landslides. Proper implementation of the the mitigation techniques includes establishment of landslide triggering factors, identification and stabilisation of currently unstable slopes, generating awareness amongst the people inhabiting the landslide prone areas. In this study, stability analysis of slopes from 5 different locations in landslide prone zone of NH-44 has been carried out in dry/ normal state and in case of a high rainfall event. The study has been carried out in three stages which are represented in Fig. 1.3.


(a)
Intercepted water


(b)
Steep cut slope

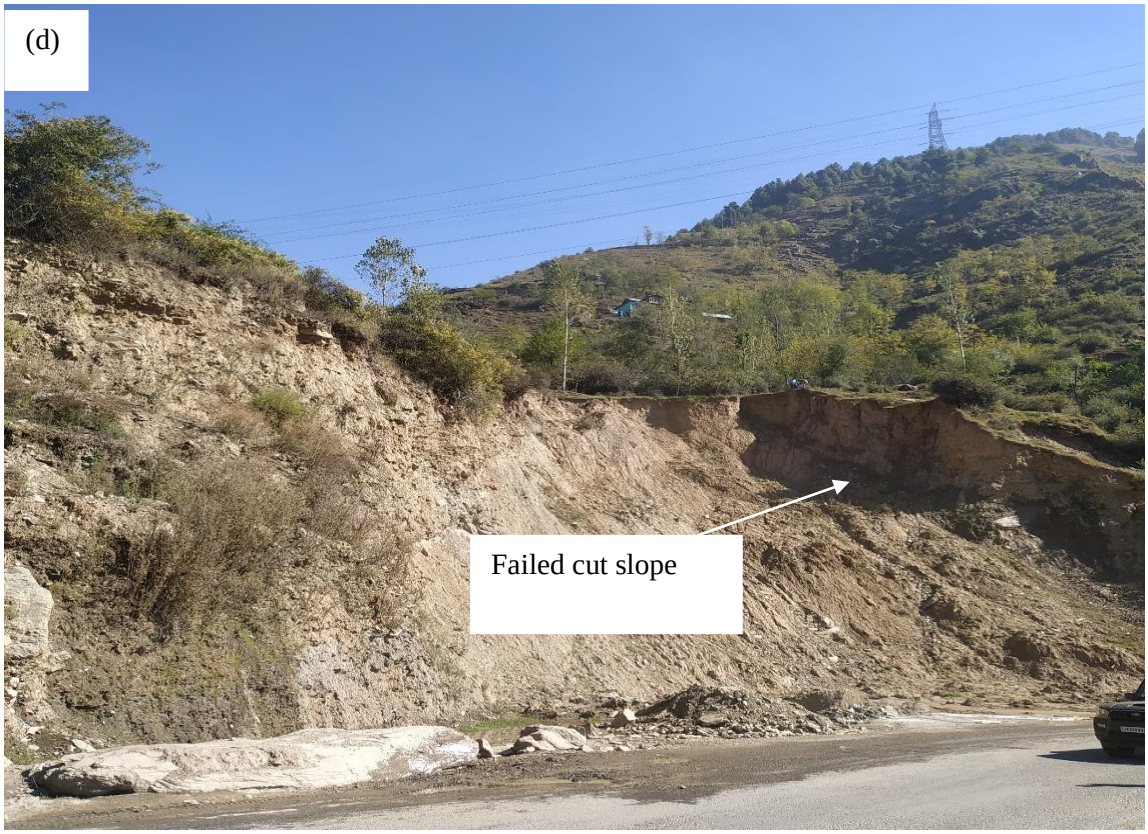

Fig. 1.2: Pictures showing (a) Intercepted water along road (b) Steep cut slope along road (c) slopes under possible progressive failure (d) Failed cut slope along road

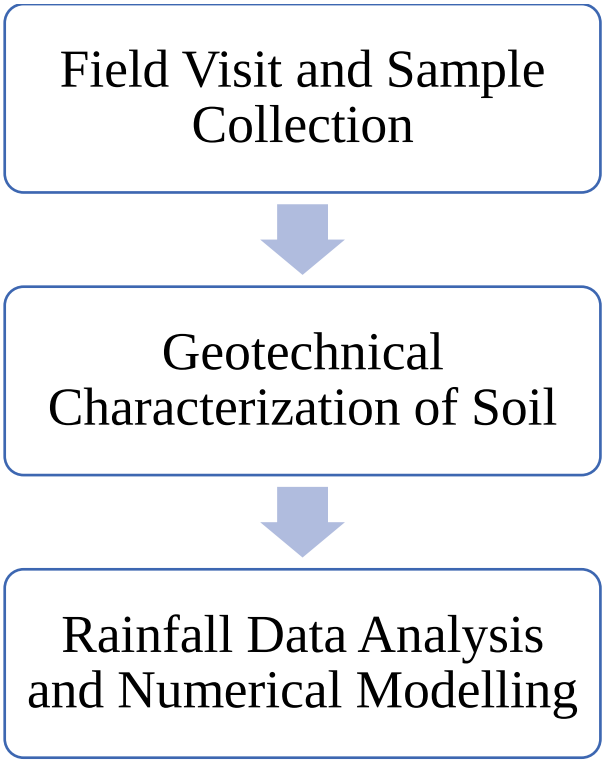

Fig. 1.3: Schematic representation of the stages involved in the present study

1.4 Objectives of the study

(1) To identify the locations suitable for the present study.

(2) To carry out sample collection and geotechnical characterisation of soil samples from the selected locations.

(3) To analyse the stability of slopes numerically under steady state condition in GeoStudio software using SEEP/W and SLOPE/W modules.

(4) To analyse pore water pressure distribution and stability of slopes under high intensity rainfall event.

1.5 Organization of the Thesis

Chapter 2 discusses the literature review relevant to the present work. Chapter 3 elaborates the different experimental methods performed for the study undertaken. Chapter 4 gives an overview of SEEP/W and Seep/W modules adopted for the numerical modelling of project. Chapter 5 shows the rainfall distribution for the past one decade. Chapter 6 discusses the results for the all the locations chosen. Chapter 7 includes conclusion and scope for future work.

Chapter 2

2.1 Literature Review

Duncan (1996) carried out detailed study to point out the advantages of Finite Element Method over conventional Limit Equilibrium Methods. The author suggested that the determination of deformations of slopes and embankments in a realistic manner are possible now mainly because the finite-element method has been developed and adapted to these applications. The FEM can explain nonlinearity in stress-strain behaviour, stress-strain behaviour which is dependent on stress, changes in geometry during construction in a sequential manner, and dissipation of excess pore pressures after construction, among other significant elements of the actual conditions. Linear elastic, multilinear elastic, hyperbolic, and elastoplastic stress-strain relationships are employed in FEM simulations. The author concluded that deformation calculated by FEM were larger in comparison to the actual deformations measured in the field. This difference was observed primarily due to the uncertainties involved in predicting actual density and water content of soils.

Griffiths and Lane., (1999) carried out 2-D plane strain finite element analysis of unreinforced slopes. Several examples of FE slope stability analysis were presented with verification against traditional stability analysis for better understanding. Elastic perfectly plastic constitutive model along with Mohr Coulomb failure criteria was used to simulate the behaviour of soil. 8-node quadrilateral elements with reduced integration were used to model the soil. The bottom boundary was kept fixed in either direction and the side boundaries were vertically free and horizontally restrained. The gravity load was applied in one step only. They compared the results of the finite element analysis with other traditional methods and argued that the finite element analysis is the powerful alternative to the traditional limit equilibrium methods.

Dawson et al., (1999) compared factors of safety obtained with the shear strength reduction technique to the factors of safety obtained with limit analysis solutions for a homogeneous embankment. Explicit finite difference method FLAC was used to compute the factor of safety. The soil is modelled as a linear elastic-perfectly plastic material with a Mohr -Coulomb yield condition and an associated flow rule. The simulation for slope stability analysis were run for trial factors of safety varying from 0.8 to 1.02. When the factor of safety was increased to 1.03, the simulations did not converge and unbalanced force exceeded to 10^{-3}. In order to evaluate the reliability of the strength reduction technique, simulations were conducted for a variety of factors. The slope angles of the simulated embankments ranged from 15˚ to 90˚. The soil was given values of ϕ ranging from 10˚ to 40˚ and values of (pore pressure coefficient) ru of 0.0, 0.25 and 0.5. After performing the analysis, it was concluded that Strength-reduction results were generally slightly higher than those predicted by limit analysis and this difference in results was further reduced with the refinement in mesh size.

Hammah et al., (2004) tried to investigate the possibilities of applying Shear Strength Reduction (SSR) FE technique to the strength model based on Generalised Hoek Brown criterion. Finding approximate values of factored Hoek Brown parameters considerably slowed down the computation time of analysis. For a specified Generalized Hoek-Brown envelope of failure, the authors recommend calculating a Mohr-Coulomb envelope equivalent to the Hoek-Brown model throughout the entire operating range of stresses. RocData program was used for finding out equivalent Mohr -Coulomb parameters and Phase2 program was used for applying SSR technique for calculating factor of safety. The results were compared with LE methods such as Bishop and Spencer's method in another software Slide. The FE factor of safety was in good agreement with those produced by LE methods.

Hammah et al., (2005) carried out comparative study between SSR method and conventional LEM methods. The performance of shear strength reduction technique was tested by applying it to 30 slopes problems which were taken from the available literature. 6 noded triangular elements were used for modelling of slopes. It was found that Young's Modulus and poison's ratio affected the magnitude of deformation but had negligible influence on computed FOS. Also, angle of dilation was found to have little significance on FOS. In case of unreinforced slopes, the number of elements chosen had no effect on SSR FOS. All the FOS calculated by SSR method have been compared with previously used LEM methods like Bishop's and Spencer's Method and the results have been found to be comparable.

Huat et al., (2006) simulated coupled hydrological/stability model for residual soil slopes of Malaysia in Seep W and Slope W programs of GeoStudio software and stability charts were designed as a function of dimensionless number with slope geometry, pore water pressure and rate of change of shear strength with change in suction . It was found that the the factor of safety of the slope reduced with increase in the slope height and the factor of safety tends to decrease with increase in permeability of soil. It was concluded by the author that lowest FOS was achieved when rainfall intensity was equal or close to saturated permeability.

Rahardjo et al., (2007) carried out a parametric study by choosing various factors affecting stability of slope followed by seepage analysis in SEEP/W module and stability analysis in SLOPE/W module of GeoStudio software to find out relative importance of parameters like soil properties, rainfall intensity, initial depth of water table and slope geometry in assessing the instability of a homogeneous soil slope under different rainfall condition. It was found that in the slopes with soils having low saturated coefficient of permeability antecedent rainfall plays a governing role in stability of slopes. The initial depth of water table determines the initial value of factor of safety while the reduction in FOS is primarily dependent on intensity of rainfall and lower initial FOS was found in slopes having steeper angles and higher values of height of slope.

Hammouri et al., (2008) used FEM and LEM to study three different problems of slopes taking in consideration the effect of rapid drawdown, undrained clay soil and crack location separately. FEM

software Plaxis Version 8 and LEM based software SAS-MCT 4.0 were used to analyse the slopes. Factor of safety and the critical slip surfaces obtained from both the methods were comparable and difference in FOS was found to be very small. The slip surface obtained with FEM is almost same for different crack location whereas LEM takes in account the crack location as a point of initiation of progressive failure.

Kanungo et al., (2013) studied three different hill slopes along a road stretch of 1.5 km at a distance of 9 km from Pipalkoti on Chamoli–Badrinath highway (NH-58) in the Garhwal Himalayas, India. 3 different slopes included one potential debris slide, one stable debris slope, and one potential rock slide. Physio-mechanical properties of the slopes have been determined by testing soil samples in the laboratory. The slopes were modelled as a continuum using 2D finite element plain strain approach to understand failure mechanism in them. Shear strength reduction analysis was performed in FEM analysis to determine critical strength reduction factor. Finite element formulation based Phase2 was used for carrying out the numerical analysis. Continuum analysis was carried out for debris and potential debris slopes whereas combined continuum-interface analysis was carried out for rock slope. After carrying out shear strength reduction analysis (SSR), it was found that potential debris slide was highly unstable along both the profile sections on both uphill and downhill sides of the road level and the results are in good conformity with field observations. For the same slope LEM analysis by Janbu's method in SLIDE software gave similar results. For the stable debris slope, FEM analysis showed that the slope was marginally stable and similar results were concluded from LEM (Bishop's Method) analysis and field observations. For the rock slope, it was observed that by incorporating all the three types of discontinuities, the FOS reduced drastically to 0.15 from 2.62 when no discontinuities were present. Thus, it was considered as a possible case of rockfall hazard. From the above studies, a landslide hazard map was also prepared for the area under study.

Chandrasekaran et al., (2013) investigated three case histories of failure which occurred in 2009 from Nilgiris district: the slope failure of railway track (Arvakandu), failure of retaining walls supporting buildings (Conoor) and failure of slope and retaining wall along national highway (Chinnabikatty). Laboratory investigations were carried out to determine index properties, and shear strength. The soil samples from all the three places were found to have high fine content 40%, 77% and 54% respectively. Finite element analysis of all the three case study sites was carried out using PLAXIS 2D software. At Aravankadu, a slope stability analysis employing the strength reduction technique was conducted to determine the slope's safety factor. It was noticed that the effective strains are close to zero towards the slope's foot. For the Coonoor site, displacement analysis was performed. The deformed mesh indicated that the two retaining walls at the top were totally displaced and tilted, while the retaining wall at the bottom was just dislocated. The deformed mesh pattern matches the observed failure pattern in November 2009 pretty closely. Analysis of slope displacement at Chinnabikatty indicated the presence of substantial displacements throughout the face and at the slope's toe.

Kanungo et al., (2013) carried out field and laboratory investigations along with finite element analysis of a potential debris slide along Chamoli -Badrinath highway (NH-58). 2 different slope profiles were used to model the slope using Shear Strength Reduction technique analysis. The landslide is spread over a length of 112 m in total at road level and it has two active stretches on left and right flank with lengths of 57 m and 15 m. The primary cause of debris slide was found to be the road widening process and triggering cause was found to be heavy precipitation during monsoon season. Four soil samples were taken at different levels of the landslide body. Laboratory investigation for the determination of grain size distribution, optimum moisture content (OMC), maximum dry density (MDD), specific gravity and permeability, cohesion (c) and frictional angle(φ) was done. These properties were further used for finite element modelling. The FEM analysis in Phase2 showed that slope is highly unstable on the both left and right flank. Janbu's simplified LEM in Slide software gave similar results. These results have further been confirmed from field observations.

Fawaz et al., (2014) examined the stability of an existing slope in Lebanon, which has collapsed due to excavation during the rainfall season. Two boreholes were drilled to the depths of 53 m and 54 m inside the slipped part of slope near Dahr el Baidar – Lebanon. and in-situ pressuremeter tests were executed at different depths. Laboratory testing was also carried out on the soil samples obtained from the boreholes and Plaxis software was used to numerically simulate the experimental pressuremeter test. The values of cohesion (c) and angle of internal friction (φ) obtained from simulation were in good agreement with those obtained from laboratory experimentation. It was further concluded that decrease in mechanical properties of soil due increase in water content is the main cause of the occurrence of slide. In presence of thin layer of low mechanical characteristics soil, the failure surface changed to planer from the originally circular failure surface. Proper drainage was suggested as an effective method to increase the stability of slope accompanied by piles and soil nails.

Raj and Sengupta (2014) studied repeated failure of railway embankment at Malda, West Bengal. Laboratory experimentation was done to obtain geotechnical properties of materials of embankment. Numerical modelling of slope failure mechanisms occurring within embankment was done using Seep W, Sigma W and Slope W modules of Geo Studio software and to observe the effect of suggested remedial measures on FOS of embankment. The embankment and top foundation material are silty in nature with low shear strength. For normal condition with water table at toe of embankment , a FOS of 1.8 was obtained. With the application of rainfall of different intensities, it was observed that with increase in the intensity of rainfall the embankment gets unstable in lesser time duration. The author suggested suitable drainage material like rockfill berm and by providing 5 m long sheet pile wall at the toe of embankment for stabilization of the embankment for higher intensity rainfall.

Tang et al., (2016) tried to investigate the effects of different initial conditions of pore water pressure distribution on slope stability in GeoStudio software using SEEP/W and SLOPE/W modules. Sandy

and clayey slopes were used as examples to investigate effects of antecedent rainfall on the slope stability and comparison of generation of initial pore water pressure by two different methods i.e by putting the value of maximum pore water pressure directly or using average annual rainfall as boundary condition in steady state analysis. When field data are unavailable, the author suggests generating the initial pore water pressure by applying the average annual rainfall to the slope for steady seepage analysis. It was observed that the effect of initial condition on slope stability reduces as antecedent rainfall duration increases. It was concluded by the author that the effect of antecedent rainfall becomes more apparent when the coefficient of permeability of soil decreases.

Kristo et al., (2017) investigated the effect of variations in rainfall patterns in Singapore and its effect on slope stability. The temporal trends in rainfall for the year 2050 and 2100 were found using Linear Regression. It was observed that the wet climate was likely to get wetter and dry climate drier in future. With the increase in rainfall intensity the FOS gets reduced subsequently. The decrease in FOS of safety was found more prominent in in next 50 years in comparison to the subsequent 50 years. The author suggested the use of preventive measures for reducing the landslide hazard in future.

Singh et al., (2018) tried to find out the mechanism that caused repeated shallow failure in Jhakri soil slopes along NH-5 through field and geotechnical investigations. Two portions of the failed slopes have been studied: one on the northern side with a slope angle of 56˚ and height between 24 m - 27 m and other on the southern side with a slope angle of 56˚ to 62˚ and height between 36 m – 43 m. The geotechnical properties were determined in the lab from the samples collected from the site. The grain size analysis showed poor to moderate sorting of soil with dominant finer fraction. The results of Atterberg limits suggested slight to moderate inorganic clay and micro images showed ill-sorted grain arrangement accompanied by sub rounded with angular to sub angular shape. LEM such as Bishop simplified (BS) and Morgenstern-Price (MP) were adopted to study the slope in Slide v.7.0 software and analysis was carried out for both pre and post failure scenarios of the slope. The slope was found to be unstable for both cases, so remedial measure of slope benching reinforced with soil nailing was suggested.

Dey and Sengupta (2018) studied the rainfall induced hillslope failure at Malin, Maharashtra. The slope has been quantified using 2-D numerical model GeoStudio. Parametric study of the effect of different rainfall intensities on the stability of slope was carried out. Seep W and Slope W programs were used to determine pore pressure variation and FOS for the slope corresponding to the different rainfall intensities. It was found by the author that for low intensity rainfall, the slope remains stable. A FOS of 1.6 was reported before rainfall which get reduced to less than unity for high intensity rainfall conditions. It was concluded that continuous rainfall infiltration developed a perched water table near the slope surface which resulted in the saturation and the positive pore water pressure build-up at a shallow depth within the slope.

Pandey (2018) studied the geological and geotechnical challenges in road widening along NH-44 from Jammu to Qazigund. The author suggested road blockage due to snowfall and landslide as a common event along the highway and is of opinion that detailed hydro geological studies must be carried out in order to mitigate the chances of landslides. Rock burst study was suggested as a preferred method for tunnel construction and various geotechnical properties of the site must be determined by testing rock core samples obtained from the respective construction site. As NH-44 is passing through outer Himalaya to Greater Himalaya, the author suggested that rock engineering properties and study of in-situ joint orientation must be considered during the preparation of geotechnical and geological report. The author presented the various geological problems faced during construction of NH-44 broadly affected by following three factors: Geological and Geotechnical Factors (landslides, rock fall, ground subsidence etc.), Hydro-meteorological disaster (cloudburst, floods etc.) and Man-Made factors (deforestation and slope excavation for construction activities). Various precautionary measures have been suggested in order to avoid or reduce the magnitude of damage that may occur during the widening process of roads such as step wise slope excavation, rock net, anchoring, shotcrete, retaining/breast wall, cladding wall, box type road cover, rock fall barrier etc.

Hussain et al., (2019) carried out detailed geotechnical investigation of soil samples from the two prominent translational landslides Dambu and Saraks along the national highway 1-A to determine inherent cause of instability there. These landslides were further analysed in Finite element software Phase2. For the geotechnical analysis, the important properties like particle size distribution, moisture content, Atterberg limits, specific gravity and shear strength parameters were determined as per Indian standard specifications. The slopes from both the slides have been modelled as debris slide in Phase2 software. DEM (digital elevation model) 12.5 m is used for the extraction of the geometry for both the slopes. Two-dimensional uniform mesh with 6 noded triangular elements were used to discretize the slopes of both the landslides. The slopes were modelled to be fixed laterally and along the bottom side whereas the upper slope surface was kept free. The results of numerical simulation showed a FOS of 1.95 for Dambu slide with a maximum displacement of 4.80 m indicating marginal slope stability whereas for Saraks slide, the FOS obtained was 0.47 with maximum displacement of 8.40 m indicating highly unstable slope. The results of FEM analysis were found to be in good compliance with the corresponding geotechnical analysis and field observations.

Sarma et al., (2020) studied rainfall induced landslides at the hill slopes of Guwahati region in India. Geotechnical characterisation of soil was carried out followed by subsequent pore pressure variation in SEEP/W and stability analysis in Slope W program in Geo Studio software. The study of landslide susceptibility and hazard using Physical models like TRIGS, SHALSTAB and SINMAP was also carried out. It was observed that in the absence of rainfall, the soil slopes are stable and reduction in FOS is observed due to the rainfall infiltration. The three models used in the study were found to be

capable of generating consistent results with observed conditions in the field, and were sufficiently capable in identifying the places prone to landslides.

Mohsin and Khader (2020) tested samples at three different sites along on NH-44 National highway in order to find the parameters that impact landslides on the national highway by using geotechnical investigations and Arc GIS software. The sites consisted of the places: one where the landslide had already occurred and is still active, the second a landslide-prone site and the third site was less prone to landslides. IMD data for the region was also observed and it was concluded that rainfall and snowfall are the main triggering factors for the landslides on Jammu & Kashmir National highway. Geomorphological studies showed that areas such as Digdol, Peera, and Ramsu which lie on tectonically active zone are susceptible to landslides even in case of a small earthquake. The samples collected from all the sites showed very low value of cohesion indicating that the soil is highly prone to landslides because a heavy shower can be enough to make it flow after it gets saturated with heavy rainfall. Early warning system on the basis of moisture content of the soil was also presented in which a low-level warning will be generated after the moisture level of the soil reaches the plastic limit value, the mid-value of liquid limit and plastic limit will be considered as the moderate level warning for the landslide as this level suggests that the moisture level of the soil is continuously increasing and the liquid limit value will be the high-level warning for landslide because the soil will have enough saturation to get flown from the slope.

Bashir and Ramkumar (2021) attempted to create a landslide inventory for Mughal Road, Shopian which lies in Pir Panjal range of Kashmir valley and is considered as an only alternate route after National Highway NH 44 by using multidate satellite data of 12 years from 2008 to 2020. Two high resolution Multidate satellite images World View of 2020 and CARTOSAT 2 of 2008 with spatial resolution of 0.6 m and 1 m respectively on a scale of 1:2000. ArcMap 10.2 which is the central application in ArcGIS has been used for database creation and GIS based analysis. The Google Earth as well as the field survey were carried out for validation of the results. It was concluded that out of the total studied area 12.62% is critical to landslides, 21.45% is highly prone and 24.84% is moderately prone while 21.94% is low and 19.13% is very low prone to landslides. Slopes with slope angle ranging from 33˚ to 40˚ are prone to landslides. Also, lack of vegetation is the main triggering point for landslide along the road.

Dhanai et al., (2022) carried out analysis of transient seepage and stability of soil slopes of three regions in India along with the effect of climate change due to global warming on the stability of slopes. Extraction of rainfall data for three periods in future was done using CMIP5. The author carried out a parametric study based on data found by different researchers followed by seepage and stability analysis in Seep W and Slope W programs of Geo Studio Software. It was found by the author that the rate of reduction of FOS is more for slopes with steeper angles and and soils with high permeability and the

rate of saturation of slope depends upon initial matric suction present in the soil above water table. It was concluded by their study that in future, the probability of short duration heavy intensity rainfall is high. In all the regions under study, a reduction in FOS with higher intensity rainfall due to reduction in pore water pressure was observed.

2.2 Gaps in Research

After conducting a thorough literature review on landslide stability assessment along NH-44 in Jammu and Kashmir, it was observed that there is a lack of geotechnical research in this domain. Lesser research has been carried on the effect of rainfall on the stability of slopes along the selected stretch. So, the research undertaken can serve to augment the information needed for the identification of landslide hotspots along the national highway.

Chapter 3

Location and Experimental studies

3.1 Study Area

Five locations along landslide prone stretch of NH-44 were selected. Table 3.1 gives the longitude and latitude of the five locations along the height and width of all the sites. The height, width, road elevation and elevation of slopes have been determined using Virtual Google Earth.

Table 3.1 Location and Geometry of slopes under study

Location	Symbol	Latitude	Longitude	Width (m)	Height (m)	Road Elevation (m) (Above mean sea level)	Elevation of slope (m)	
Ramsoo	S_1	33˚20’46.081” N	75˚11’12.559” E	373	499	1246	Top	1709
							Bottom	1210
Sheerbibi	S_2	33˚22’13.450” N	75˚11’37.580” E	278	109	1466	Top	1560
							Bottom	1451
Shabinbas	S_3	33˚24’54.281” N	75˚12’12.959” E	322	118	1636	Top	1687
							Bottom	1569
Darshipora	S_4	33˚26’59.234” N	75˚11’41.117” E	246	101	1685	Top	1778
							Bottom	1677
Chareel	S_5	33˚28’23.869” N	75˚11’39.968” E	296	98	1795	Top	1860
							Bottom	1762

3.2 Experimental studies

3.2.1 Grain Size Distribution

Wet sieving 300 g of oven dried soil sample on 75 IS sieve was used to determine grain size. The soil sample fraction retained on the 75 IS sieve was oven dried at a constant weight at 105 °C. The process was then conducted for dry sieve analysis according to IS:2720 (Part 4)-1985. Hydrometer analysis was performed on the fraction passing through the 75 IS sieve. Calgon solution 33:7 (comprising 33 grammes of sodium hexametaphosphate and 7 grammes of sodium carbonate mixed in 1 litre of water) was used as a de-flocculating agent and 50g of soil passing through a 75 IS sieve was used for

hydrometer analysis. A semi-logarithmic graph was plotted between sieve size (mm) on the X-axis and % finer on the Y-axis after hydrometer and sieve analysis.

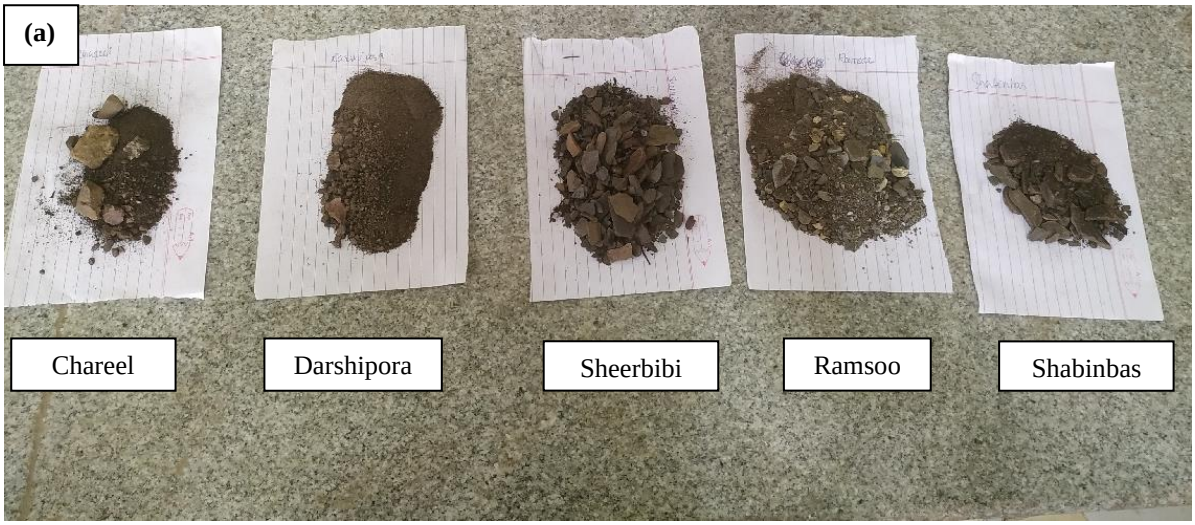

Fig. 3.1: (a) Soil fraction retained on 75 µ IS sieve after wet sieving (b) Sieve arrangement for coarse sieve analysis.

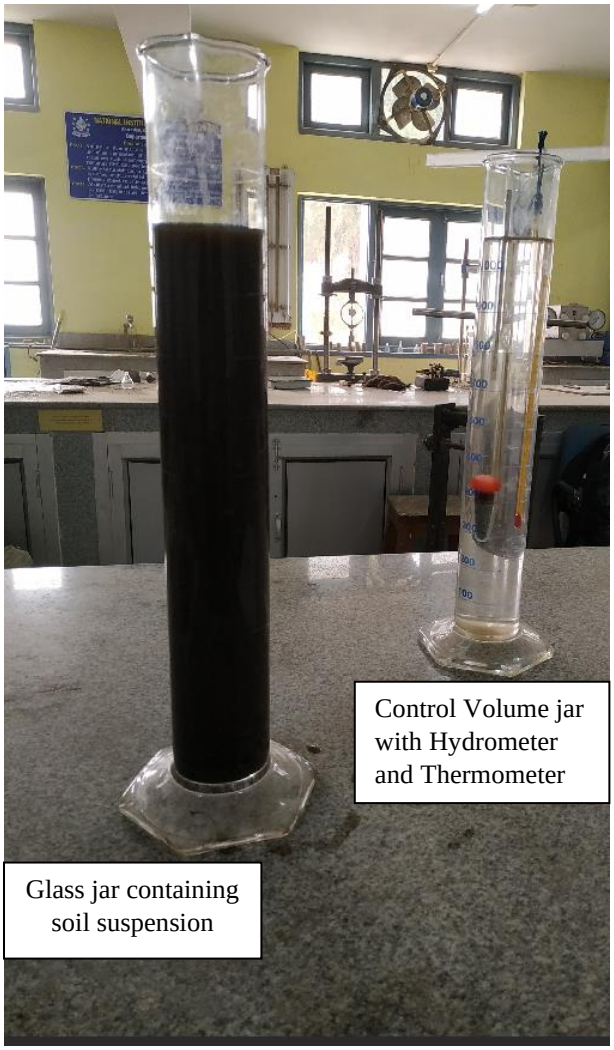

Fig.3.2: Experimental set up for Hydrometer analysis

3.2.2 Atterberg Limits

IS:2720 (Part 5)-1985 was followed to determine liquid limit, plastic limit and plasticity index of soil samples. 120 g of oven dried soil sample passing through 425 μ IS sieve was taken for the test. The soil sample is thoroughly mixed with sufficient quantity water to form a uniform paste. A portion of the prepared soil sample is transferred to the brass cup of Casagrande's Apparatus and is levelled to have a depth of 1 cm at the point of maximum thickness. By using an appropriate grooving tool, a cut is made in the soil sample and the handle is rotated at a speed of 2 revolutions per second. Number of blows are recorded when the groove made in the soil sample comes in contact by a distance of 12 mm. The numbers of blows should be in the range of 15 – 35. A specimen of the soil sample is taken for water content determination in the direction perpendicular to the groove especially from the region of groove which came in contact due flowing. The test is repeated 4-5 times and a graph is plotted between log of number of blows and water content. The water content corresponding to the 25 number of blows gives the liquid limit of soil sample. After the determination of liquid limit, about 8 g of soil mass is rolled between the fingers on a glass plate using sufficient pressure until a thread of 3 mm diameter is formed.

After that the soil is remoulded again and the process is repeated till cracks appear on the surface of soil thread when rolled to 3 mm diameter. A representative specimen of soil sample is taken from the cracked portion of thread for water content determination. The moisture content determined is the plastic limit of soil sample. The plasticity index of soil sample is determined by subtracting plastic limit from liquid limit of soil.

3.2.3 In-Situ Bulk Density and In-Situ Moisture Content

In-situ bulk density was determined by Core Cutter method as recommended by IS:2720 (Part 29)-1975. The internal diameter and height of core cutter was 10 cm and 13 cm respectively. After determination of in-situ bulk density, soil samples were taken from core cutters of respective sites for the determination of in-situ moisture content. Moisture content was determined as per IS:2720 (Part 2)-1973. The determination of moisture content is important because the moisture content of soil is responsible for reactivating and accelerating of landslides (Crozier, 1986).

3.2.4 Specific Gravity

Specific gravity for S_1 and S_2 sites has been determined using Pycnometer and S_3, S_4 and S_5 by density bottle method. IS:2720 (Part 3, Section 1)-1980 has been used to calculate the specific gravity of the soil samples from all the sites. The specific is calculated by using the equation below:

$$\text{Specific Gravity (G)} = \frac{W_2 - W_1}{(W_2 - W_1) - (W_3 - W_4)}$$

Where W_1 = Weight of empty pycnometer/ density bottle

W_2 = Weight of pycnometer/ density bottle+ oven dry soil

W_3 = Weight of pycnometer/ density bottle+ oven dry soil + water

W_4 = Weight of pycnometer/ density bottle+ water

All the weights in the above equation are in grams (g).

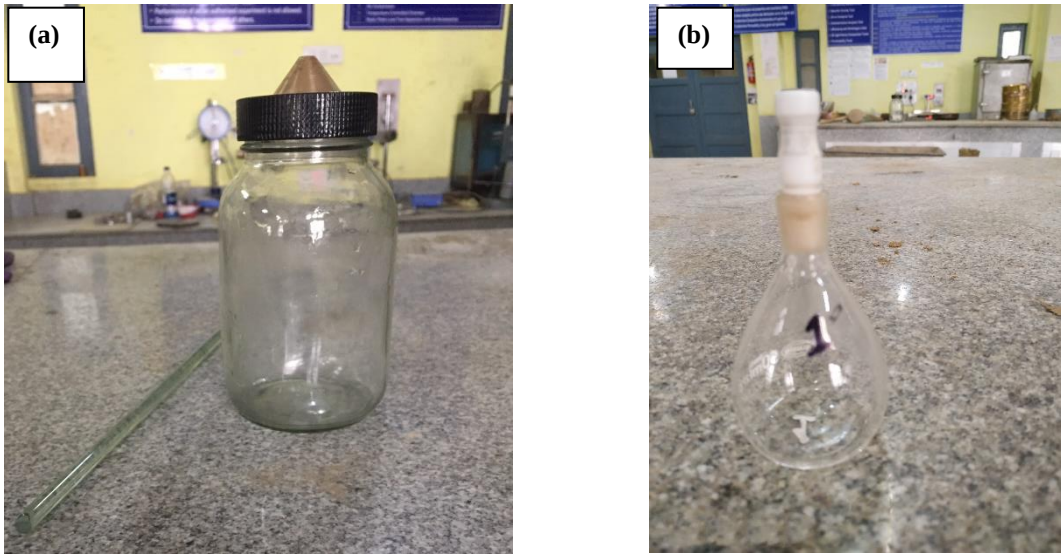

Fig. 3.3: shows (a) Pycnometer and (b) density bottle for the determination of specific gravity of coarse and fine-grained soil

3.2.5 Shear Strength

The maximum value of shear stress that can be mobilised within a soil mass is known as its shear strength (Ranjan and Rao, 1991). Direct shear test (DST) has been used to evaluate shear strength parameters cohesion (c) and angle of internal friction (φ)of soil samples. These two parameters are required for design of slopes, foundation, retaining walls, slab bridges, sheet piles, calculation bearing capacity of any strata etc. Direct shear test is suitable for drained condition although it can be used for undrained condition but only the way to achieve it is to prevent drainage by applying loads quickly which often results in overestimated strengths due to strain rate effects (Duncan et al., 2014). Plain gride plates are placed at the top and bottom of soil sample in the shear box. Loading pad is placed on the top grid plate and normal load is applied. A gap of 1 mm is maintained between the upper and lower halve of shear box. Shear load is applied till a shear displacement of 12 mm is obtained (i.e., 20% of longitudinal dimension). The proving ring assembly provides the shear loads and and the horizontal dial gauge provide corresponding horizontal displacement. DST has been performed on soil samples under two conditions: Undisturbed/ Natural/ Unsaturated and Inundated. Undisturbed samples were extracted from core cutter moulds. For inundated condition, remoulded samples were prepared using in situ moisture content and dry density values. The test was repeated three times at normal loads of 49.05 kN/m^2, 98.1 kN/m^2 and 147.15 kN/m^2 (0.5 kg/cm^2 kg/cm^2 and 1.5 kg/cm^2). The strain rate of 0.25 mm/min was kept constant for all the tests. IS:2720 (Part 13)-1986 has been followed for various specifications.

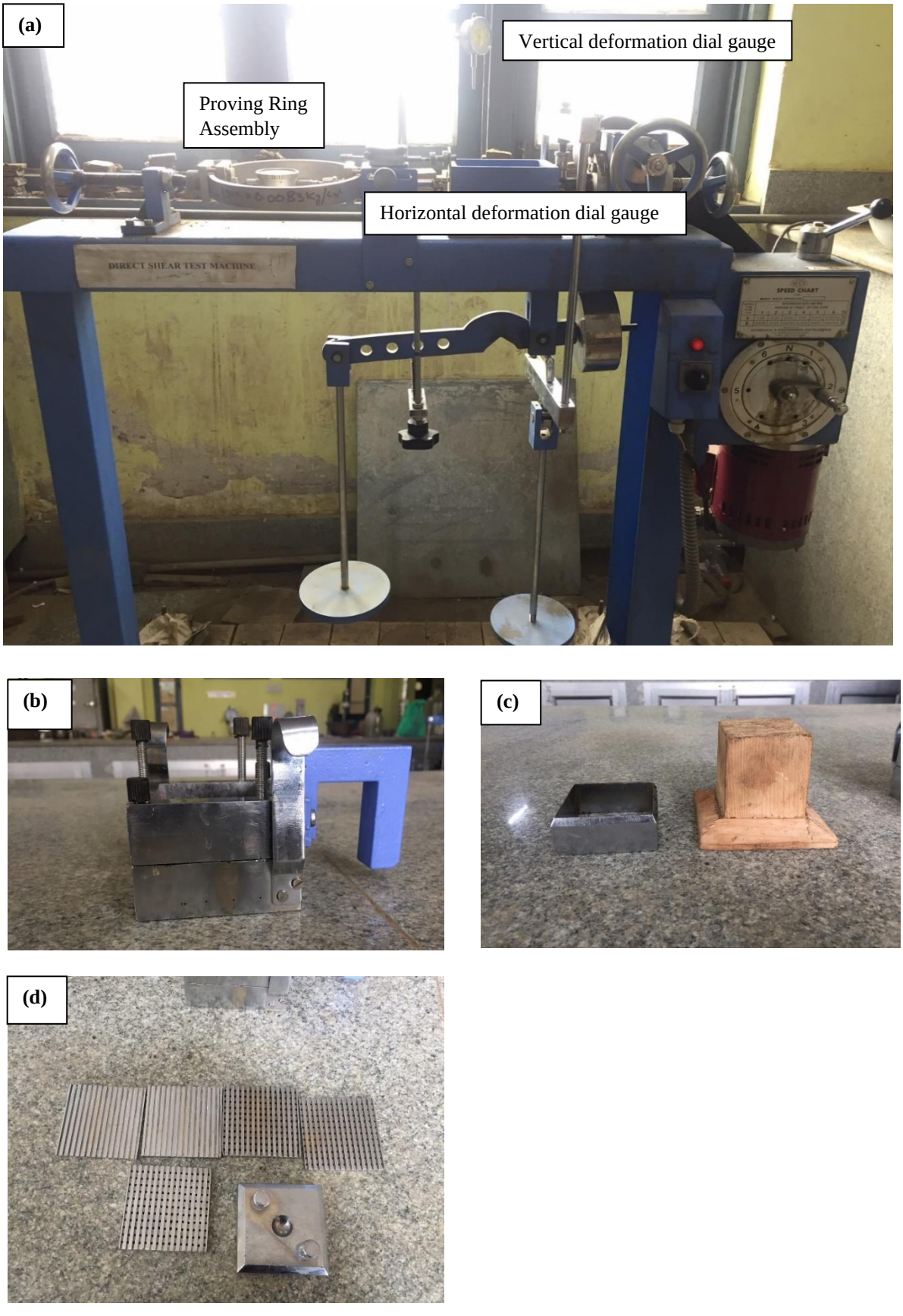

Fig. 3.4: (a) Direct Shear test apparatus (b) Shear box (c) Sample cutter and sample extractor (d) Grid plates and loading pad

3.2.6 Consolidation Characteristics

Consolidometer or Oedometer is used in laboratory to determine the consolidation parameters of soil by following the standard procedure recommended by IS:2720 (Part 15)-1986. In standard oedometer the soil is loaded in axial direction only and restrained in lateral directions. Consolidation settlement and the time for consolidation under a given loading condition can be determined from the consolidation parameters. The results of this test can be used in the design of foundation also. The test was performed on remoulded sample prepared in the laboratory at in situ moisture content and dry density. When weight is applied to a saturated soil mass, it is carried first by water existing in the pores, and when water begins to escape through these voids, the hydrostatic pressure is dissipated, and load is transferred to the soil solids, resulting in a decrease in overall soil mass volume. The soil samples are prepared in oedometer rings of diameter 6 cm and height 2 cm. After setting up the whole assembly, a seating load of 4.91 kN/m^2 was applied for 24 hrs till there is no change in dial gauge (least count = 0.0002 cm). After this, loads were applied successively after every 24 hrs in the order of 9.81 kN/m^2, 19.62 kN/m^2, 49.05 kN/m^2, 98.1 kN/m^2, 196.2 kN/m^2, 392.4 kN/m^2 and 784.8 kN/m^2. Unloading was done in 3 steps by reducing the load to 1/4th of present load.

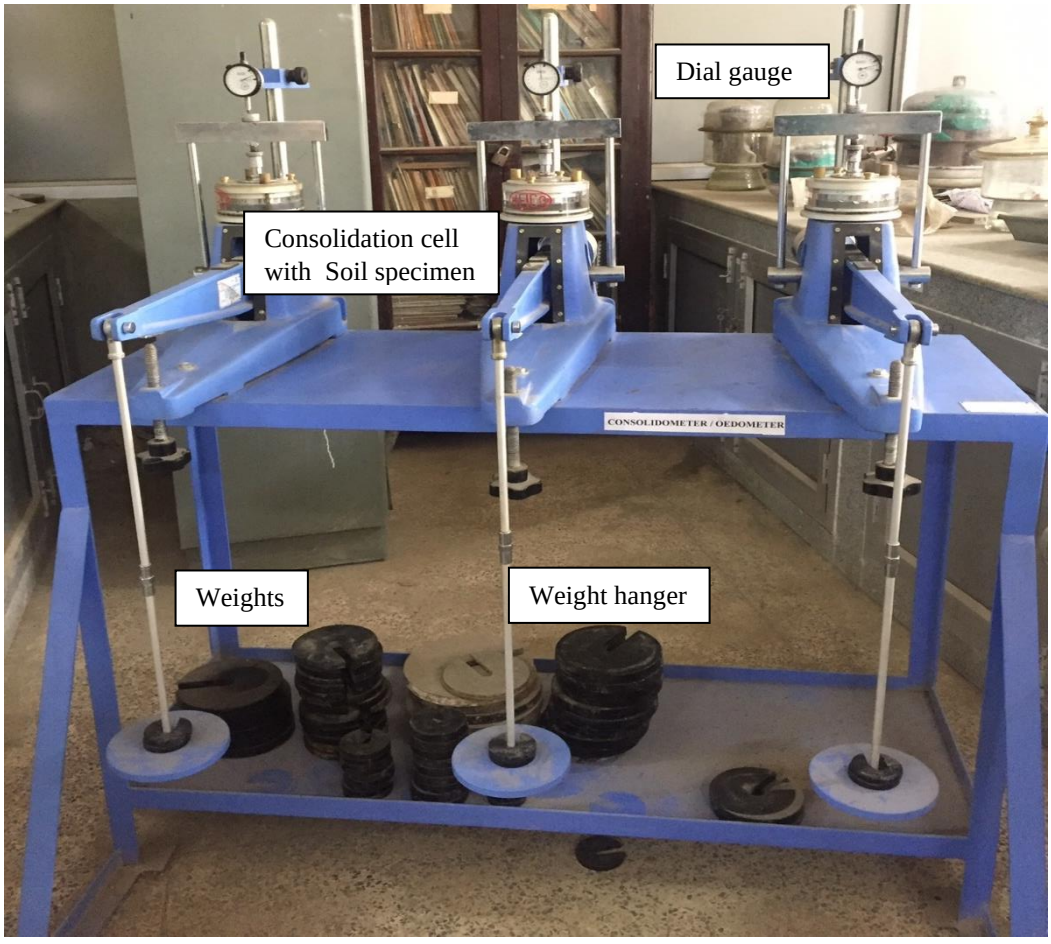

Fig. 3.5: 1- Dimensional consolidation test apparatus (Oedometer)

Chapter 4
Numerical Modelling

4.1 Seepage Analysis

The slopes have been analysed with the commercial software GeoStudio 2018 R2. The Seep/W module of GeoStudio was used to model the slope's hydrological behaviour. In SEEP/W, there are two types of flux boundaries that can be specified: a nodal flux boundary (Q) and a unit flux boundary (q). On the boundary nodes, a nodal flux boundary (Q) can be set directly. A unit flux boundary (q) is provided along the element's boundary edges. Before transient analysis is performed, steady-state analysis is performed to develop the initial pore water condition within the slope (Tang et al., 2016). On the surface of the slope, an input of yearly average rainfall in the form of rainfall flux was used to analyse steady seepage. For transient analysis, the steady-state parent for pore pressure was used, and precipitation was applied as the flux boundary condition. For transient analysis, the precipitation rate was calculated by dividing the total rainfall on the day of highest precipitation by 24 hours. The results were recorded at intervals of 1.2 hours.

The SEEP/W module is based on the premise that the flow through saturated and unsaturated soil is governed by Darcy's Law, which states:

$$q = ki \tag{2}$$

where q is specific discharge, i is hydraulic gradient and k represents the hydraulic conductivity of soil. This equation applies to both saturated and unsaturated soil situations, with the exception that, in unsaturated soil, the hydraulic conductivity varies with the change in soil moisture content. For seepage in two dimensions, the general governing equation is:

$$\frac{\partial}{\partial x}\left(k_x \frac{\partial H}{\partial x}\right) + \frac{\partial}{\partial y}\left(k_y \frac{\partial H}{\partial y}\right) + Q = \frac{\partial V}{\partial t} \tag{3}$$

Where H represents the totals head, k_x and k_y are the hydraulic conductivity in x and y directions, Q represents the applied boundary flux, V is the volumetric water content and t is time. In SEEP/W module, it is assumed that during transient processes pore air pressure remains constant at atmospheric pressure. Thus, the change in volumetric water content varies with pore water pressure only. Thus, equation in this module reduces to:

$$\frac{\partial}{\partial x}\left(k_x \frac{\partial H}{\partial x}\right) + \frac{\partial}{\partial y}\left(k_y \frac{\partial H}{\partial y}\right) + Q = m_w \gamma_w \frac{\partial H}{\partial t} \tag{4}$$

Where m_w is the slope of storage curve.

For seepage analysis, input data such as soil properties and boundary conditions are needed. SWCC (soil water characteristic curve) and HCF (hydraulic conductivity function) in unsaturated / saturated

material model require soil property input. Volumetric data point function, Fredlund-Xing function, Van Genuchten function, and Sample Function define the volumetric water content function in GeoStudio. Among these functions, the Volumetric data point function was chosen for this investigation. For predicting unsaturated hydraulic conductivity, SEEP/W utilizes two models, Fredlund-Xing and Van Genuchten, as hydraulic data point functions with SWCC as input. In addition to SWCC, the saturated hydraulic permeability (ks), the saturated volumetric water content (s), and the residual water content (r) are required as input parameters for the computation of unsaturated hydraulic conductivity using the Van Genuchten and Mualem equation, which is given as follows:

$$k_w = k_s \frac{\left[1-\left(a\Psi^{(n-1)}\left(1+(a\Psi^n)\right)^{-m}\right]^2}{\left[\{(1+a\Psi)^n\}^{\frac{m}{2}}\right]} \quad (5)$$

where a, m and n are the curve fitting parameters and Ψ is the matric suction range. Input parameters for SEEP/W are shown in Table 4.1. Fig. 4.1 to Fig. 4.5 show the SWCC and HCF for soil samples from all the locations.

Table 4.1 Input parameters required for estimation of SWCC and HCF in SEEP/W module for the selected locations

S. no.	Parameters	S_1	S_2	S_3	S_4	S_5
1	D_{60} (mm)	1.417	1.663	0.029	0.043	0.023
2	D_{10} (mm)	0.010	0.005	0.0011	0.0062	0.0016
3	Saturated hydraulic conductivity (k_s) (m/s)	1.23×10^{-5}	1.23×10^{-5}	1.25×10^{-6}	1.25×10^{-6}	1.25×10^{-6}
4	Saturated volumetric water content (θ_s)	0.221	0.215	0.289	0.236	0.271
5	Residual volumetric water content (θ_r)	0.022	0.022	0.029	0.024	0.027
6	Liquid limit (w_L) (%)	39.38	40.08	22.63	20.83	27.98
7	Rainfall flux for steady state analysis ($m^3/sec/m^2$)	3.21×10^{-8}	2.89×10^{-8}	2.61×10^{-8}	2.65×10^{-8}	2.54×10^{-8}
8	Rainfall flux for transient state analysis (mm/day)	99.49	110.56	103.86	112.20	107.61

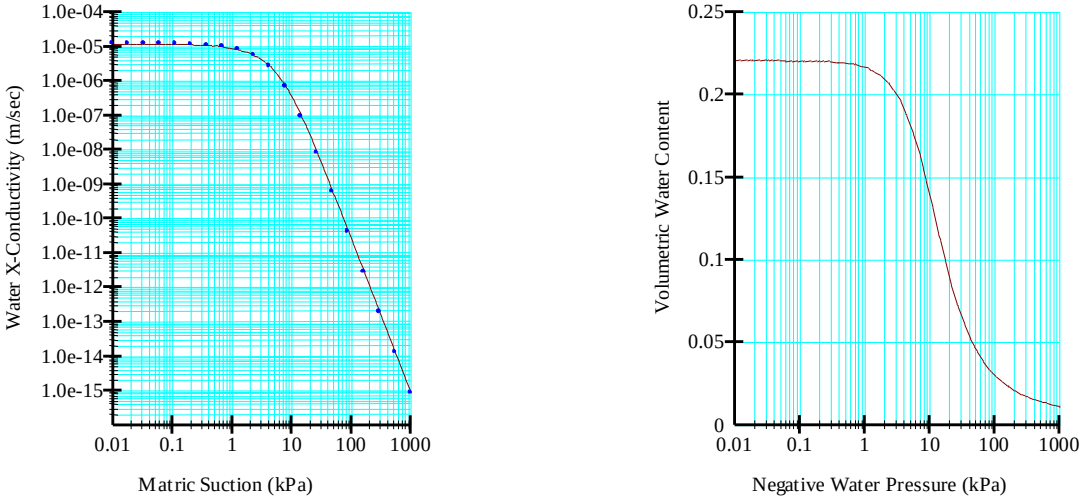

Fig. 4.1: HCF and SWCC for S_1 location

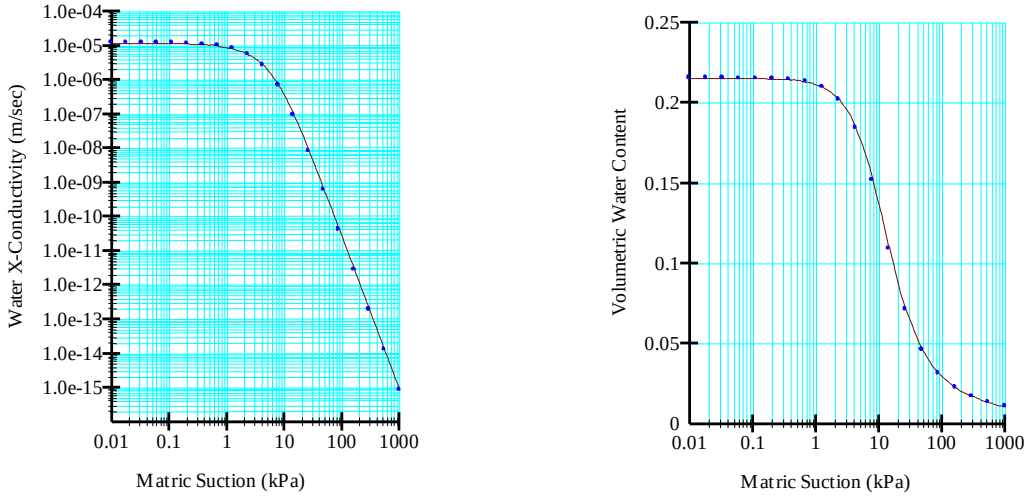

Fig. 4.2: HCF and SWCC for S_2 location

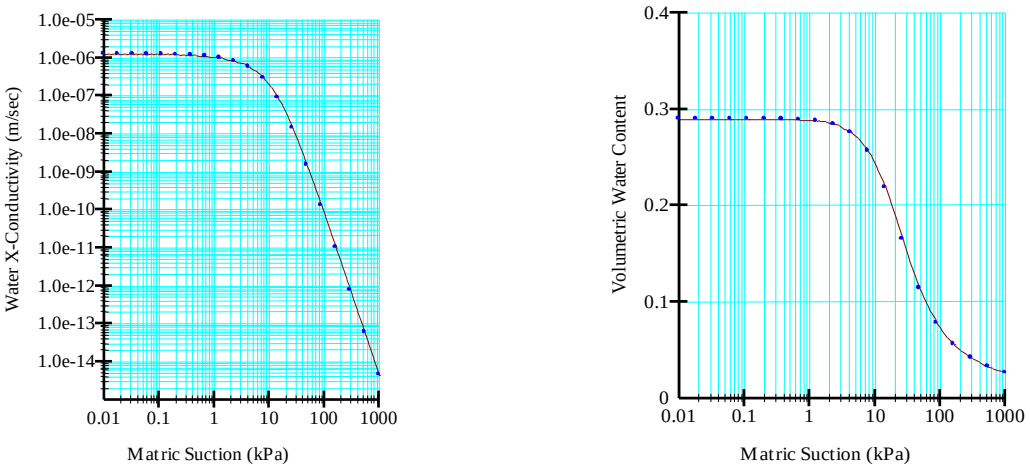

Fig. 4.3: HCF and SWCC for S_3 location

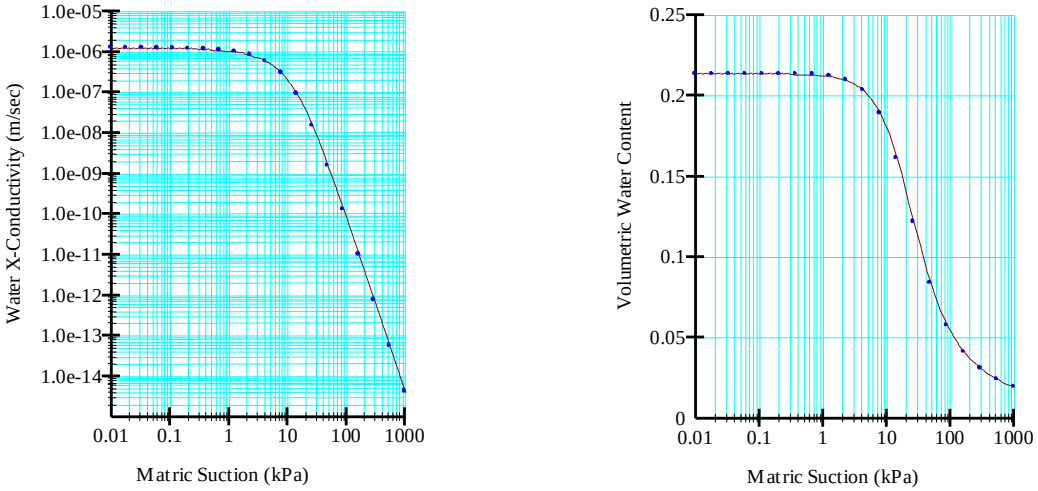

Fig. 4.4: HCF and SWCC for S_4 location

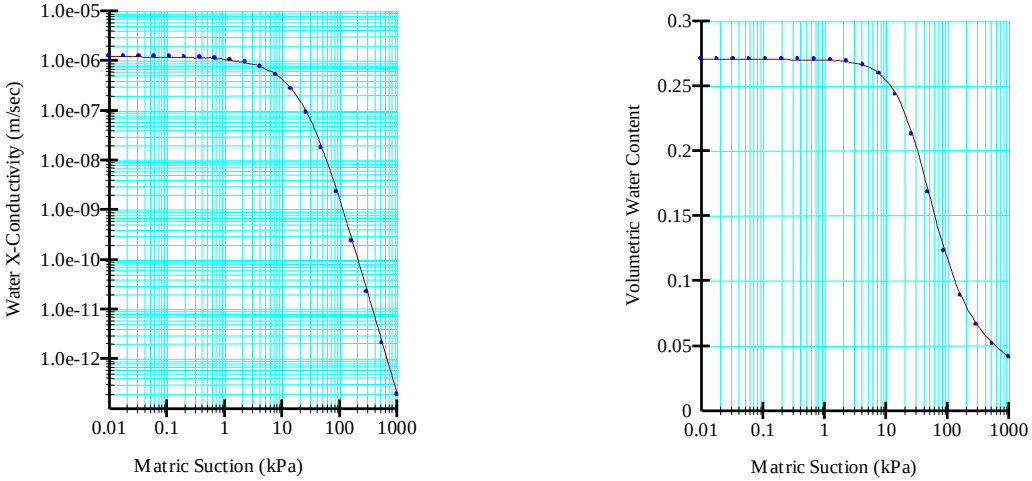

Fig. 4.5: HCF and SWCC for S_5 location

4.2 Slope stability analysis

Seep/W module's estimated pore water pressure is utilised as an input for Slope/W module's initial pore water pressure. To incorporate the effect of negative pore water pressure, the Fredlund et al (1978) equation is utilised in the Slope/ W module, which is presented as follows:

$$\tau = c' + (\sigma_n - u_a) \tan\phi' + (u_a - u_w) \tan\phi^b \quad (6)$$

where τ is the shear strength of unsaturated soil, c' is the effective cohesion, σ_n is the total normal stress, u_a is the pore air pressure, u_w is the pore water pressure, $(\sigma_n - u_a)$ is the net normal stress, $(u_a - u_w)$ is the matric suction, ϕ^b is the angle representing rate of increase in shear strength relative to the matric suction and ϕ' is the effective angle of internal friction. In eq. 5 ϕ^b is taken as a constant value but it is found that ϕ^b changes with change in degree of saturation in the zone of capillary saturation. Another option for the calculation of unsaturated shear strength of soil is also available within SLOPE/W module given by Vanapalli et al (1996) is given below:

$$\tau = c' + (\sigma_n - u_a) \tan\phi' + (u_a - u_w) \left[\left(\frac{\theta_w - \theta_r}{\theta_s - \theta_r}\right) \tan\phi'\right] \quad (7)$$

where θ_w is the volumetric water content, θ_r is the residual water content and θ_s is the saturated water content. The factor of safety of the sliding surface is given by:

$$FOS = \frac{\sum \tau_r}{\sum \tau_m} \quad (8)$$

Where $\sum \tau_r$ represents the total resisting shear stresses and $\sum \tau_m$ represents the total mobilised shear stresses.

In SLOPE/W module, there are ten methods based on limit equilibrium for analysing slopes. Amongst them, in this study Morgenstern and Price method is used because it considers both interslice shear and normal forces and satisfies both force and moment equilibrium equations. It is a precise method which is applicable to a variety of soil profiles and slope geometries. The geometry of slopes used in present study are shown below:

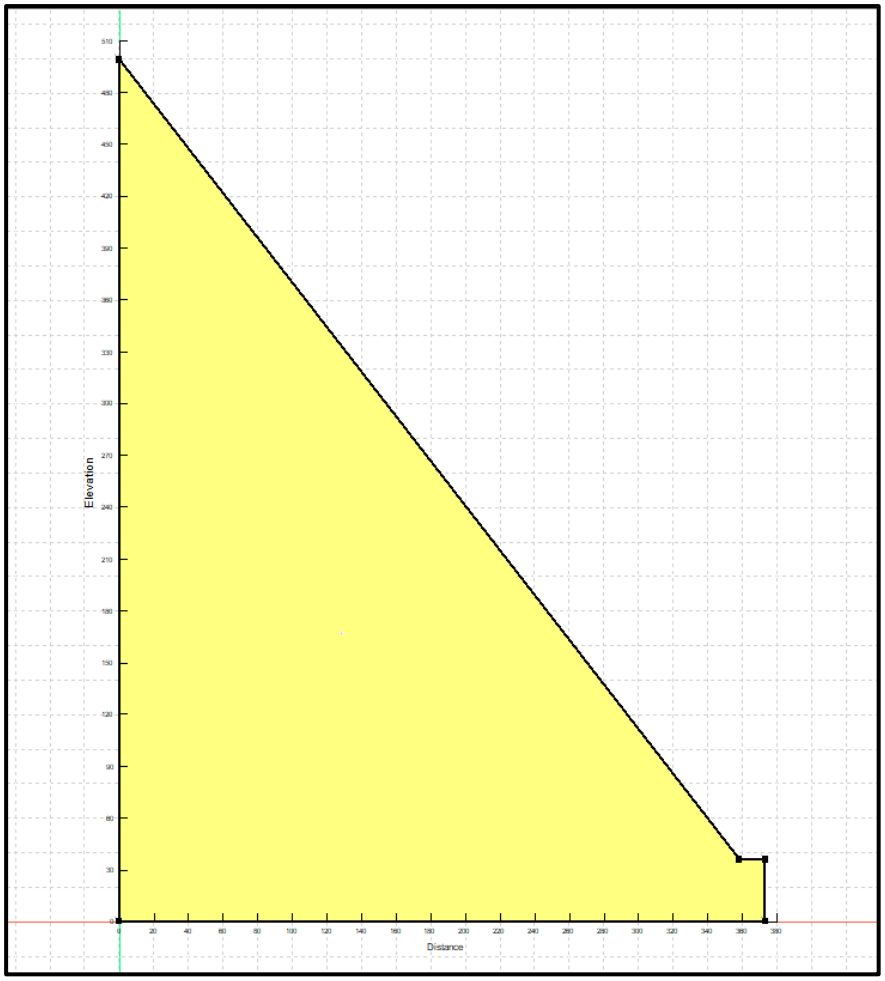

Fig. 4.6: Geometry of slope S_1

Fig. 4.7: Geometry of slope S_2

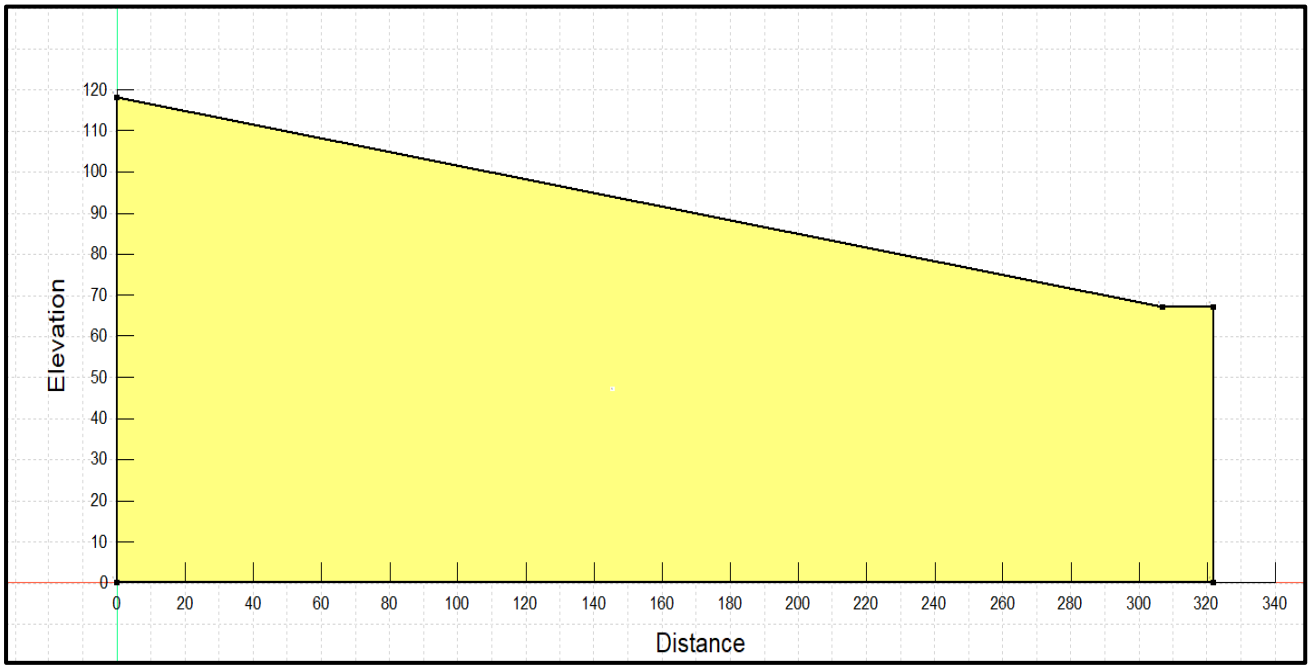

Fig. 4.8: Geometry of slope S_3

Fig. 4.9: Geometry of slope S_4

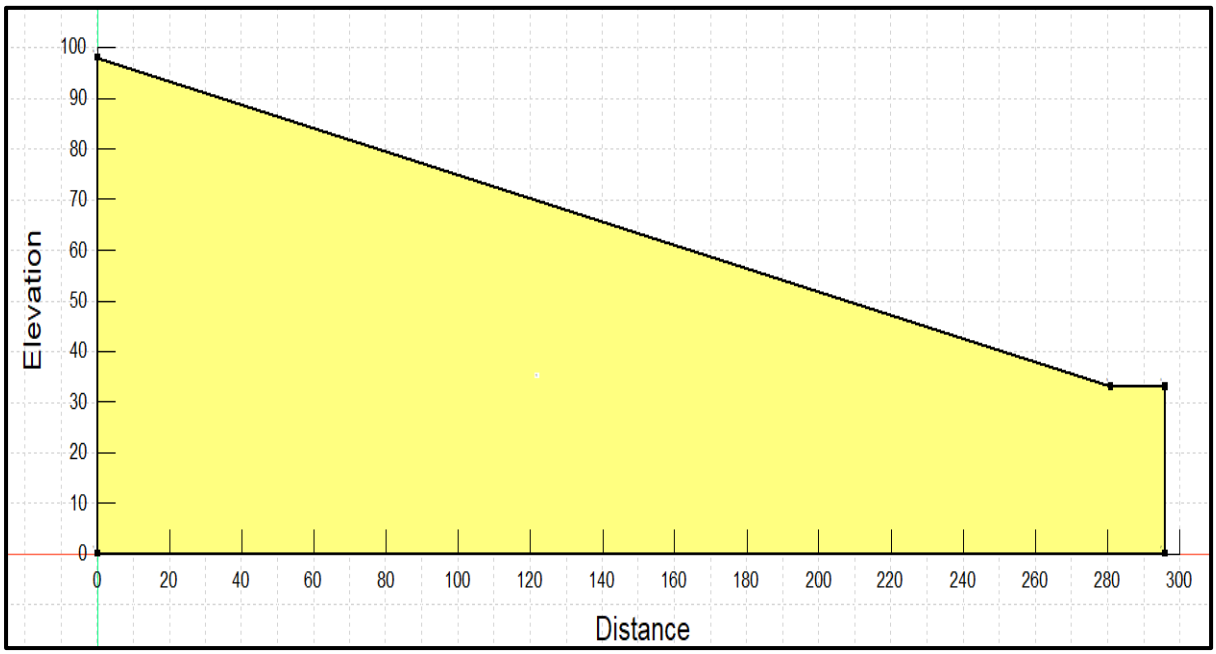

Fig. 4.10: Geometry of slope S_5

Chapter 5

Rainfall Data Analysis

There are many factors that affect the stability of slopes like tectonic, seismic activities, slope cutting, hill side constructions, precipitation etc. Out of these factors, rainfall has been found to have a profound effect on the stability of slopes. Rain water seeps within the soil and increases the pore water pressure within the slope. With the increase in the pore water pressure, the effective stresses within the soil reduces. As shear strength of soil depends upon effective stress, with the decrease in the effective stress of soil its shear strength also reduces resulting in lowering the overall FOS of slope. For the present study, rainfall data for five selected slope locations as shown in Fig. 5.1 have been extracted using CHIRPS: Rainfall estimates in mm from rain gauges and satellite observations. Fig. 5.2 shows the annual rainfall data for all the 5 sites for the past 10 years (2011-2021). From the annual data, it was found that 2015 was the year with maximum rainfall. Monthly rainfall data for the year 2015 (Fig. 5.3) for all the locations was further analysed and it was found that march was the month with maximum rainfall intensity and for the same month, daily rainfall data was also observed in order to get the maximum daily rainfall intensity for each location. Fig. 5.4 shows the daily rainfall intensity for the month of march for all the 5 locations.

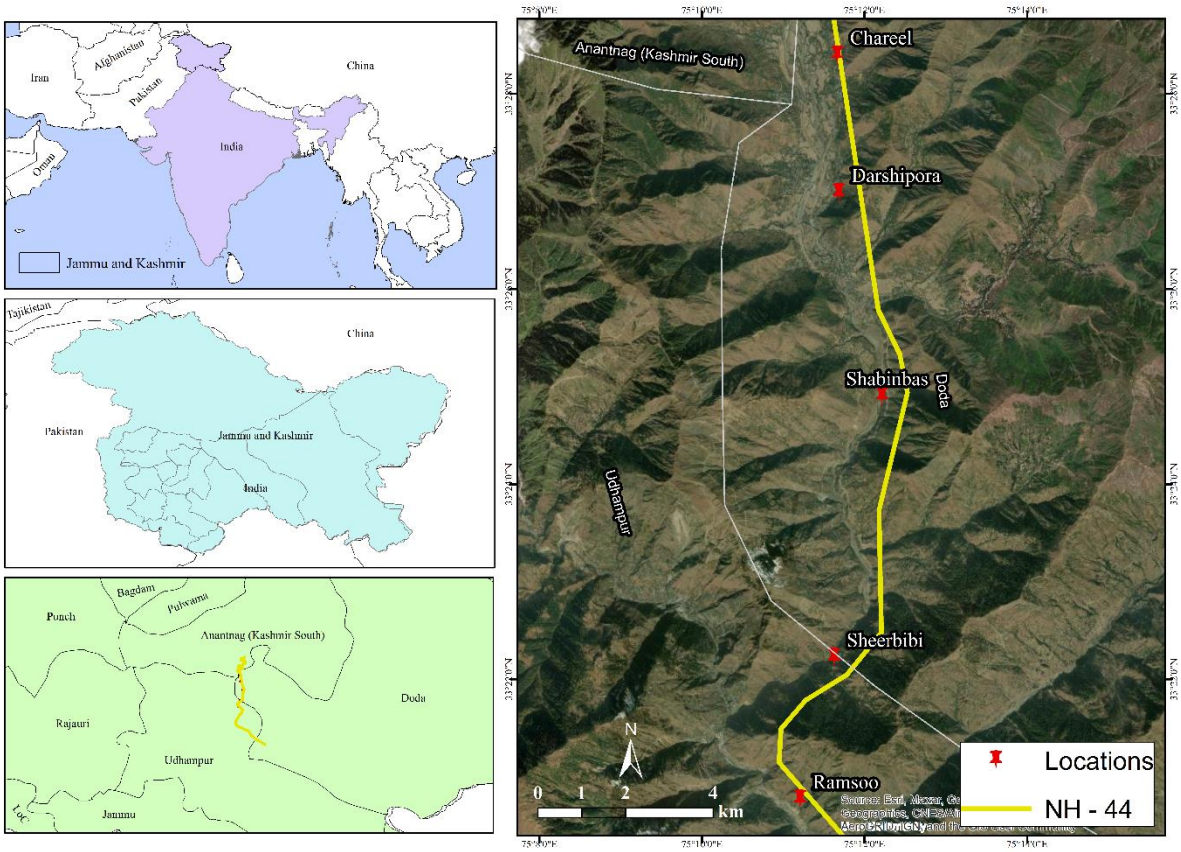

Fig. 5.1: Location map of the study area

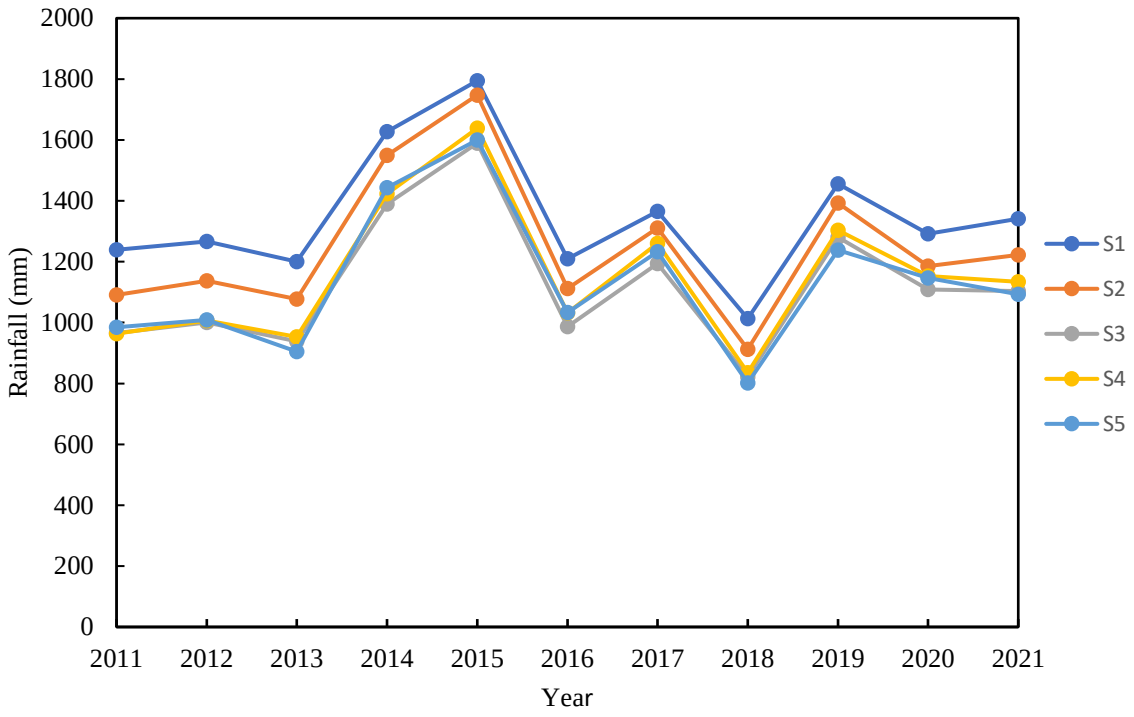

Fig. 5.2: Annual rainfall data of all locations for the past 10 years (CHIRPS)

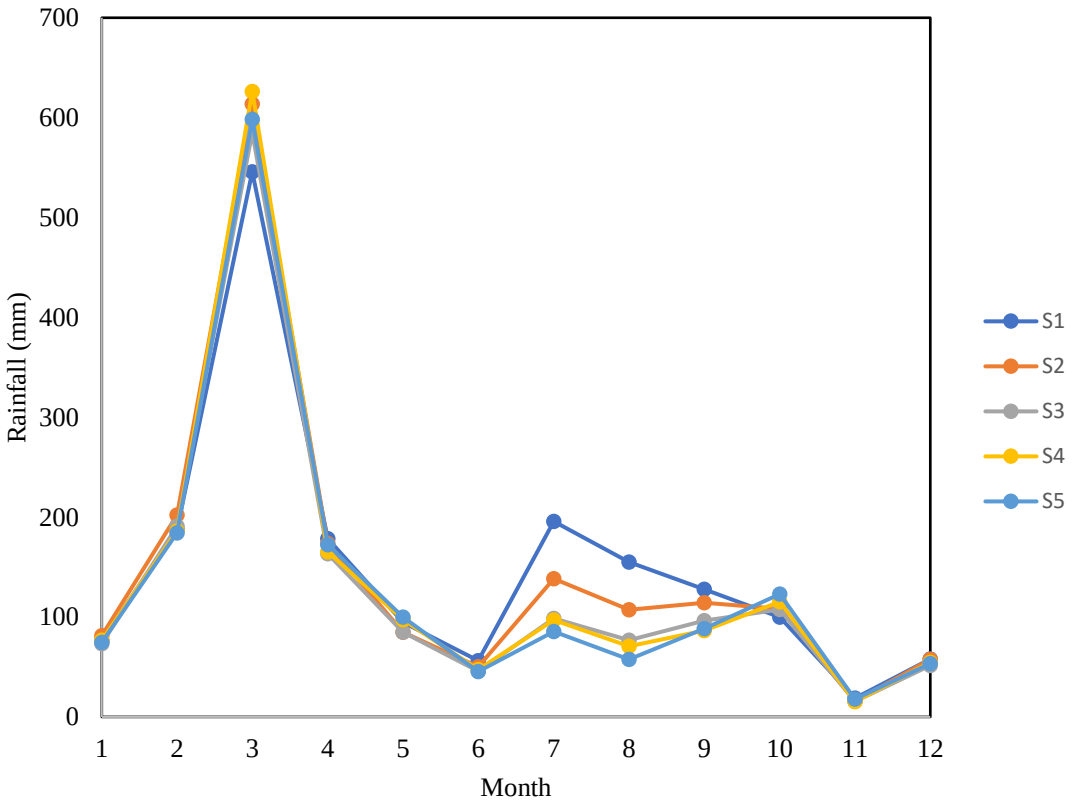

Fig. 5.3: Monthly rainfall data of all locations for the year with maximum precipitation (CHIRPS)

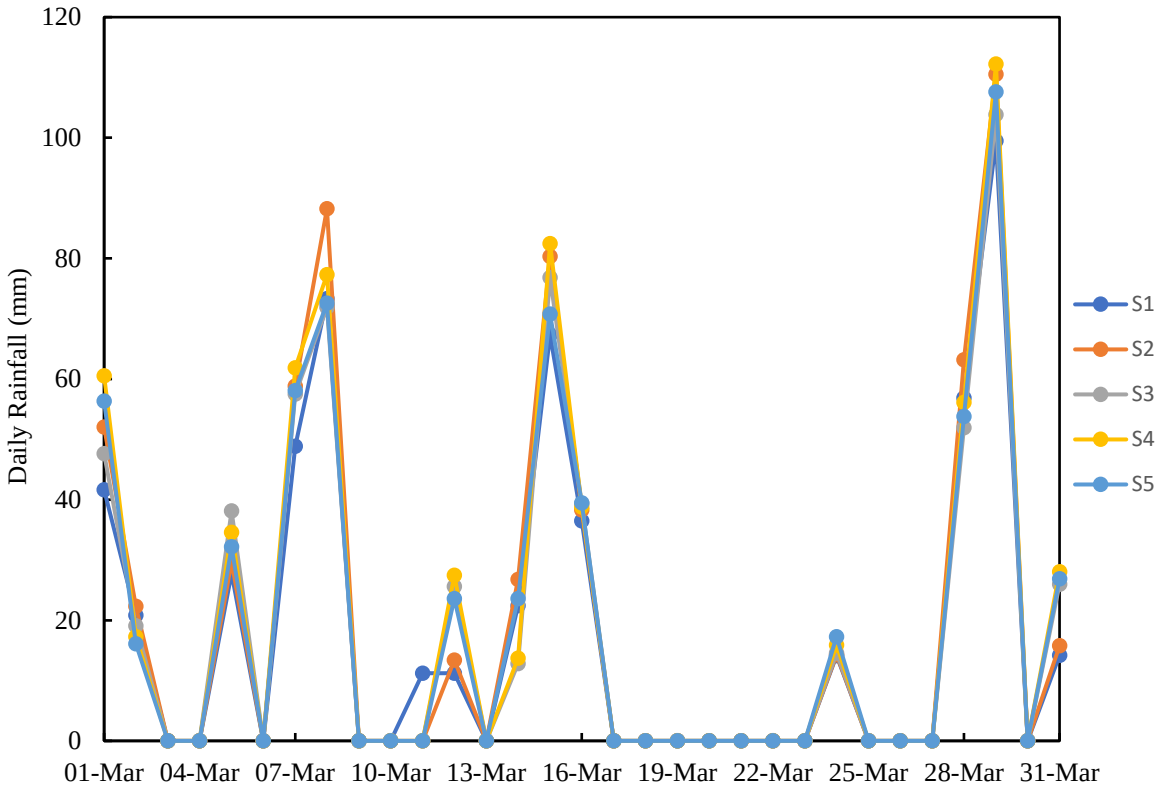

Fig. 5.4: Daily rainfall data for the month of maximum rainfall for all the locations (CHIRPS)

Chapter 6

Results and Discussion

6.1 Laboratory Investigation

The important geotechnical properties determined for this research include:

6.1.1 Results for Grain Size Distribution

Soil samples from S_1 and S_2 were classified as coarse-grained soils as more than 50% by weight of soil sample was retained on 75μ IS sieve while soil samples from S_3, S_4 and S_5 were classified as fine-grained soils. The soils were classified as per Unified Soil Classification System (USCS) as Silty Sand (SM) for S_1, S_2, Low Compressible Silt (ML) for S_3 and S_4 and Low Compressible Silt with Clay (CL-ML) for S_5 (Table 3). The grain size distribution curve of soils for all sites are shown in Fig. 6.1

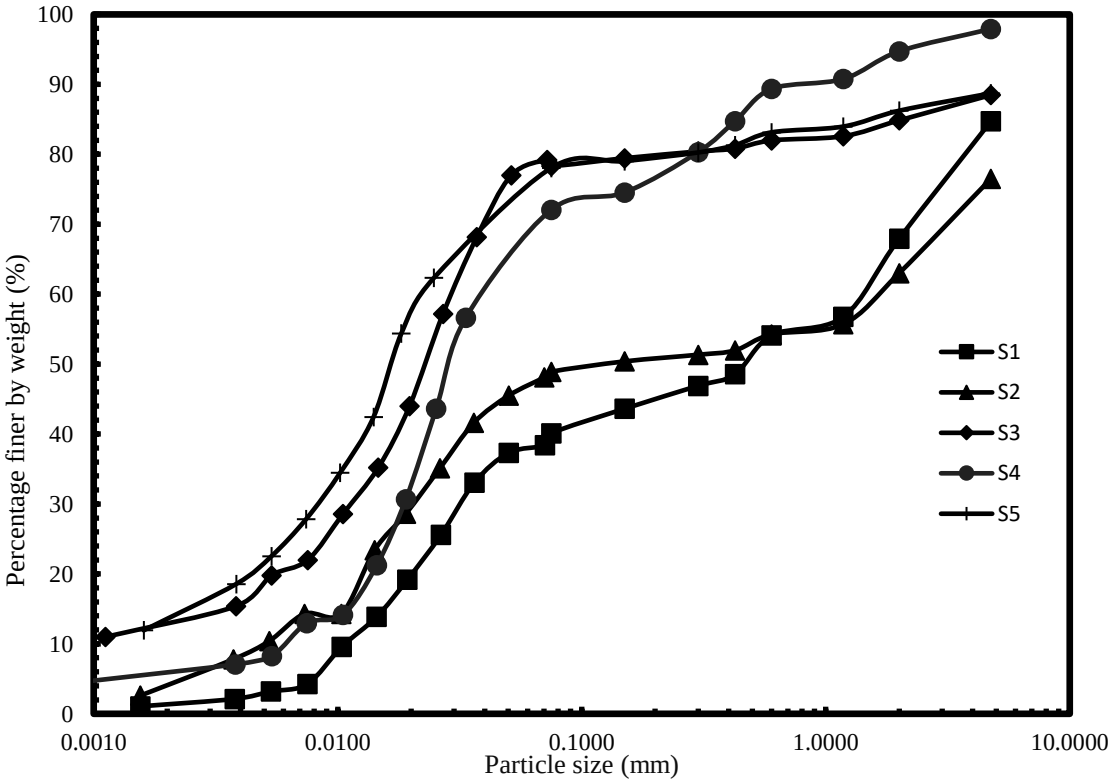

Fig. 6.1: Grain Size Distribution plots for soil samples collected from 5 sites

6.1.2 Results for Atterberg Limits

The liquid limit(w_L) of 5 sites varies between (20-40) %, Plastic Limit (w_P) between (17-34) % and Plasticity Index (I_P) between (3-9) %. The soil was described as low plastic for S_1 and S_4, and medium plastic for S_2, S_3 and S_5. The results obtained for Liquid Limit, Plastic Limit and Plasticity Index for all the 5 sites are presented in Table 6.1. Similar results were obtained by Mokwa (1999).

Table 6.1 Laboratory results for Grain size distribution and Atterberg limits

Site	Grain Size Distribution (%)				USCS Classification	Liquid Limit (w_L) (%)	Plastic Limit (w_L) (%)	Plasticity Index (I_P) (%)
	Gravel	Sand	Silt	Clay				
S_1	15.28	44.61	39.04	1.07	SM	39.38	36.13	3.25
S_2	23.50	27.59	46.31	2.60	SM	40.08	32.27	7.81
S_3	11.53	10.17	65.85	12.47	ML	34.10	24.99	9.11
S_4	2.08	25.86	66.61	5.45	ML	20.83	17.60	3.23
S_5	11.28	10.67	64.90	13.15	CL-ML	27.99	22.51	5.48

6.1.3 Results for In-Situ Bulk Density, In-Situ Moisture Content and Specific Gravity

The bulk density of soil samples varies from (1700-1900) kg/m^3 and in-situ moisture content varies from (13-24) % for different sites. The specific gravity was found to range between 2.65-2.68. Table 6.2 shows the bulk density, in-situ moisture content and specific gravity of soil from all locations.

Table 6.2 Laboratory results for density, moisture content and specific gravity

Site	Bulk Density (ρ_b) (kg/m^3)	Dry Density (ρ_d) (kg/m^3)	Saturated Density (ρ_{sat}) (kg/m^3)	In-Situ Moisture Content (%)	Specific Gravity(G)
S_1	1690	1480	1930	13.53	2.68
S_2	1710	1410	1870	21.54	2.68
S_3	1840	1490	1930	22.63	2.65
S_4	1880	1610	2000	16.89	2.65
S_5	1910	1540	1960	23.92	2.65

6.1.4 Results for Shear Strength Parameters

Table 6.3 shows the laboratory results for both conditions. Similar results were obtained by Pandit et al (2021). The reason for high cohesion values may be attributed to the high percentage of silt. Non-Plastic silt behaves more like sand and plastic silt behaves more like clay, so higher cohesion values may be attributed to the presence of plastic silt. Upon inundation significant decrease in cohesion values was observed in soil samples with high percentage of silt. This indicates that water can significantly affect strength properties of soil for the locations under study. Fig. 6.2- 6.6 shows the Mohr -Coulomb strength envelope and plot of shear stress vs horizontal displacement for each location.

Table 6.3 Cohesion and friction angle values obtained from DST

Site Location	Direct Shear Strength Parameters			
	Unsaturated		Inundated	
	Cohesion (c) (kN/m^2)	Friction Angle (φ) (°)	Cohesion (c) (kN/m^2)	Friction Angle (φ) (°)
S_1	37.39	27.60	33.73	27.28
S_2	47.52	28.44	22.99	32.01
S_3	62.68	21.34	19.92	33.69
S_4	32.94	34.28	0.098	40.78
S_5	56.27	22.83	2.55	37.81

(a)

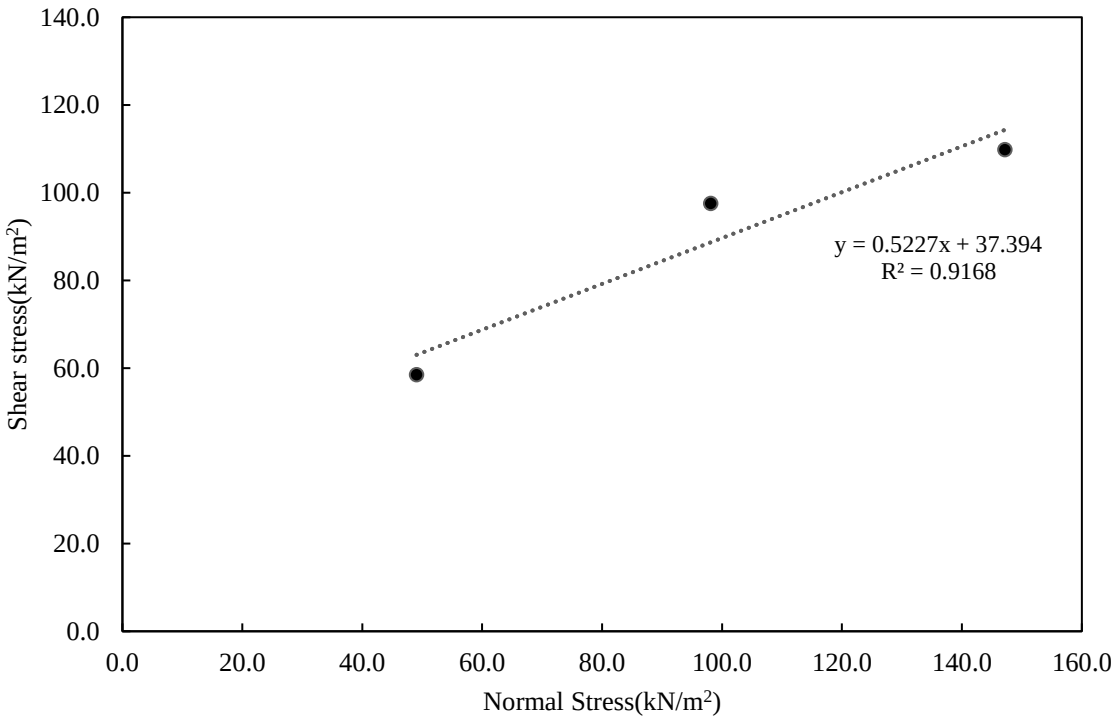

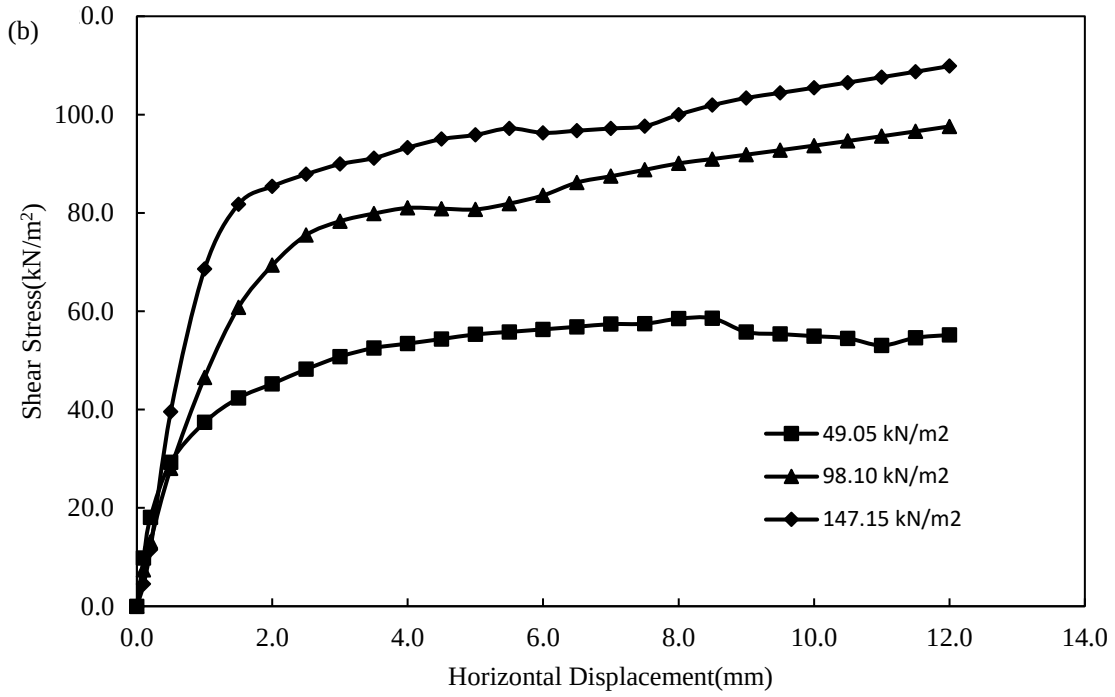

Fig. 6.2: Direct shear test results for S_1 (a) Mohr-Coulomb strength envelope (b) shear stress versus horizontal displacement

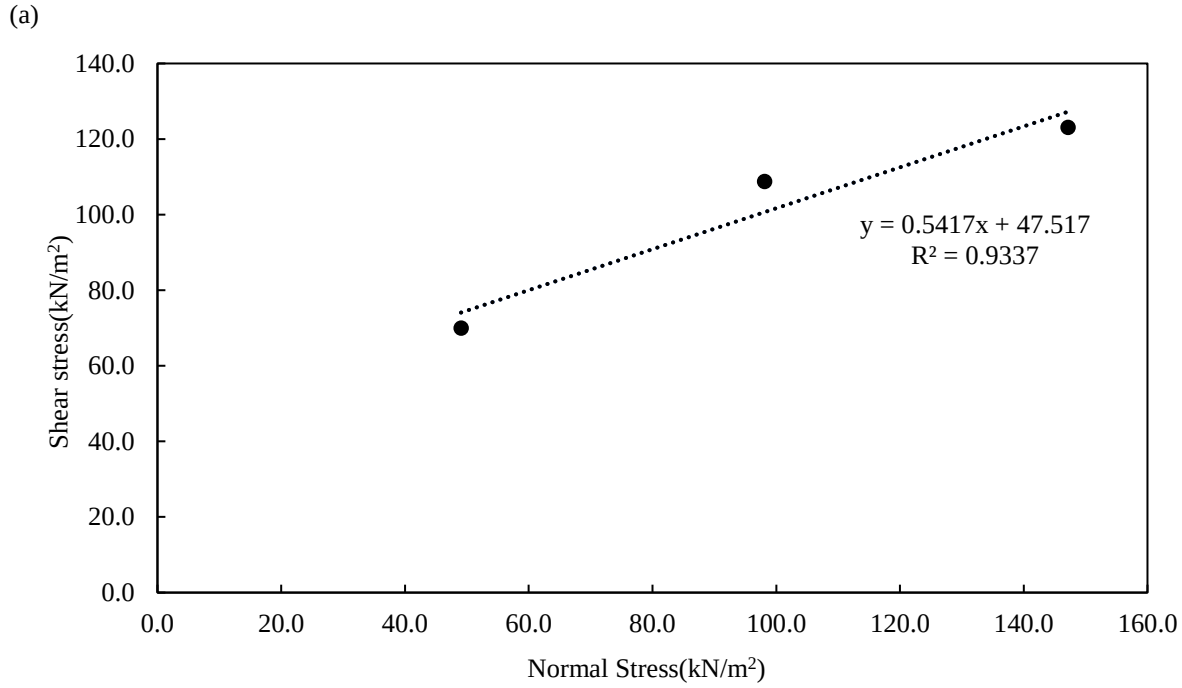

(b)

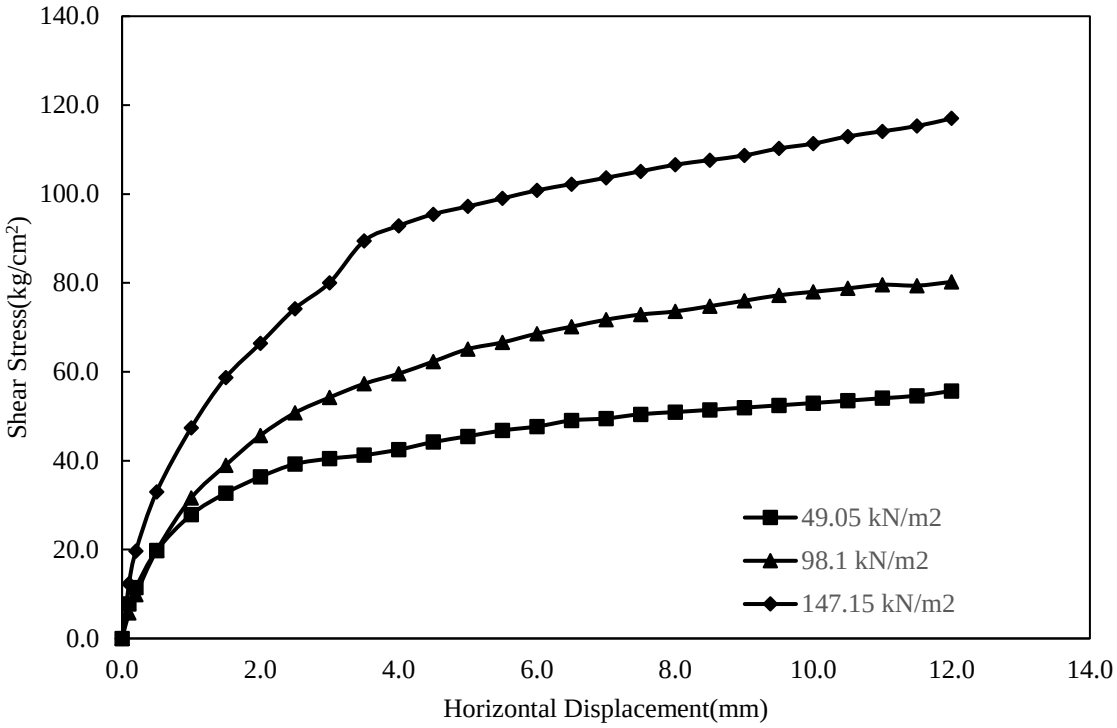

Fig. 6.3: Direct shear test results for S_2 (a) Mohr-Coulomb strength envelope (b) shear stress versus horizontal displacement

(a)

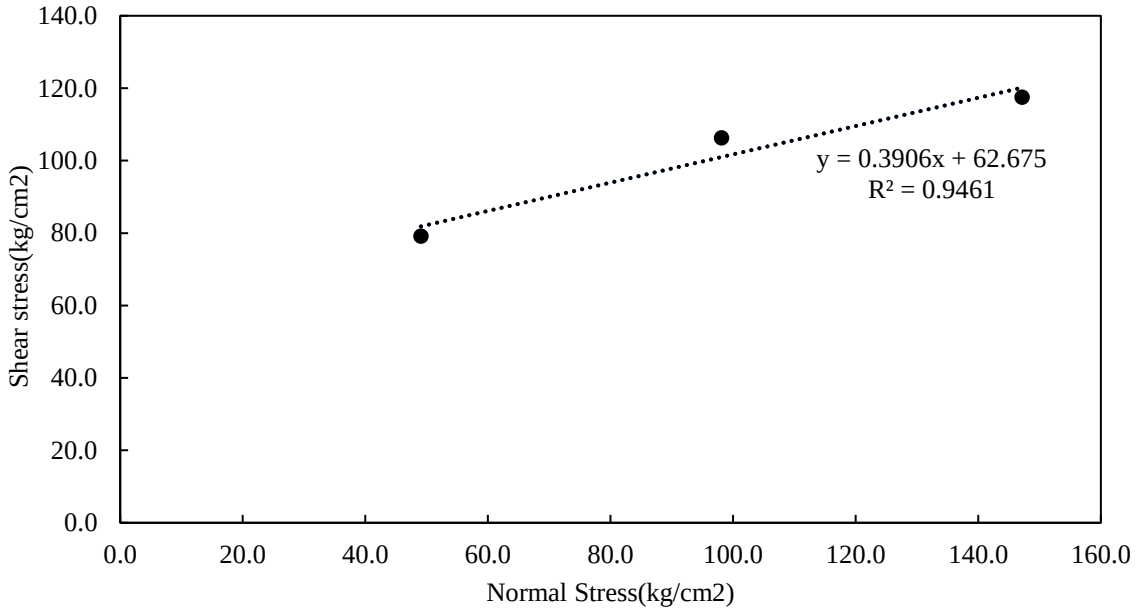

(b)

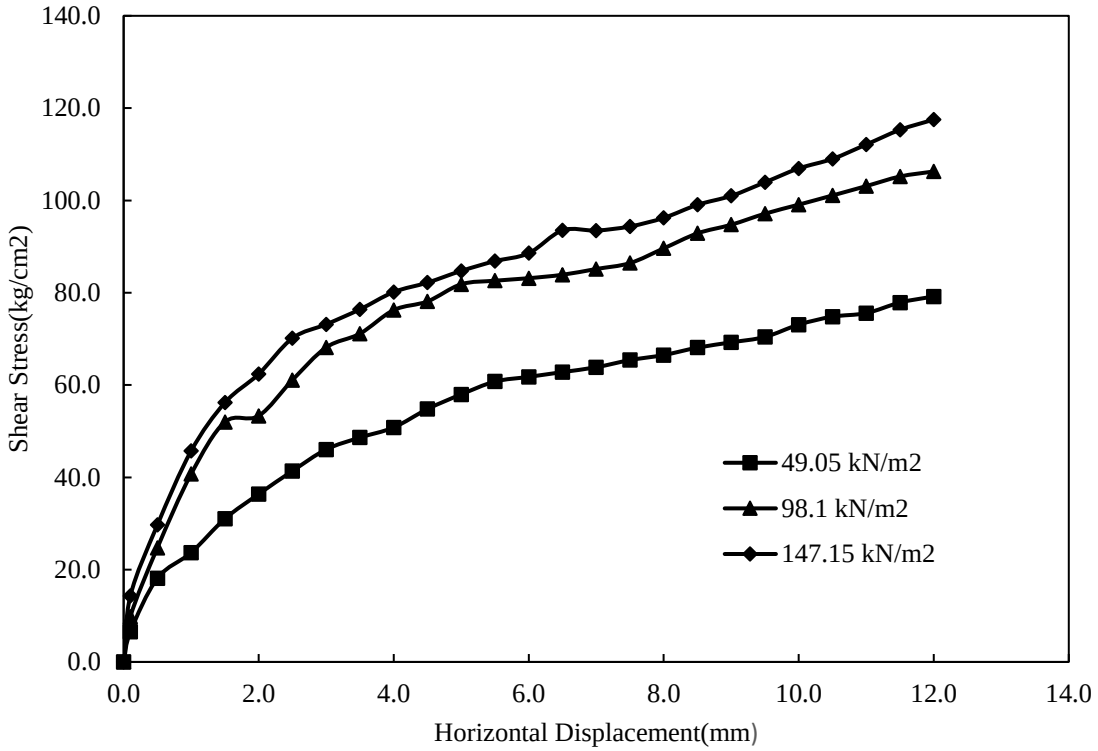

Fig. 6.4: Direct shear test results for S_3 (a) Mohr-Coulomb strength envelope (b) shear stress versus horizontal displacement

(a)

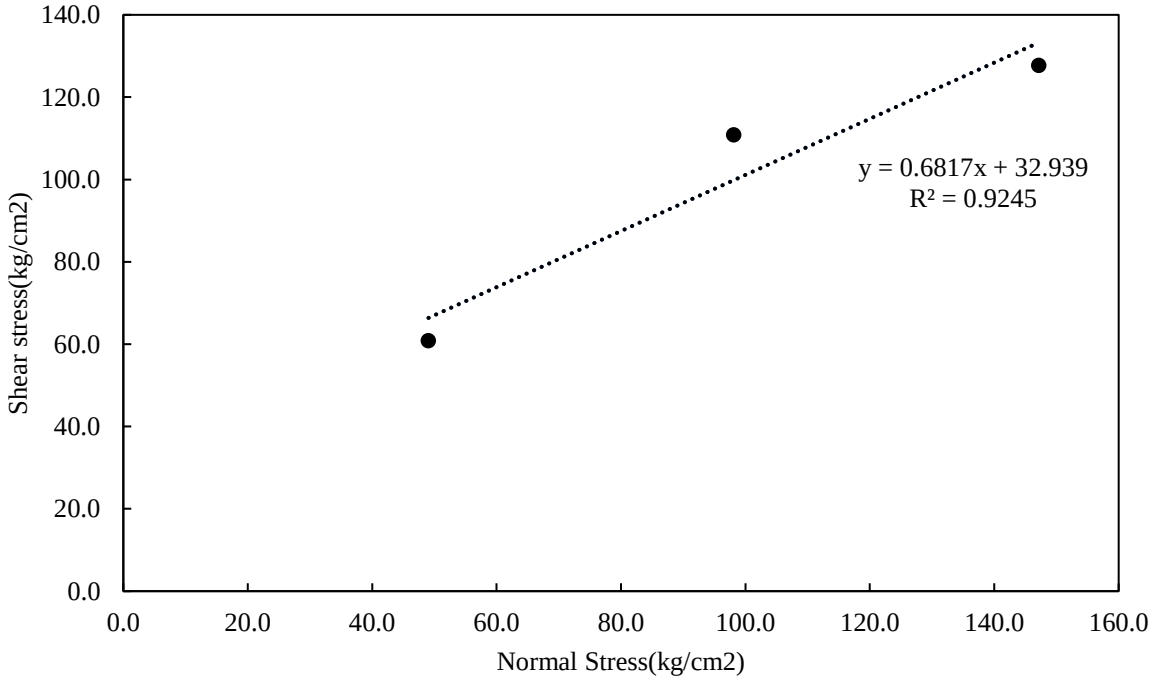

(b)

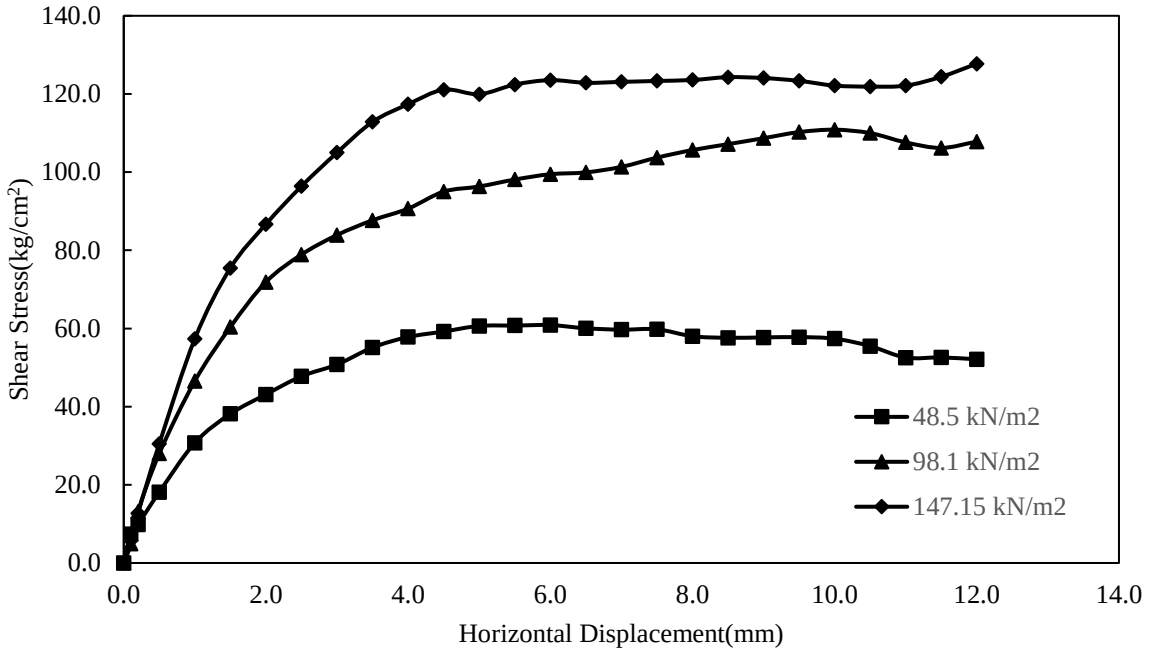

Fig. 6.5: Direct shear test results for S_4 (a) Mohr-Coulomb strength envelope (b) shear stress versus horizontal displacement

(a)

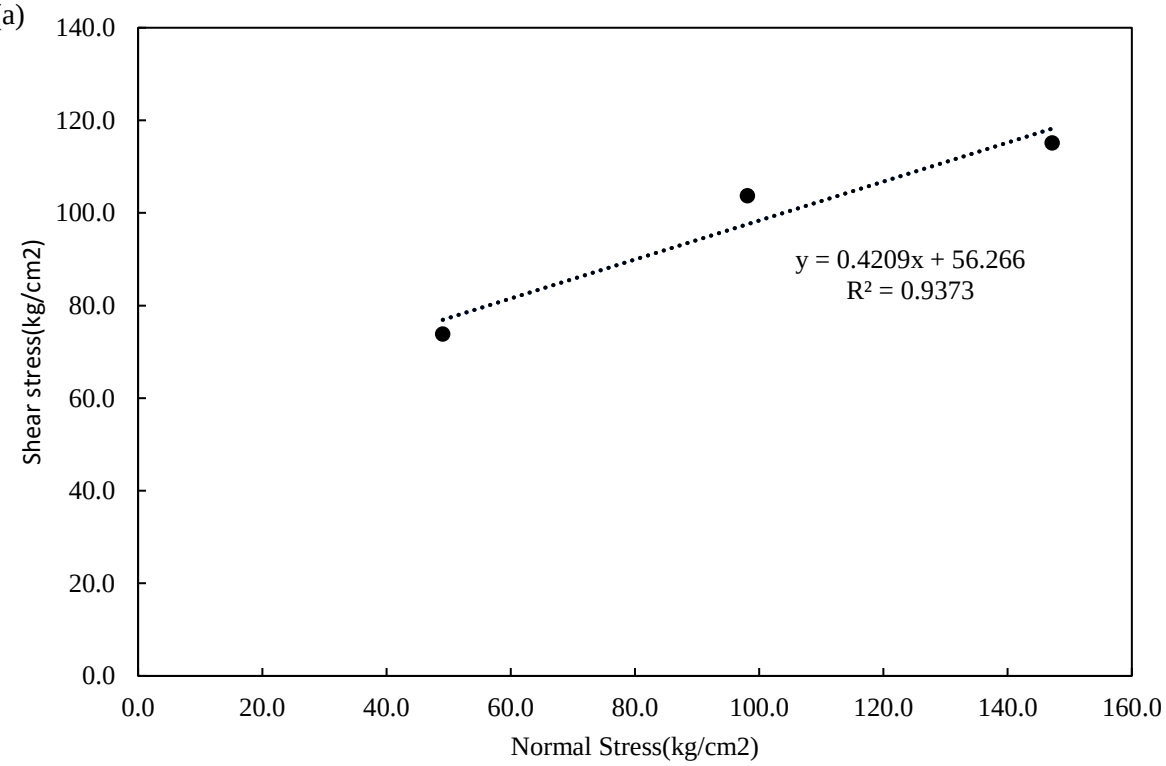

(b)

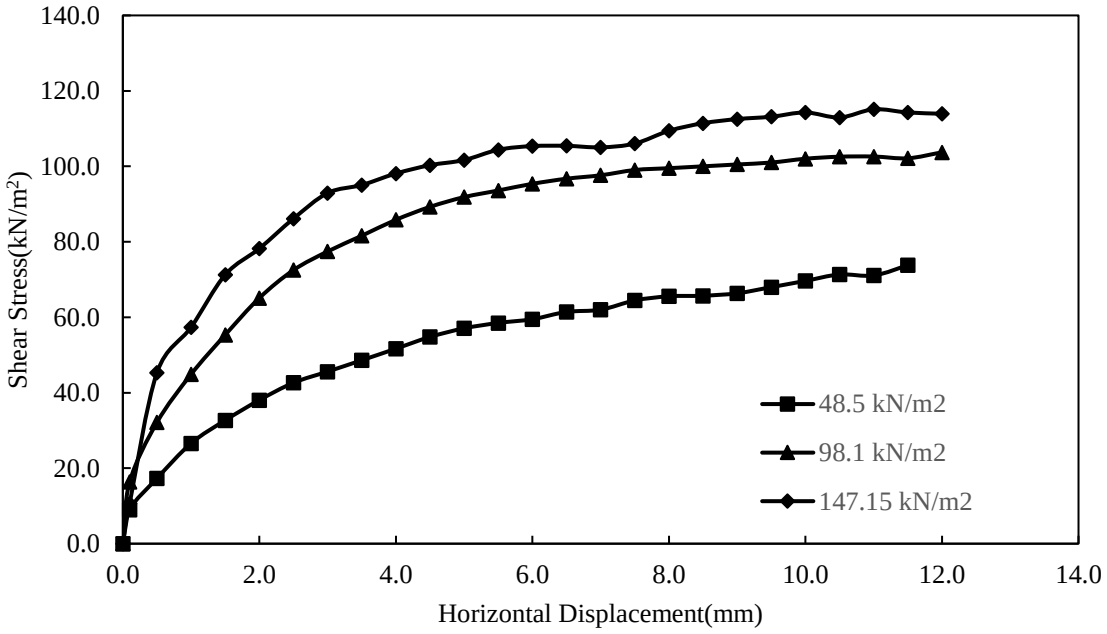

Fig. 6.6: Direct shear test results for S_5 (a) Mohr-Coulomb strength envelope (b) shear stress versus horizontal displacement

6.1.5 Results for Consolidation Characteristics

The consolidation parameters obtained from this test are presented in Table 6.4. The plot for e vs log p and normal stress vs shear stress are for each location are presented in Fig 6.7 – Fig 6.11

Table 6.4 Consolidation parameters obtained from 1-D consolidometer test.

Site	S_1	S_2	S_3	S_4	S_5
Initial Void Ratio (e_0)	0.7620	0.9077	0.7185	0.5739	0.7258
Height of Soil Solids (H_S)	1.1351	1.0484	1.1638	1.2707	1.1589
Compression Index (Cc)	0.2230	0.2712	0.1347	0.1833	0.1711
Recompression Index (Cr)	0.0404	0.0447	0.0251	0.0203	0.0254
Pre-Consolidation Pressure (kN/m^2)	206.01	107.91	215.82	166.77	88.29
Coefficient of Compression(a_v) (m^2/kN)	1.44×10^{-4}	2.65×10^{-4}	1.02×10^{-4}	2.08×10^{-4}	3.12×10^{-4}
Coefficient of Volume Compressibility (m_v) (m^2/kN)	8.15×10^{-5}	1.39×10^{-4}	4.79×10^{-4}	1.31×10^{-4}	1.80×10^{-4}
Average Coefficient of Consolidation (Cv) (m^2/sec)	7×10^{-8}	8×10^{-8}	1×10^{-7}	1.1×10^{-7}	1.1×10^{-7}

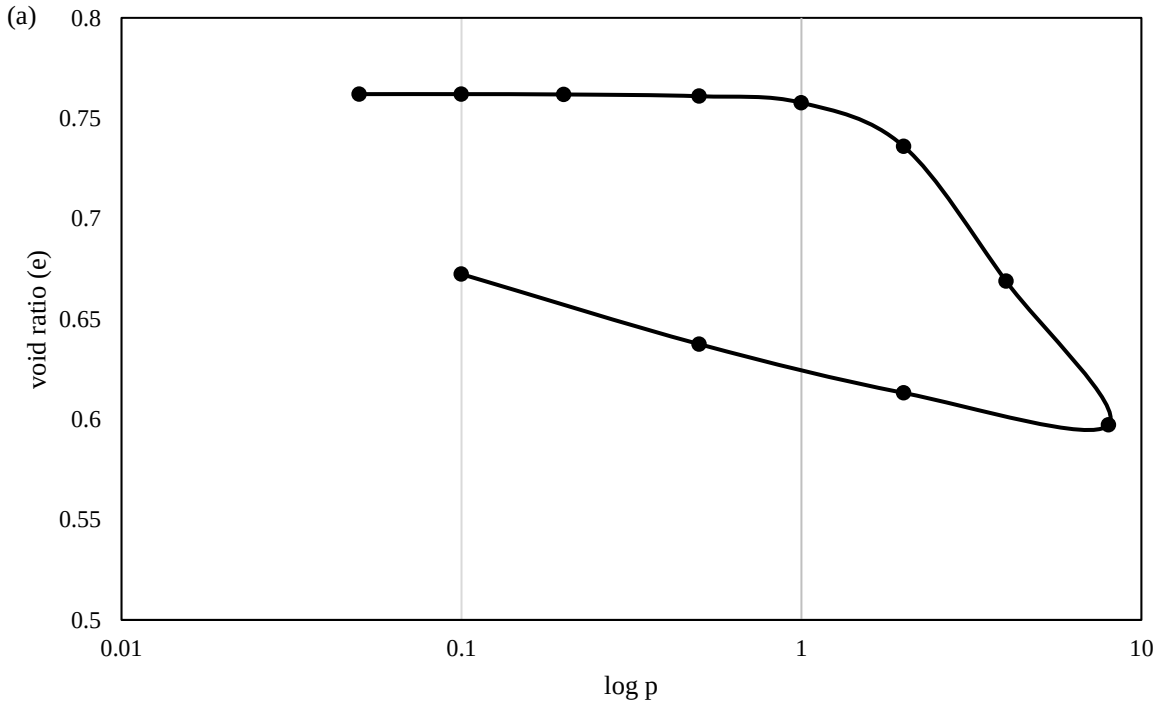

(b)

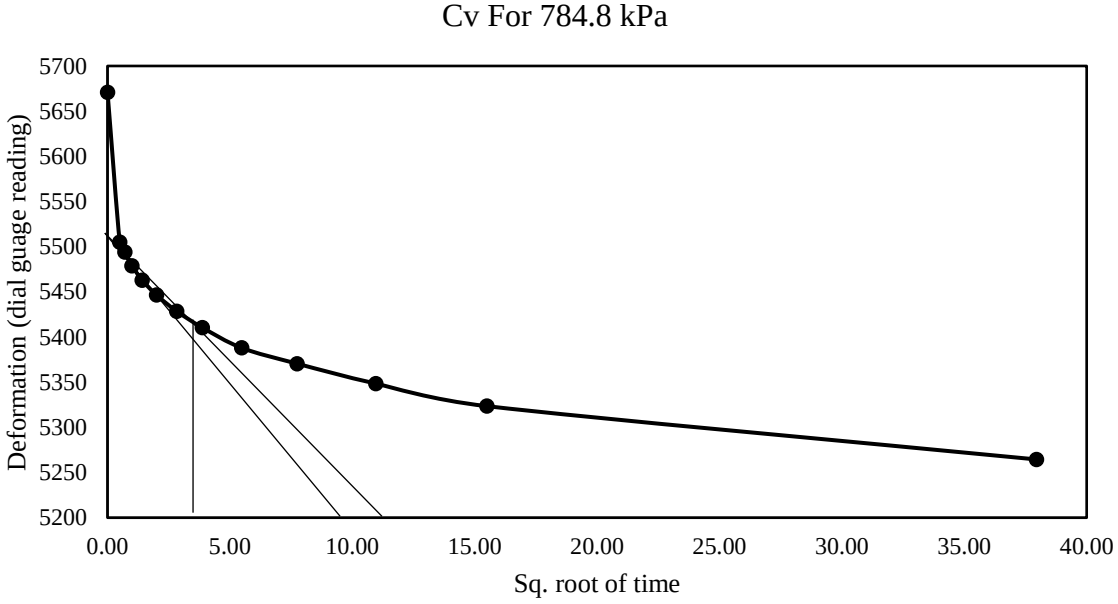

Fig. 6.7: Consolidation test results for S_1 (a) plot of e vs log p (b) coefficient of consolidation for 784.8 kPa by Taylor's square root of time fitting method

(a)

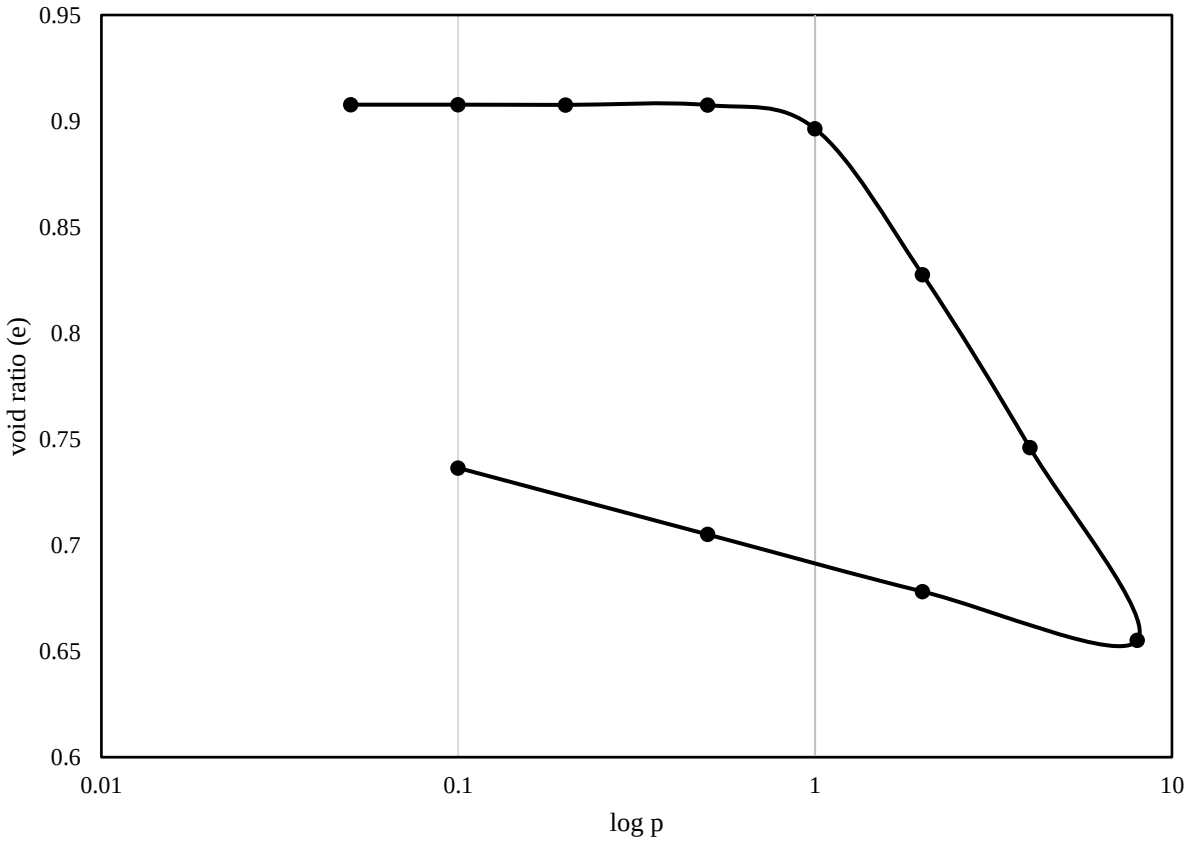

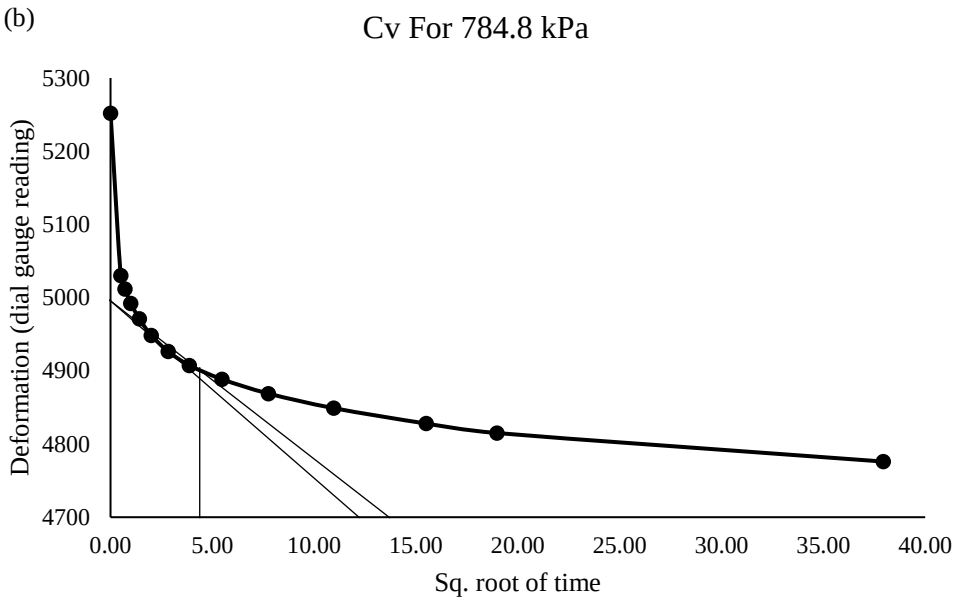

Fig. 6.8: Consolidation test results for S_2 (a) plot of e vs log p (b) coefficient of consolidation for 784.8 kPa by Taylor's square root of time fitting method

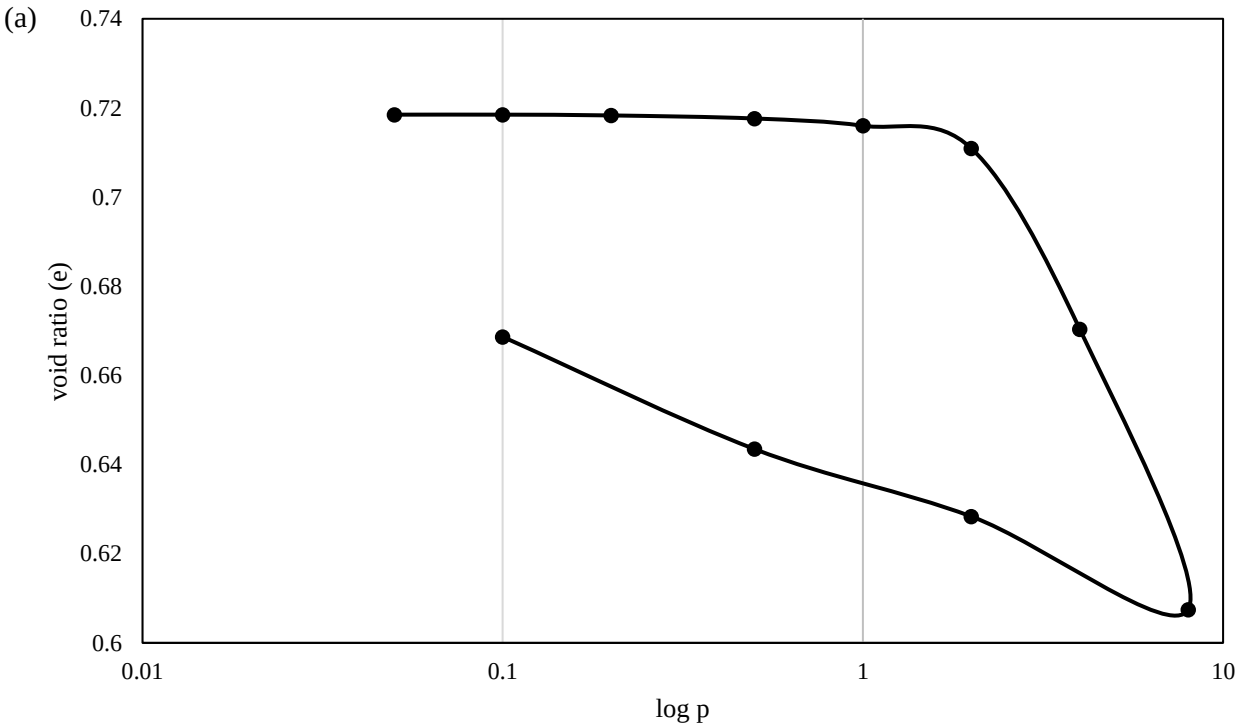

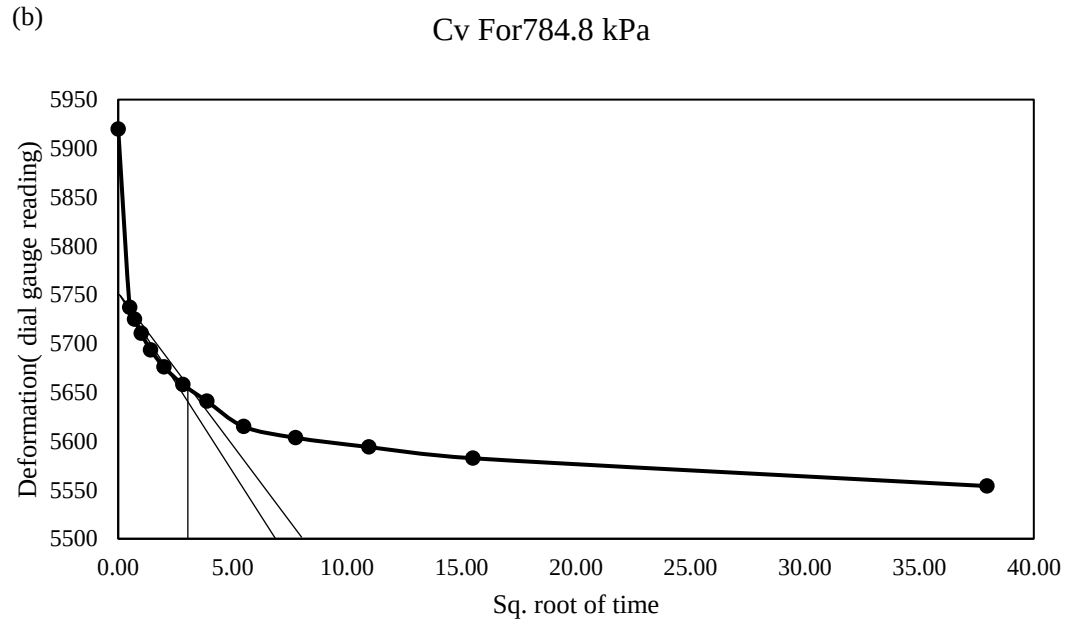

Fig. 6.9: Consolidation test results for S_3 (a) plot of e vs log p (b) coefficient of consolidation for 784.8 kPa by Taylor's square root of time fitting method

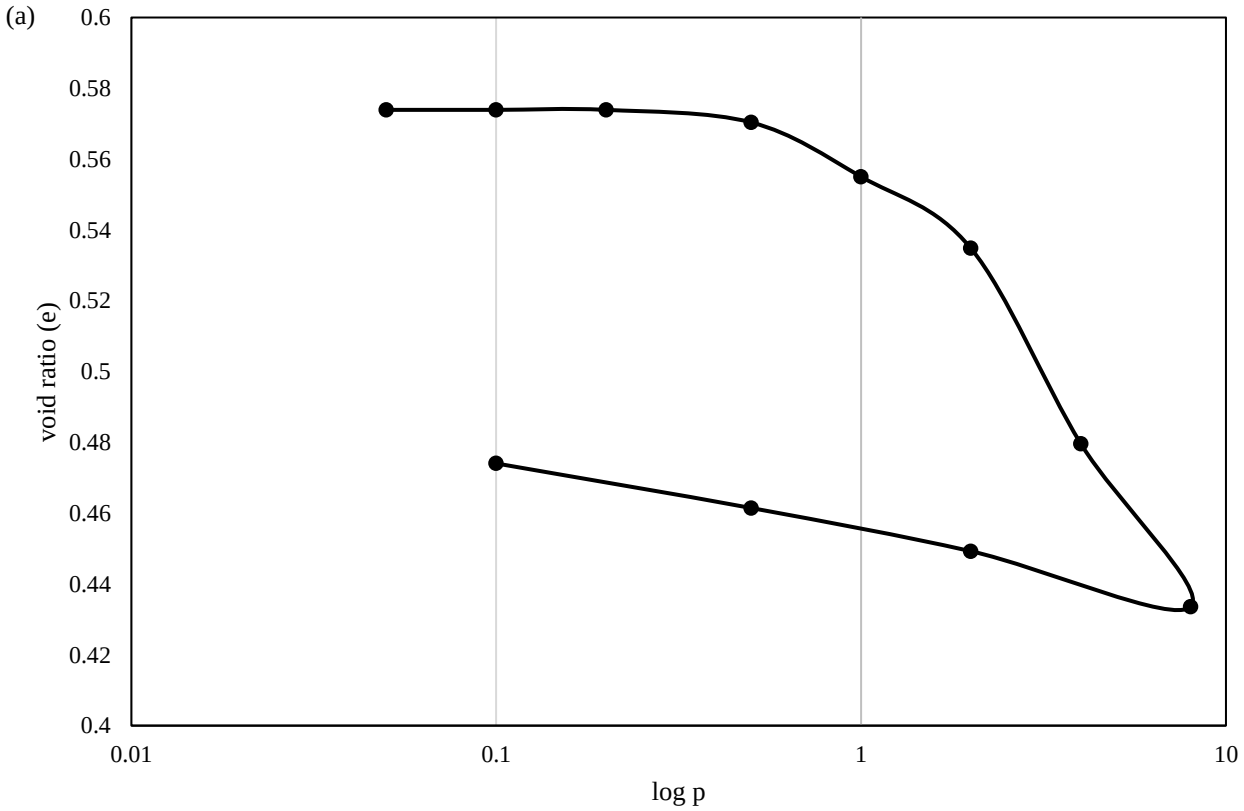

(b)

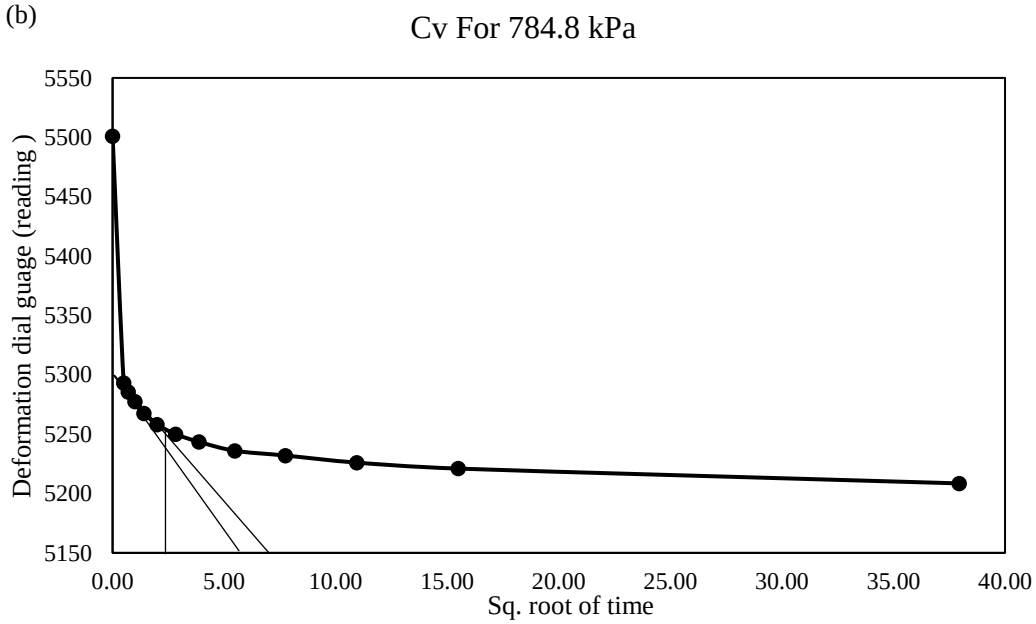

Fig. 6.10: Consolidation test results for S_4 (a) plot of e vs log p (b) coefficient of consolidation for 784.8 kPa by Taylor's square root of time fitting method

(a)

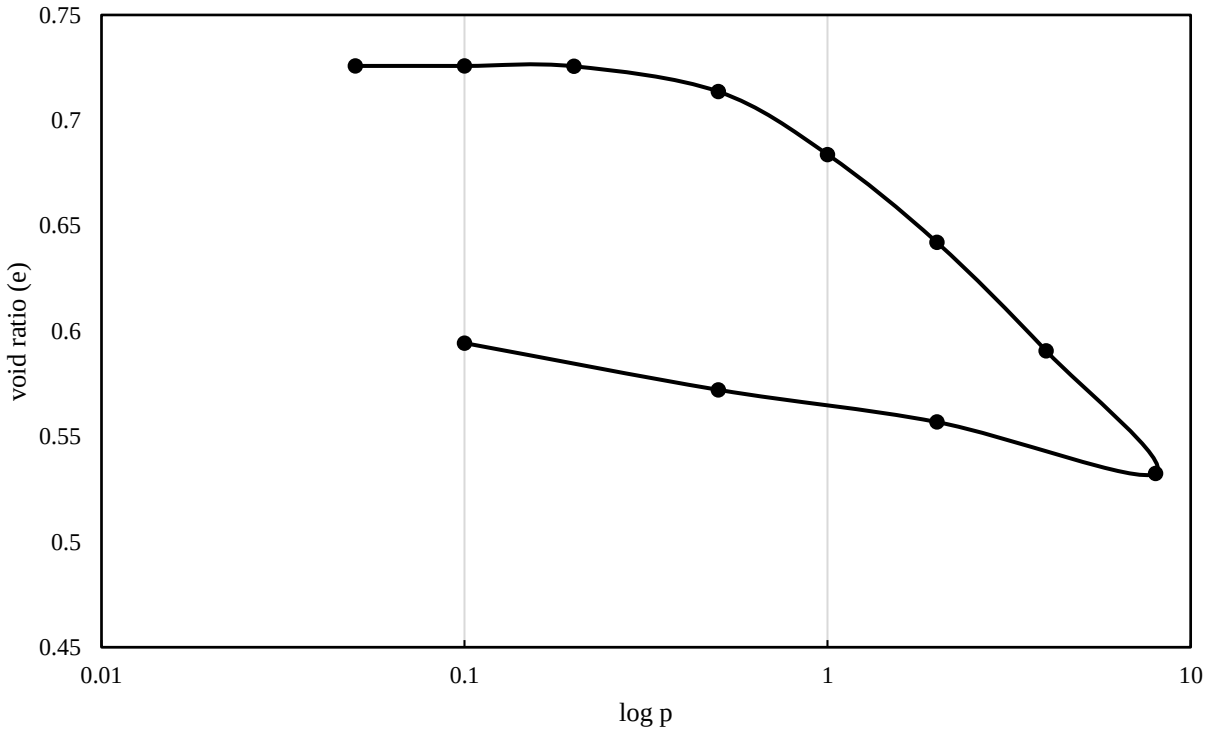

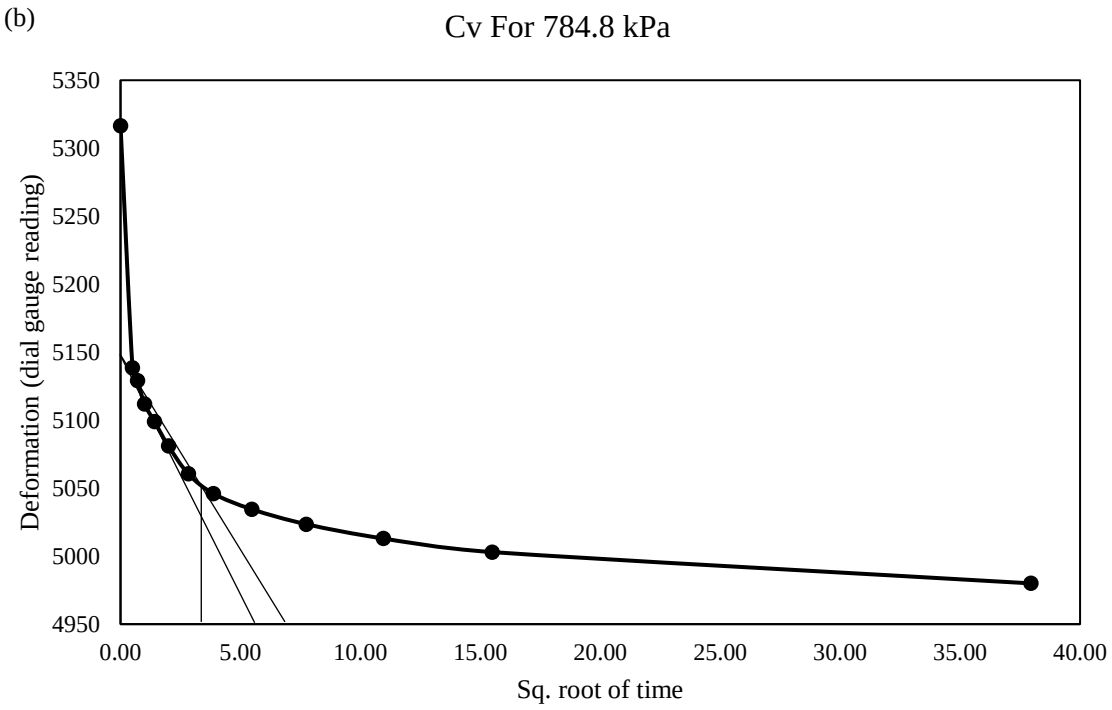

Fig. 6.11: Consolidation test results for S_5 (a) plot of e vs log p (b) coefficient of consolidation for 784.8 kPa by Taylor's square root of time fitting method

6.2 Output from numerical analysis

Change in pore water pressure within slope with time before and after the rainfall event, change in FOS with time, and relative change in FOS of slopes before and after the rainfall event are the outcomes of numerical study. The seepage analysis boundary conditions include no drainage at the slope's base and left boundary, rainwater flux at the slope's surface, and a zero-pressure boundary condition at the slope's right boundary and initial water table location near the bottom of slope. The same boundary condition has been applied to all the slopes under examination. In seepage analysis, a global element mesh size of 5 m comprised of triangular elements was used. For the purpose of simplifying numerical analysis, it is assumed that the slopes of the current study are uniform throughout.

6.2.1 Pore water distribution within the slope under normal conditions without rainfall for all locations

For the development of initial pore water pressure condition within the slope S_1, S_2, S_3, S_4 and S_5, steady state seepage analysis is carried out with the rainfall influx of 3.21×10^{-8} $m^3/sec/m^2$, 2.89×10^{-8} $m^3/sec/m^2$, 2.61×10^{-8} $m^3/sec/m^2$, 2.65×10^{-8} $m^3/sec/m^2$ and 2.54×10^{-8} $m^3/sec/m^2$ respectively. Fig. 6.12 to Fig. 6.16 shows the distribution of pore water pressure within the respective slopes under normal conditions.

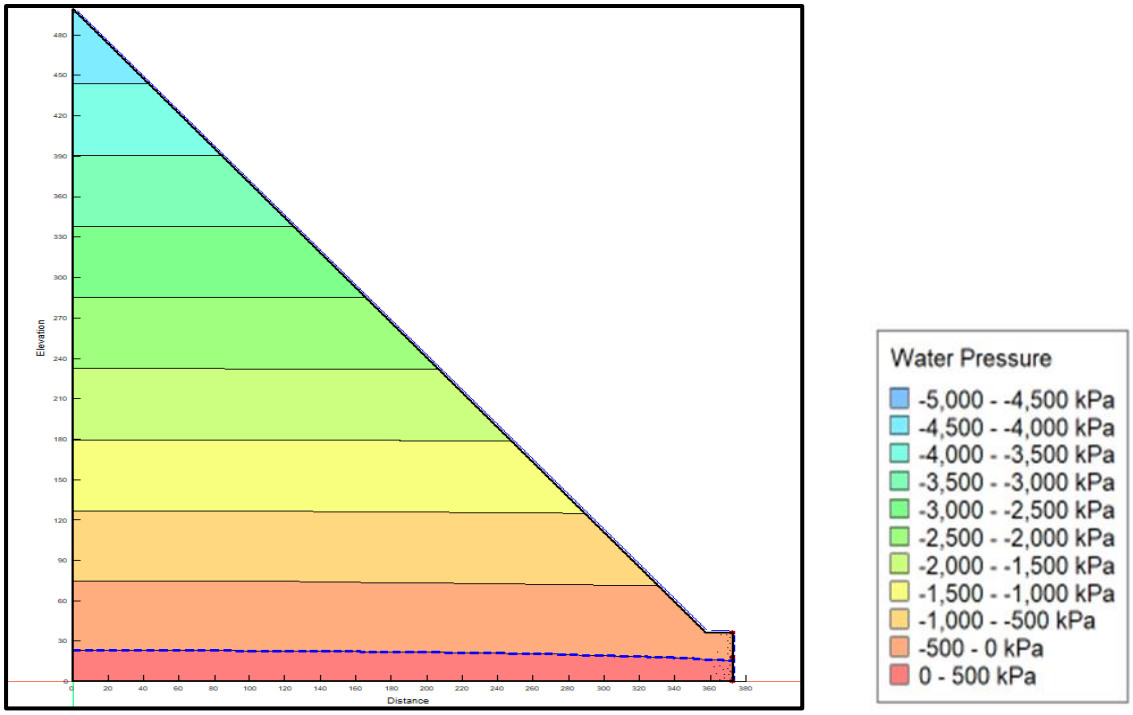

Fig. 6.12: Distribution of pore water pressure within the slope under normal conditions without rainfall for S_1

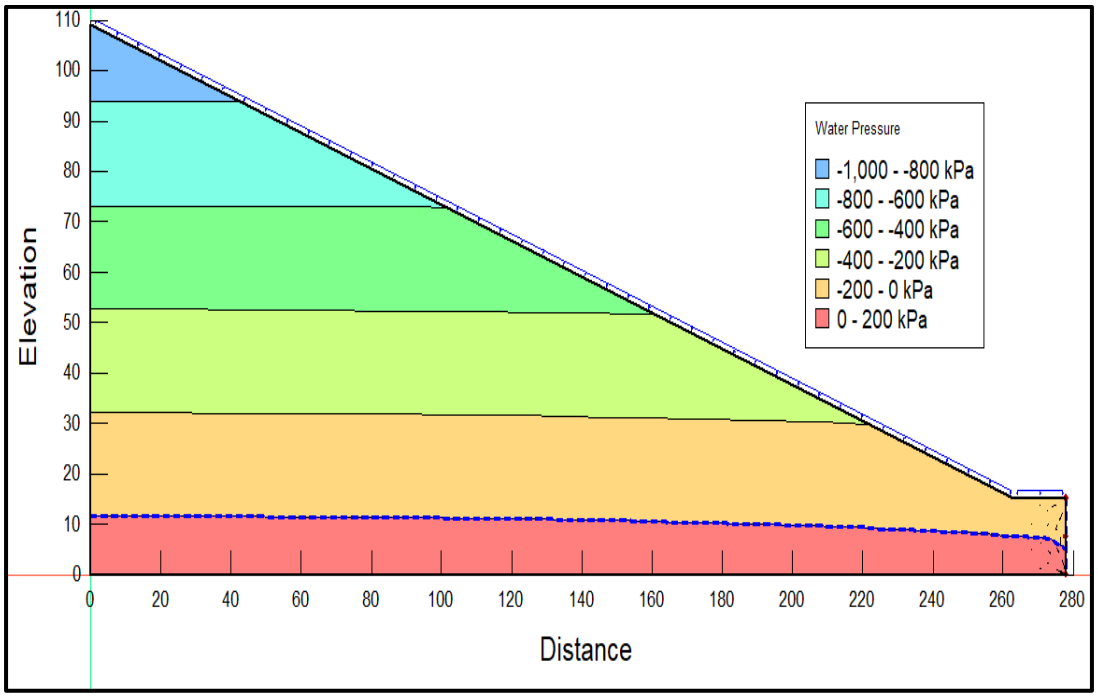

Fig. 6.13: Distribution of pore water pressure within the slope under normal conditions without rainfall for S_2

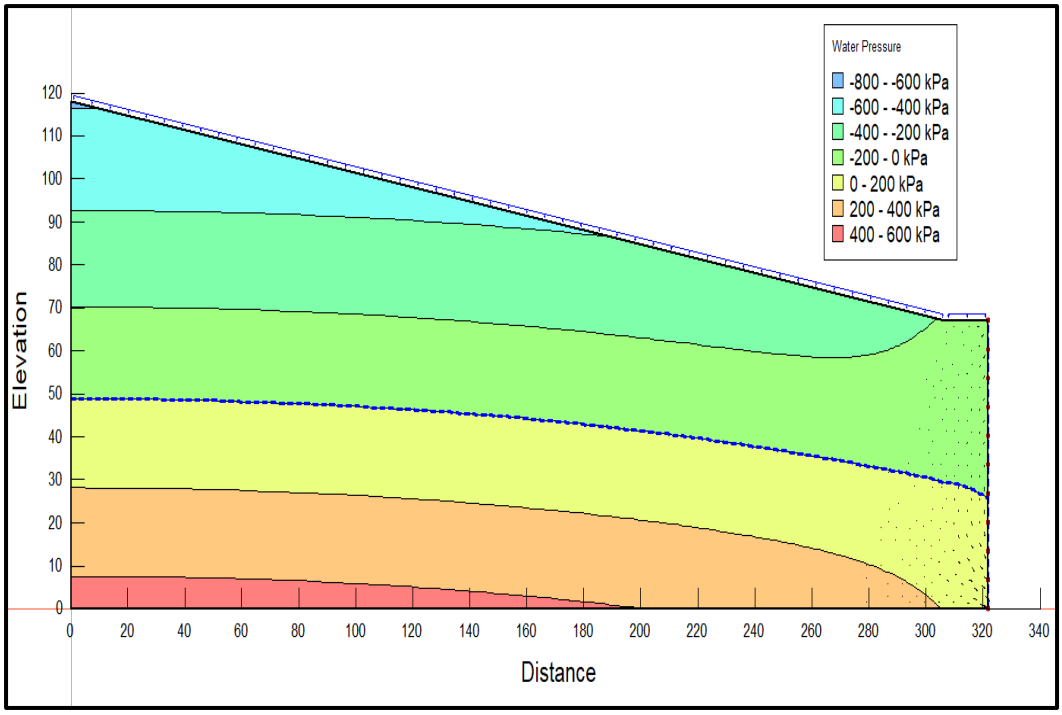

Fig. 6.14: Distribution of pore water pressure within the slope under normal conditions without rainfall for S_3

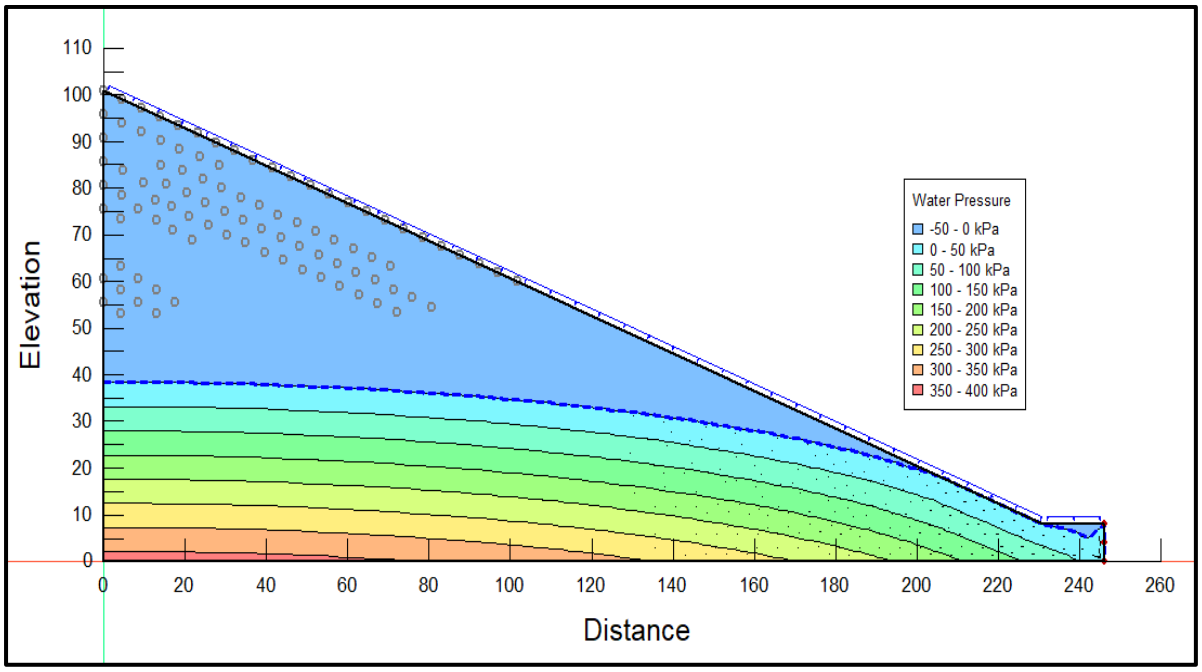

Fig. 6.15: Distribution of pore water pressure within the slope under normal conditions without rainfall for S_4

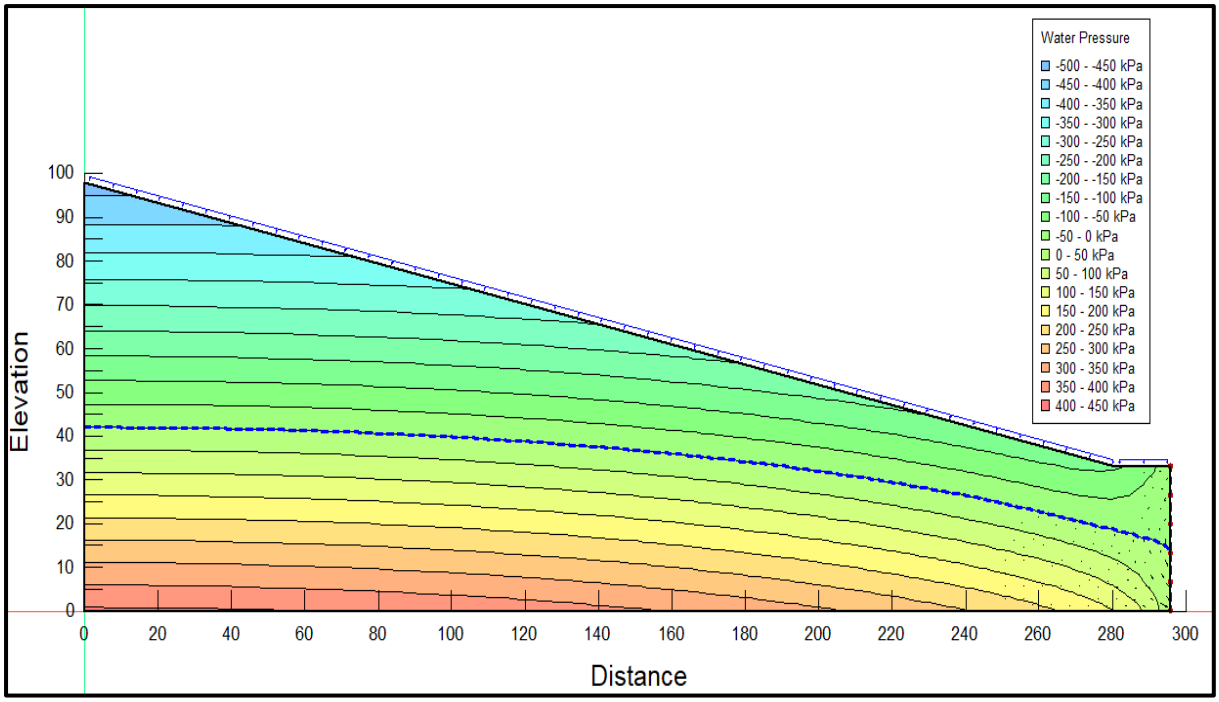

Fig. 6.16: Distribution of pore water pressure within the slope under normal conditions without rainfall for S_5

6.2.2 Factor of safety of slope under normal conditions for all locations

Fig. 6.17 to Fig 6.21 shows the factor of slope for each location along with the critical slip surface using Morgenstern-Price method.

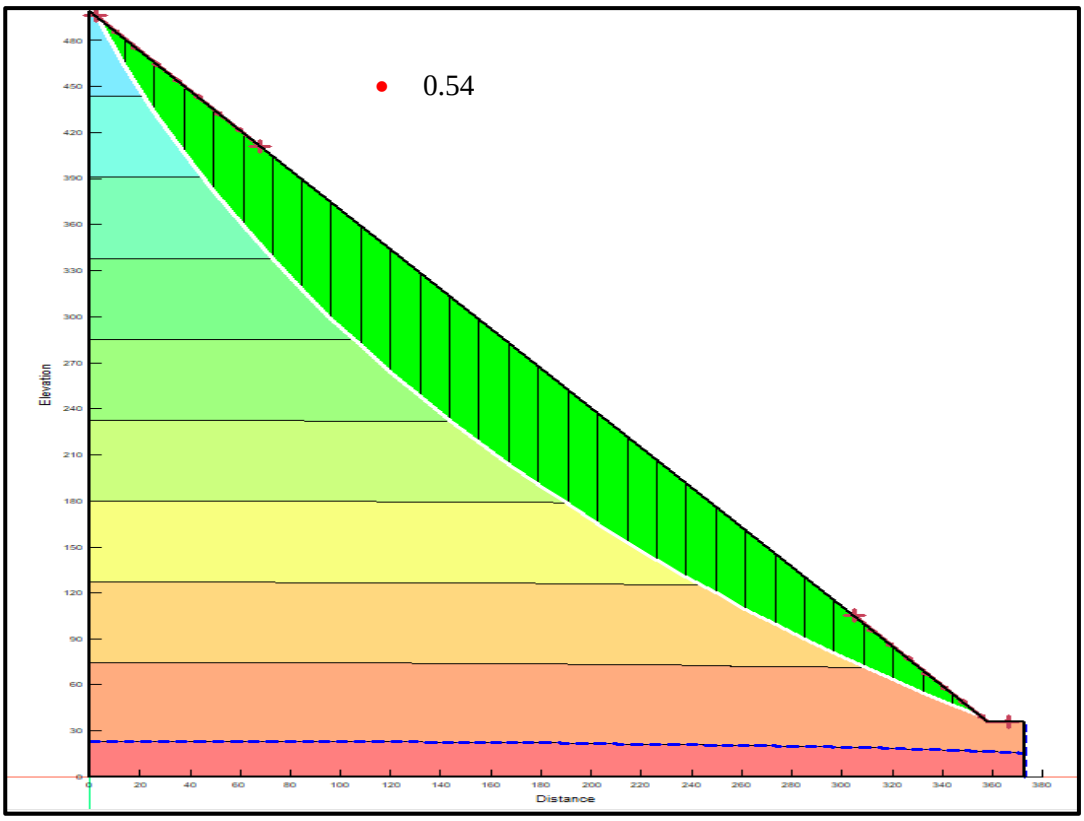

Fig. 6.17: Critical slip surface for S_1 location under normal conditions with corresponding FOS of 0.54

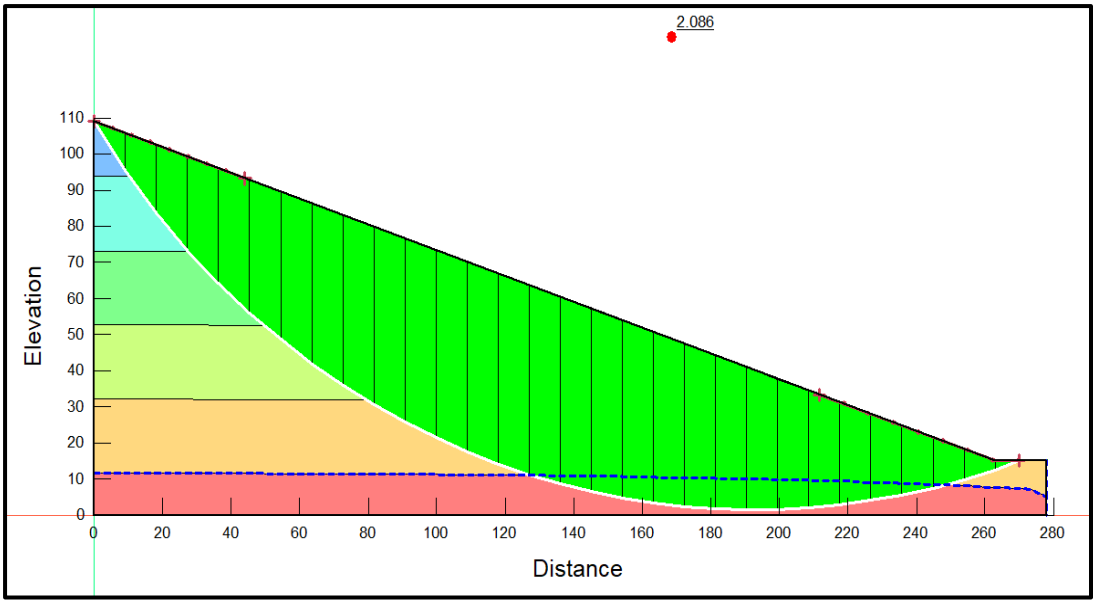

Fig. 6.18: Critical slip surface for S_2 location under normal conditions with corresponding FOS of 2.086

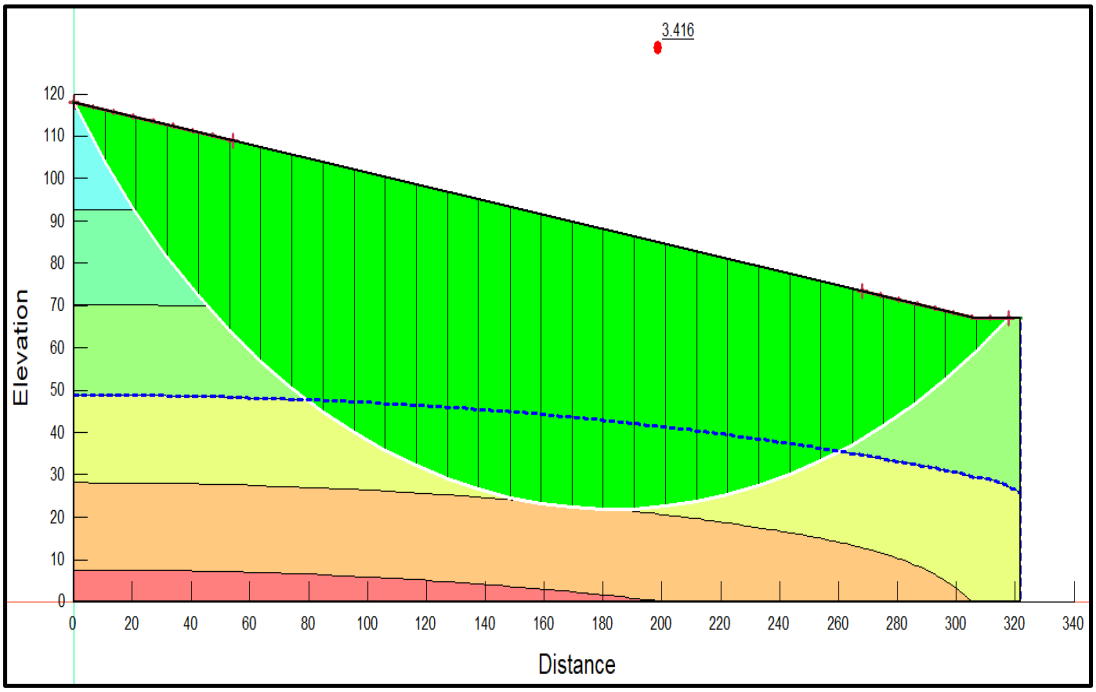

Fig. 6.19: Critical slip surface for S_3 location under normal conditions with corresponding FOS of 3.416

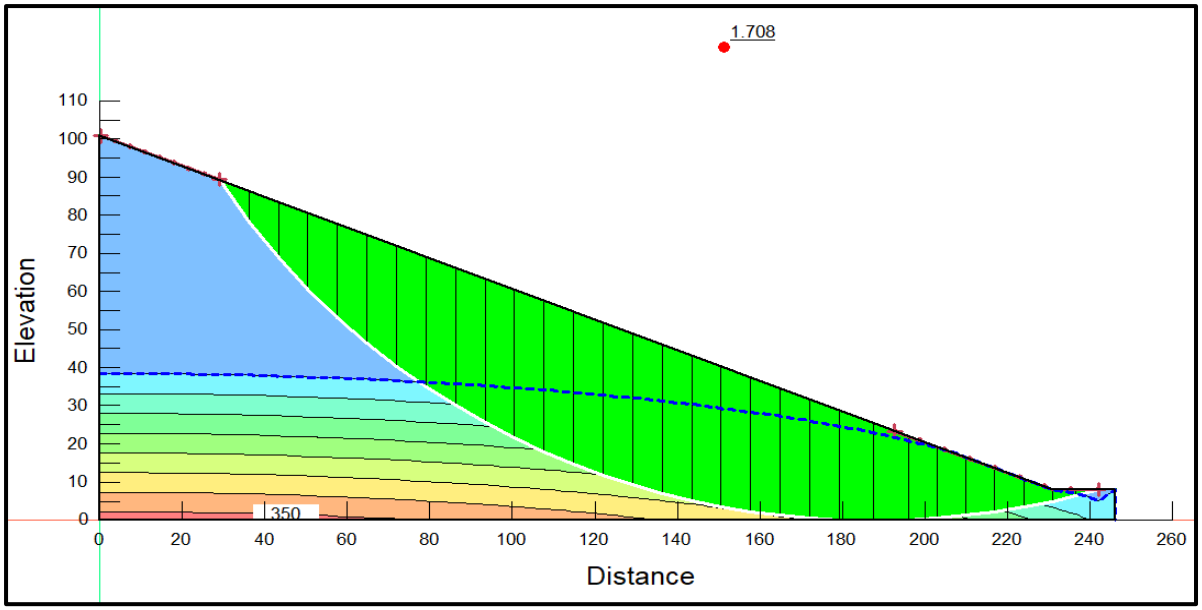

Fig. 6.20: Critical slip surface for S_4 location under normal conditions with corresponding FOS of 1.708

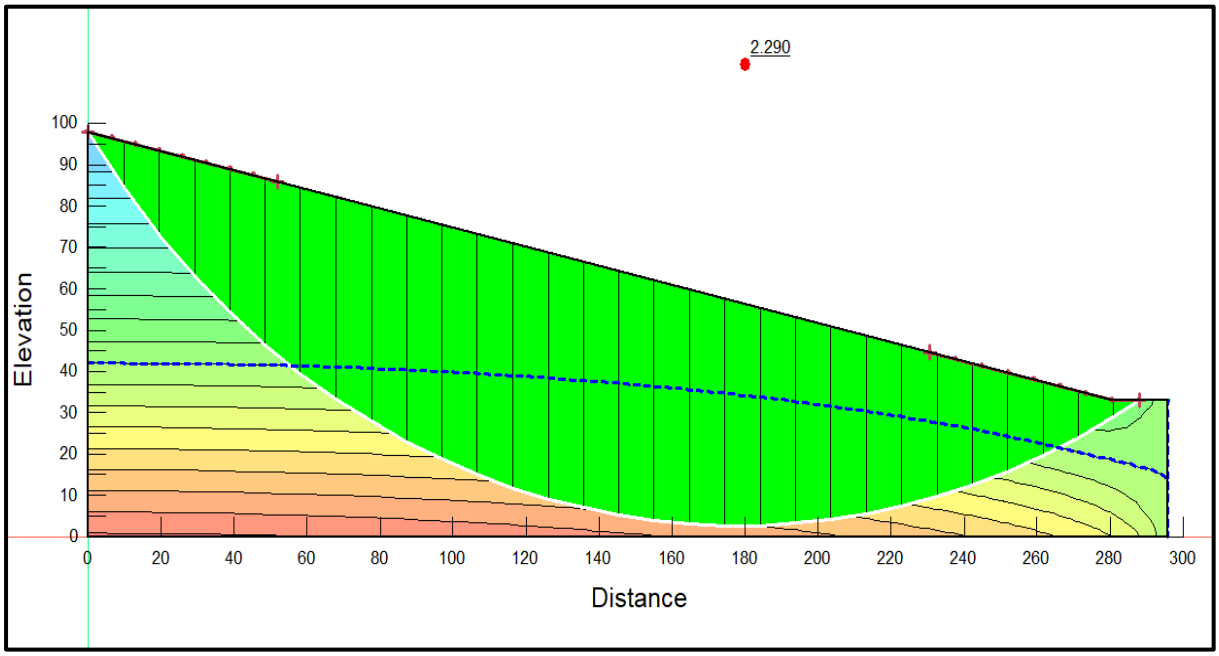

Fig. 6.21: Critical slip surface for S_5 location under normal conditions with corresponding FOS of 2.209

6.2.3 Factor of safety of slope after high intensity rainfall event for all locations

For S_1 location transient analysis is not carried out because the slope is unstable even under normal weather conditions. Fig. 6.22 to Fig. 6.25 shows the factor of safety of each slope after high intensity rainfall event.

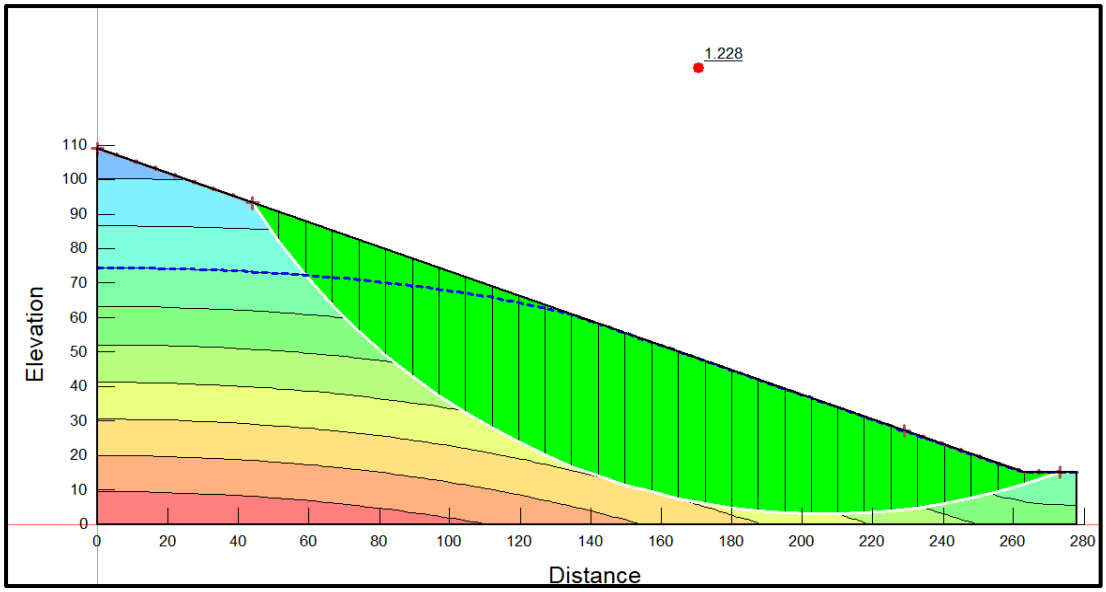

Fig. 6.22: Critical slip surface for S_2 location under rainfall condition and corresponding FOS of 1.228

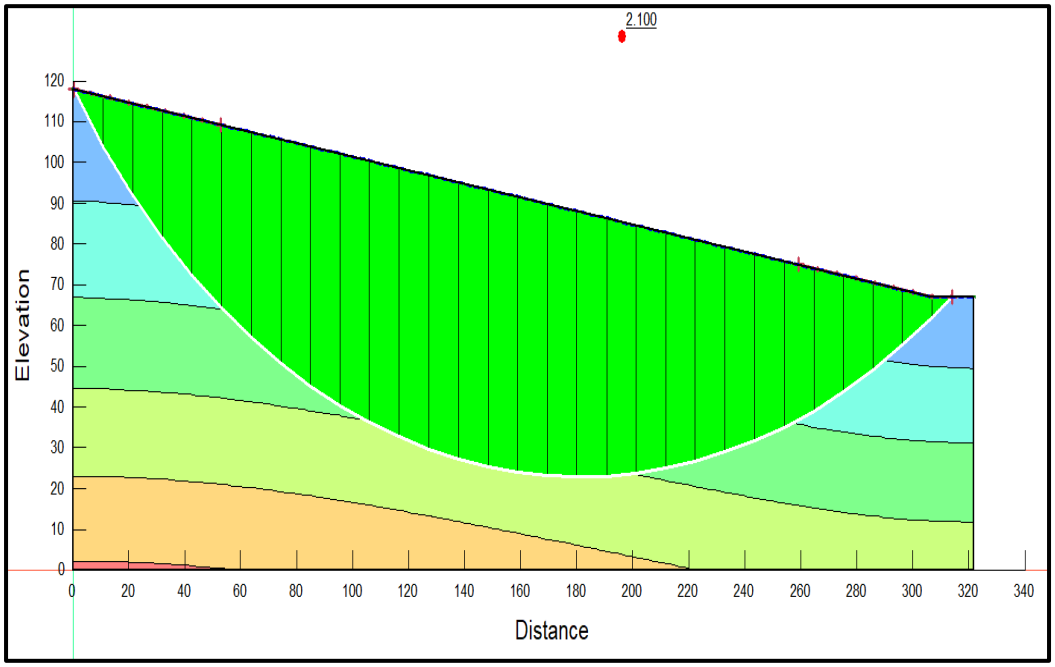

Fig. 6.23: Critical slip surface for S_3 location under rainfall condition and corresponding FOS of 2.1

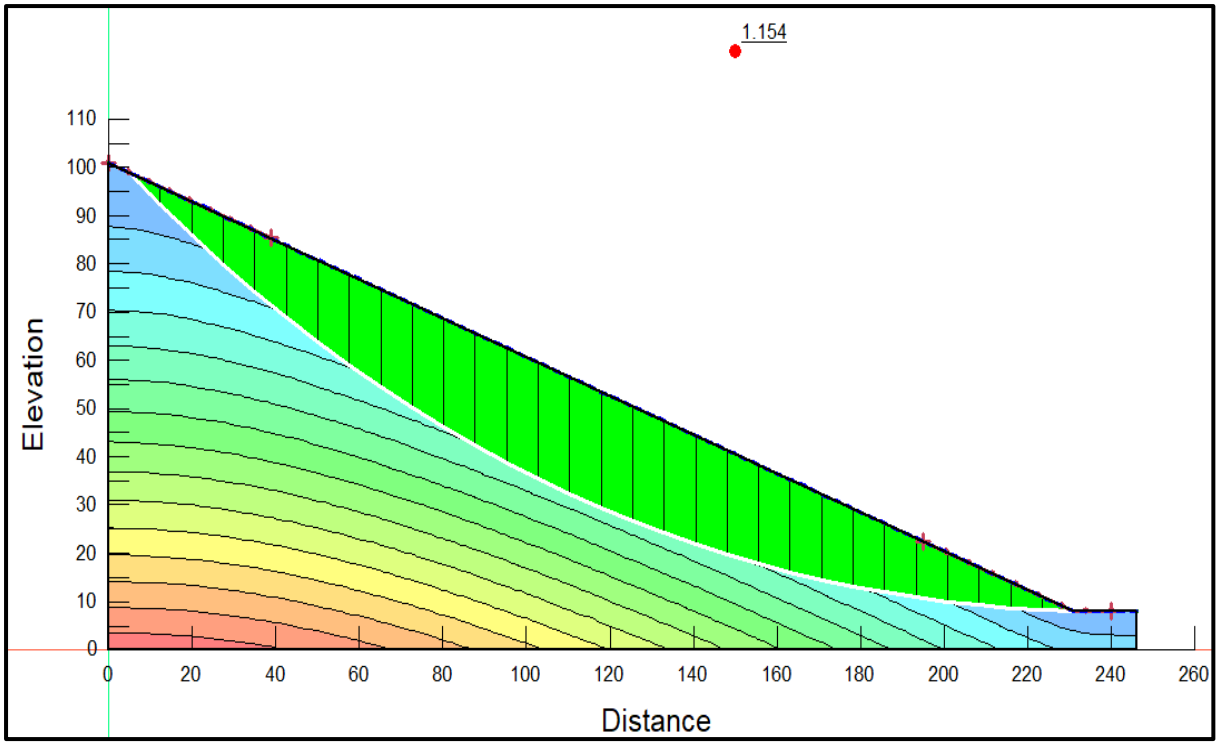

Fig. 6.24: Critical slip surface for S_4 location under rainfall condition and corresponding FOS of 1.154

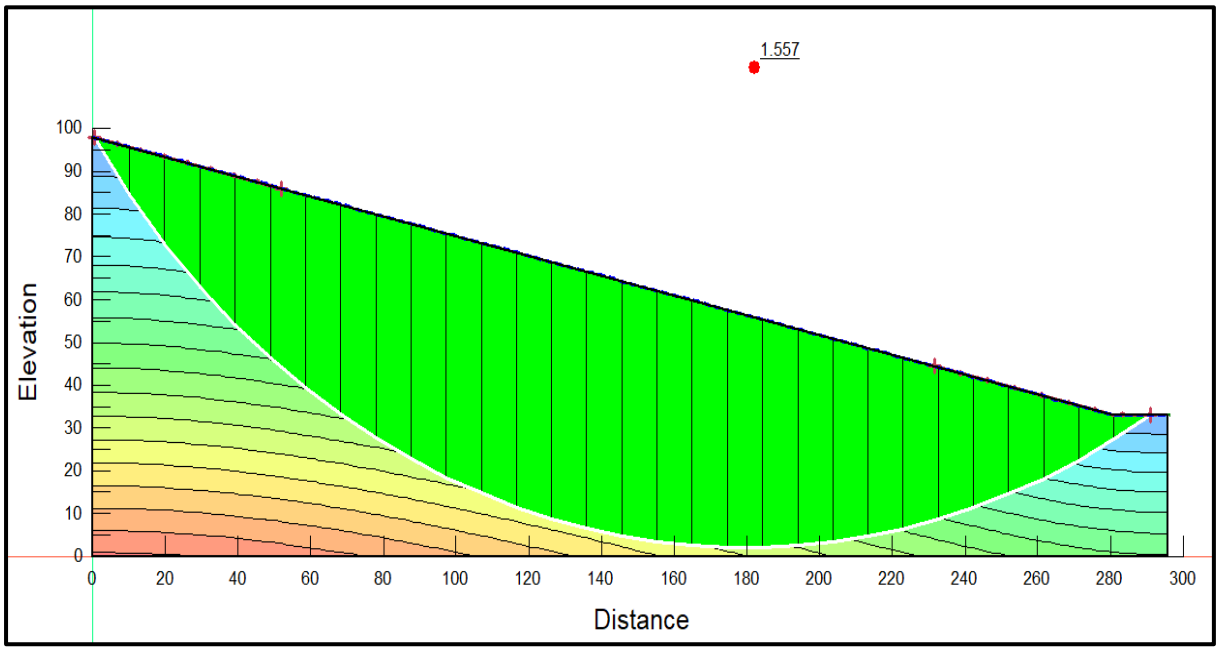

Fig. 6.25: Critical slip surface for S_5 location under rainfall condition with corresponding FOS of 1.557

6.3 Stability analysis of slope S_5 using manual calculations

In order to validate the results of numerical analysis, manual calculations using Fellinius or Swedish Circle method has been performed. In this method, equilibrium of moments is satisfied but the equilibrium of forces is not satisfied. A trial circular slip surface is assumed and the soil above the slip surface is divided into 8 slices. Except for the first and the last slice the width of each slice is fixed to 40 m. The forces acting on each slice are individually analysed. The FOS of slope is calculated for initial state of slope prior to the rainfall event. The geometry of slope (drawn to a horizontal scale of 1 cm = 20 m, and vertical scale of 1cm = 10 m) is shown in figure 6.26 and results are presented in table 6.5. The FOS calculated using Fellinius method is under estimated in comparison to other limit equilibrium methods (Zolkepli et al., 2019). Despite the limitations, this method has been used for validation due to simpler calculations. The FOS computed using this method is 20% less in comparison to the FOS computed using Morgenstern and Price method. Hence validating the findings of researchers who have worked in the same domain.

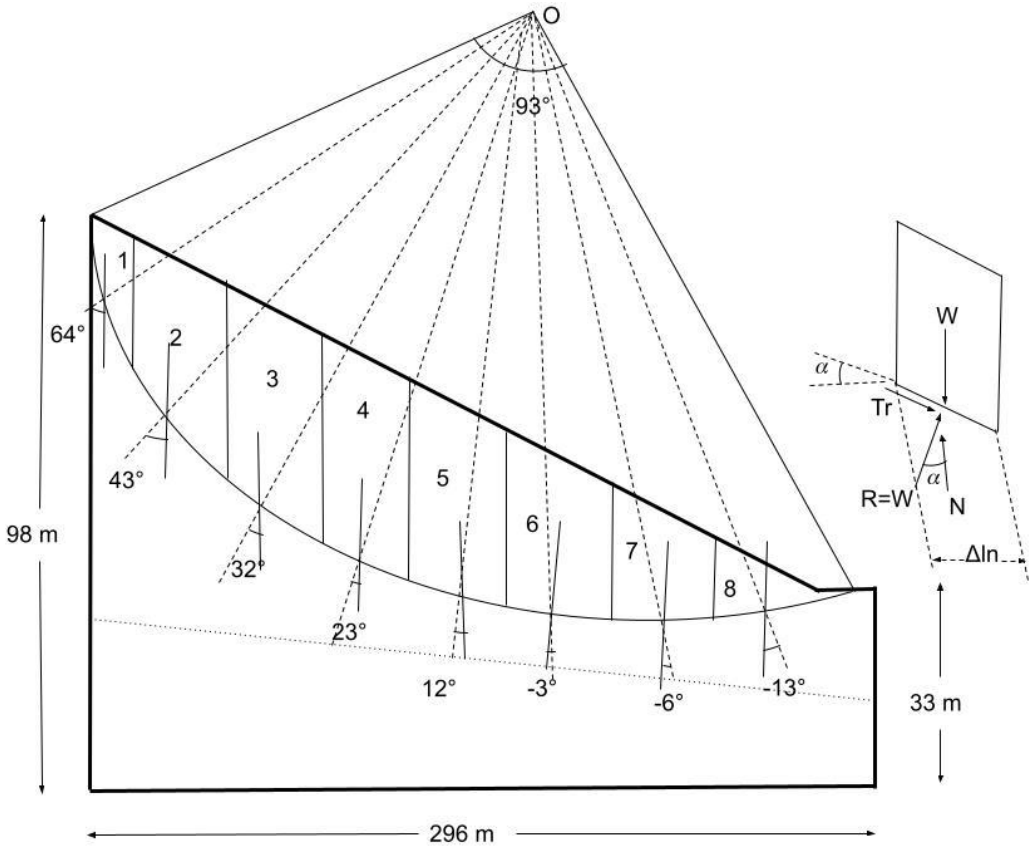

Fig. 6.26: Assumed critical slip surface for S_5 location under normal conditions using Fellinius method

Table 6.5 Calculation table for computation of FOS by Fellinius Method

Slice No.	**Weight (W_n) (kN/m)**	**α_n (degrees)**	**sin α_n**	**cos α_n**	Δl_n	**W_n sin α_n (kN/m)**	**W_n cos α_n (kN/m)**
1	$\frac{1}{2}\times 20\times 16\times 18.75 = 3000$	64	0.898	0.438	45.66	2694	1314
2	$\frac{1}{2}\times(16+29)\times 40\times 18.75$ = 168755	43	0.682	0.731	54.72	11508.75	12335.63
3	$\frac{1}{2}\times(29+34)\times 40\times 18.75$ = 23625	32	0.529	0.848	47.169	12497.63	20034
4	$\frac{1}{2}\times(34+34)\times 40\times 18.75$ = 25500	23	0.391	0.921	43.431	9970.5	23485.5
5	$\frac{1}{2}\times(34+30)\times 40\times 18.75$ = 24000	12	0.208	0.978	40.89	4992	23472
6	$\frac{1}{2}\times(30+23)\times 40\times 18.75$ = 19875	-3	-0.052	0.998	40.056	-1033.5	19847.18
7	$\frac{1}{2}\times(23+11)\times 40\times 18.75$ = 12750	-6	-0.104	0.994	40.221	-1326	12679.87
8	$\frac{1}{2}\times 11\times 18.75$ = 3506.25	-12	-0.225	0.974	41.07	-788.91	3415.09
$\sum_{1}^{8}$ **slice**					353.23	38514.46	116583.27

$$FOS = \frac{(c\times L)+\tan\phi \sum W_n \cos\alpha_n}{\sum W_n \sin\alpha_n} \qquad (9)$$

Where c is the effective cohesion, L is $\sum \Delta l_n$, ϕ is effective angle of internal friction, W_n is weight of individual slice, $\Delta l_n = \frac{\text{width of slice base}}{\cos\alpha_n}$

$$FOS = \frac{(56.27\times 352.23)+\tan 22.83(116583.27)}{38514.465}$$

FOS = 1.80

6.4 Discussion

6.4.1 Ramsoo (S_1)

The soil from Ramsoo has been identified as silty sand with only 1.07% clay fraction. The height and width of slope are 499 m and 373 m respectively. From the analysis of rainfall data, it is observed that amongst the 5 locations chosen for carrying out the study, this location receives the highest rainfall. The results of steady state analysis show that the water table is very low with respect to the height of slope. The pore water pressure is negative for throughout the slope except below the water table where the pore water pressure is positive. The maximum negative pore water pressure within the is -4000 kPa and maximum positive pore water pressure is 500 kPa. After carrying out steady seepage analysis, stability analysis is performed taking pore water pressure from parent steady seepage analysis. The FOS obtained is 0.54, indicating the slope is highly unstable. The reason for the instability is attributed to the geometry of slope having a steep slope angle of 52.29˚ and high slope height. The slope height and angle affect the initial FOS of slope (Rahardjo et al., 2007). The instability caused due to unstable geometry predominates the stabilising effect of high suction pressure within the slope. For this location, transient seepage analysis is not carried out because the slope is unstable even under normal/ no rainfall conditions. Fig. 6.27 shows the variation of pore water pressure with elevation, from the graph it can be seen that the suction pressure increases hydrostatically above the water table to the top of slope.

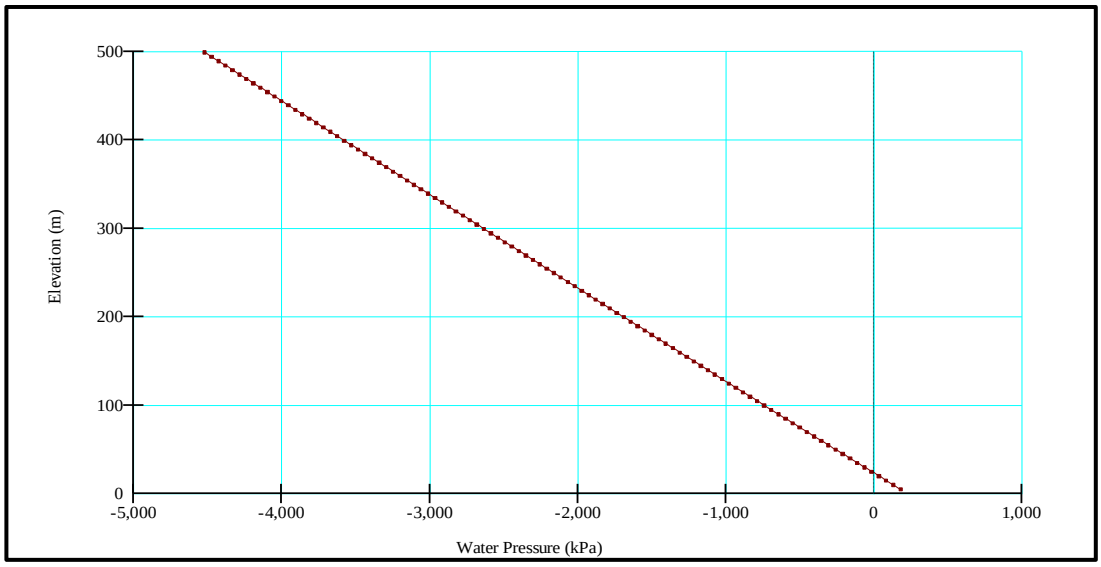

Fig. 6.27: Variation of pore water pressure along the elevation of slope under normal conditions

6.4.2 Sheerbibi (S_2)

The soil from Sheerbibi has been been identified as silty sand with only 2.60% clay fraction. The height and width of slope are 109 m and 278 m respectively. For the development of initial pore water pressure conditions within the slope, steady seepage analysis is performed with rainfall flux of 2.89×10^{-8} $m^3/sec/m^2$. The maximum negative pore water pressure within the slope is -800 kPa and maximum positive pore water pressure is 200 kPa. The stability analysis is performed after steady state seepage

analysis in order to find the FOS of slope under normal/ no rainfall condition. The FOS obtained is 2.086, indicating the slope is stable under normal conditions. The higher safety factor obtained may be attributed to the deep location of water table and higher matric suction within the slope. After the steady state seepage analysis, transient seepage analysis is carried out using initial pore water pressure from parent seepage analysis. The transient analysis is carried out for 1 day using the rainfall intensity corresponding to the maximum daily rainfall obtained from the Fig. 5.4, the results are computed after every 1.2 hr interval. Fig. 6.28 shows graphically the variation of pore water pressure throughout the elevation of the slope with time. From the fig. it can be seen that at the beginning of rainfall, the pore water pressure distribution throughout the slope is negative except for the small portion below the water table but as the duration of high rainfall event increases, the water table rises due to infiltration of rainwater resulting in development of positive pore water pressure. The FOS after 1 day of high intensity rainfall event obtained is 1.228. Heavy rainfall causes the rain water to infiltrate within the slope, causing reduction in matric suction. The reduction in matric suction in turn decreases the shear strength of soil which results in reduced FOS of the slope. From Fig. 6.29 it can be seen that the FOS of slope reduces sharply within first 14 hours of rainfall, this can be attributed to the material property of slope, the slope material is silty sand which has relatively high permeability, also the percentage of clay is less, enabling rain water to easily percolate within the slope. Thus, after 1 day of heavy rainfall, the slope is marginally stable.

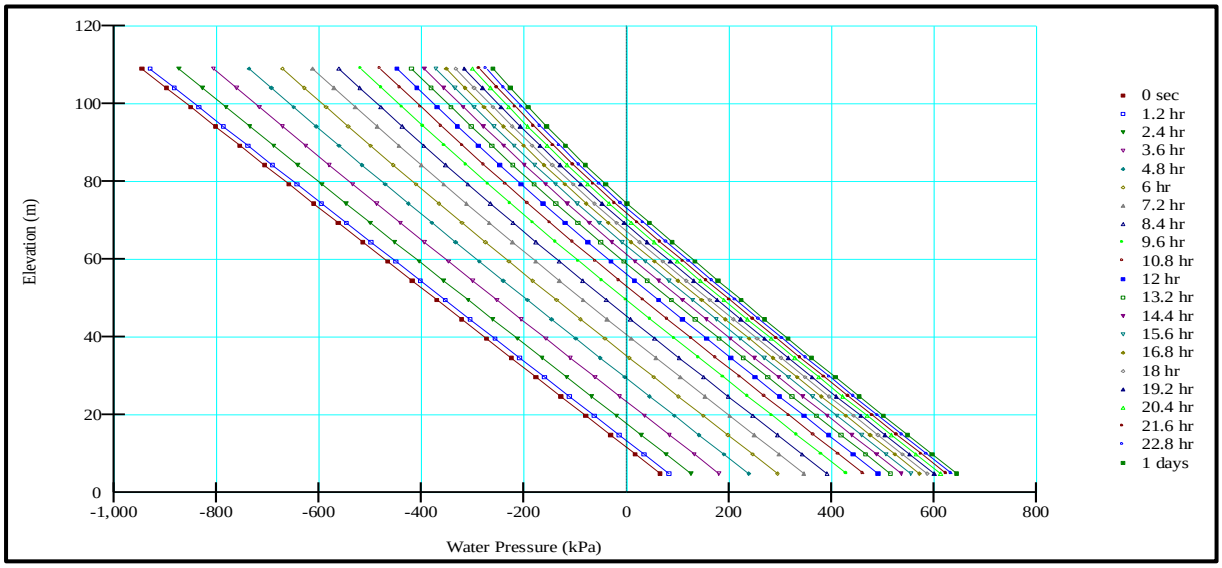

Fig. 6.28: Variation of pore water pressure along the elevation of slope with time during high intensity. rainfall event

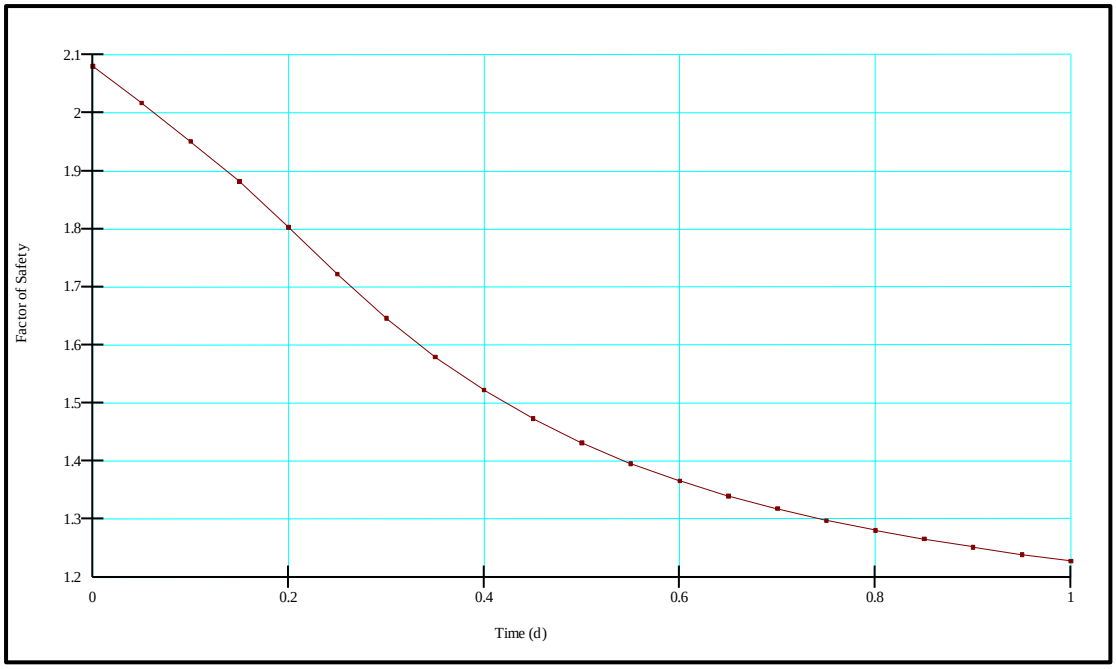

Fig. 6.29: Variation of FOS of slope with time during high intensity rainfall event

6.4.3 Shabinbas (S_3)

The soil from Shabinbas has been identified as low compressible silt. The height and width of slope are 322 m and 118 m respectively. An input of rainfall flux of 2.61×10^{-8} $m^3/sec/m^2$ is made for the development of initial pore water pressure conditions within the slope. The maximum suction/ negative pore water pressure of -600 kPa and maximum positive pore water pressure is 400 kPa after steady state analysis within the slope. The FOS obtained after steady seepage analysis is 3.416 indicating the slope is stable under normal or no rainfall condition. The stability of slope is attributed to the geometry of slope and material properties of slope. The slope angle is gentle and slope material comprises of 12.47% clay fraction providing higher cohesive strength to the slope, thereby increasing stability. Additionally, the apparent cohesiveness given by matric suction within the soil increases the soil's stability. Fig. 6.30 depicts the distribution of pore water pressure within the slope as determined by a transient seepage examination. At the beginning of a rainfall event, there is matric suction above the water table and positive pore water pressure below it. As the duration of the rainfall grows, these conditions alter. The slope becomes saturated within the first twelve hours of a rainfall event. This is a result of the saturated permeability of the soil. When the rainwater flux exceeds the saturated permeability of the soil, positive pore water pressure develops until the slope becomes saturated (Dey and Sengupta, 2018). The fluctuation in FOS with time is depicted in Figure 6.31; after 12 hours, there is no further decrease in FOS, due to saturation of slope and possible runoff. After transient analysis, the FOS of slope decreases to 2.1, showing that the slope is stable following the heavy precipitation event.

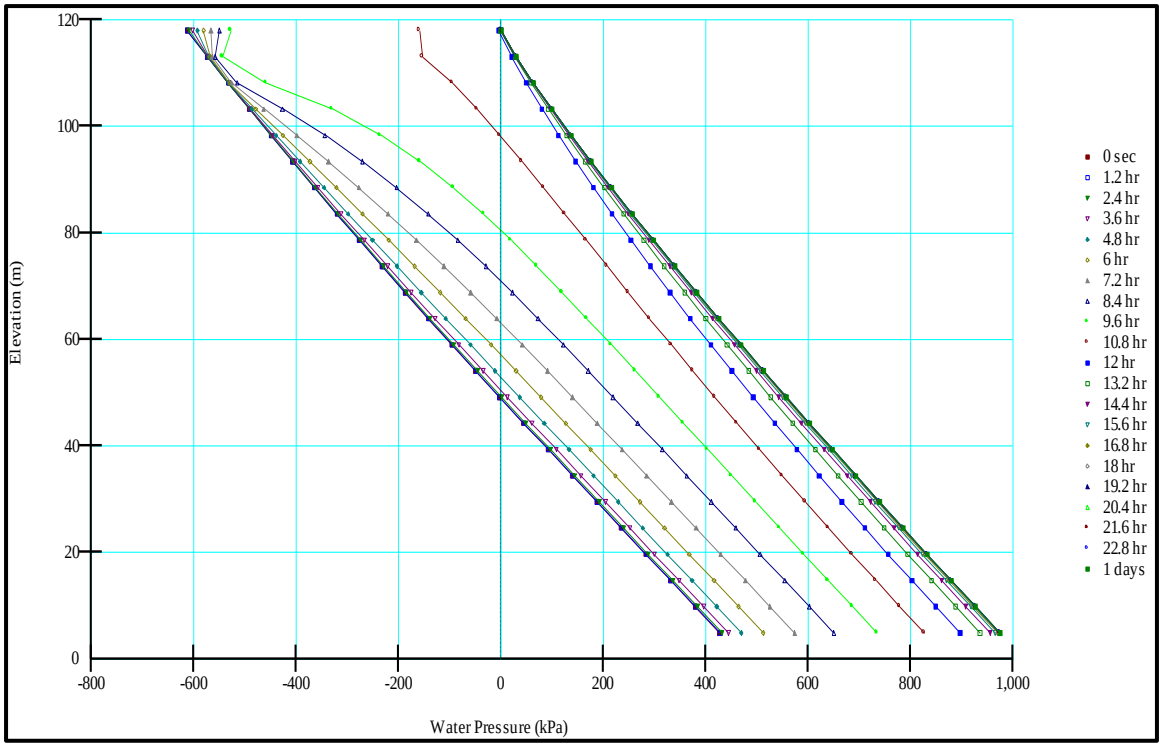

Fig. 6.30: Variation of pore water pressure along the depth of slope with time during high intensity rainfall event

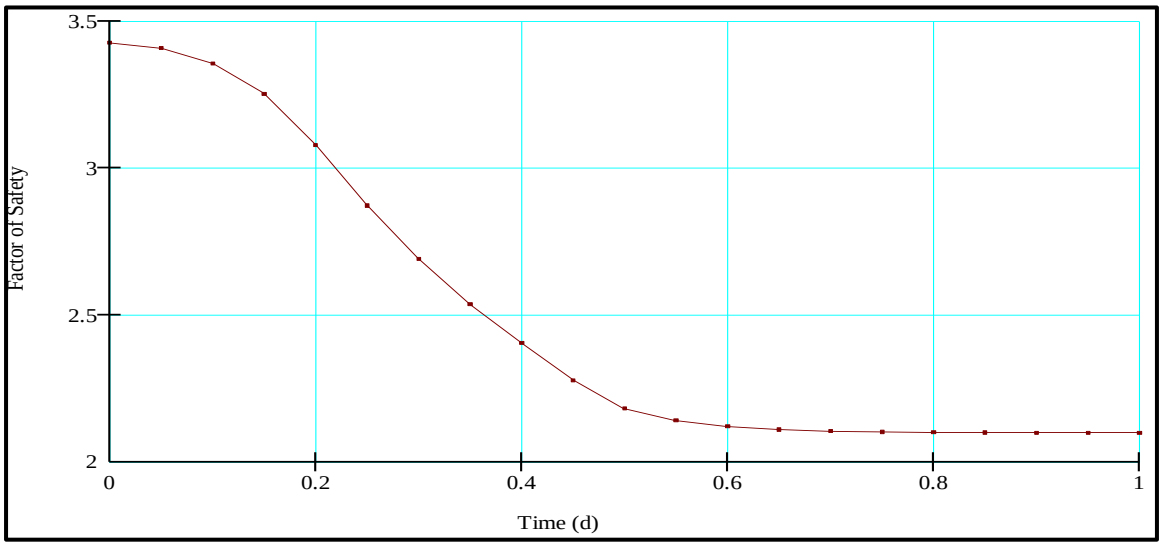

Fig. 6.31: Variation of FOS of slope with time during high intensity rainfall event

6.4.4 Darshipora (S_4)

The soil from Darshipora has been identified as low compressible silt with clay fraction of 5.45%. The height and width of slope are 101 m and 246 m respectively. The rainfall flux for the development of initial pore water condition within the slope is 2.65×10^{-8} $m^3/sec/m^2$. The maximum suction pressure within the slope is -50 kPa and maximum positive pore water pressure within the slope is 400 kPa. The matric suction for this location is lowest and does not increase hydrostatically to the top of slope. This can be attributed to the composition of soil which consists of material of higher permeability i.e., sand

and silt. The stability analysis carried out for the slope after steady seepage analysis gave out a safety factor of 1.708. The transient seepage analysis is carried taking pore water pressure from parent seepage analysis for 1 day. The pore water pressure variation throughout the elevation of slope at different time periods is shown in Fig. 6.32. From the fig, it can be seen that after steady seepage analysis, both negative and positive pore water pressure exist above and below the water table but with the increase in the duration of rainfall, the slope gets saturated due to the rainfall infiltration and there is an overall decrease in the shear strength of soil. The FOS after high rainfall event of 1 day is 1.154, indicating the slope is marginally stable after 1 day of heavy rainfall. The variation of FOS with time is shown in Fig. 6.33, the factor of safety reduces sharply within first 12 hours of rainfall resulting in the saturation of slope and after that any additional rainfall may be manifested in the form of surface runoff.

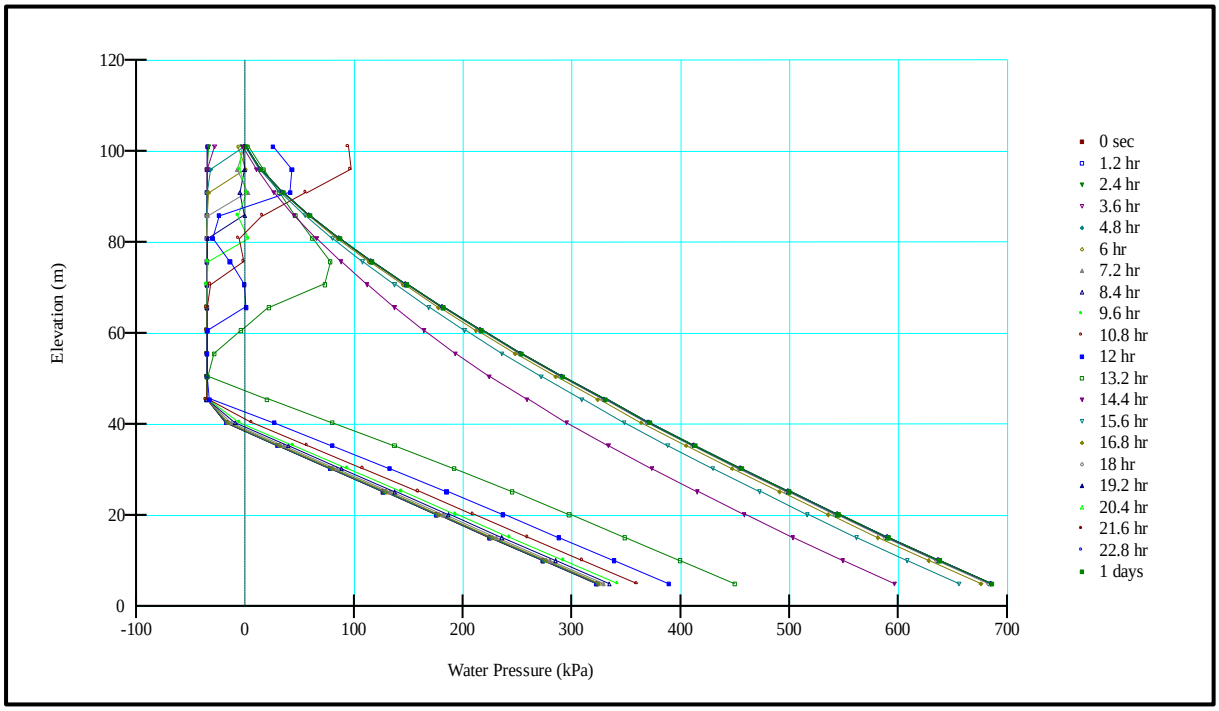

Fig. 6.32: Variation of pore water pressure along the depth of slope with time during high intensity rainfall event

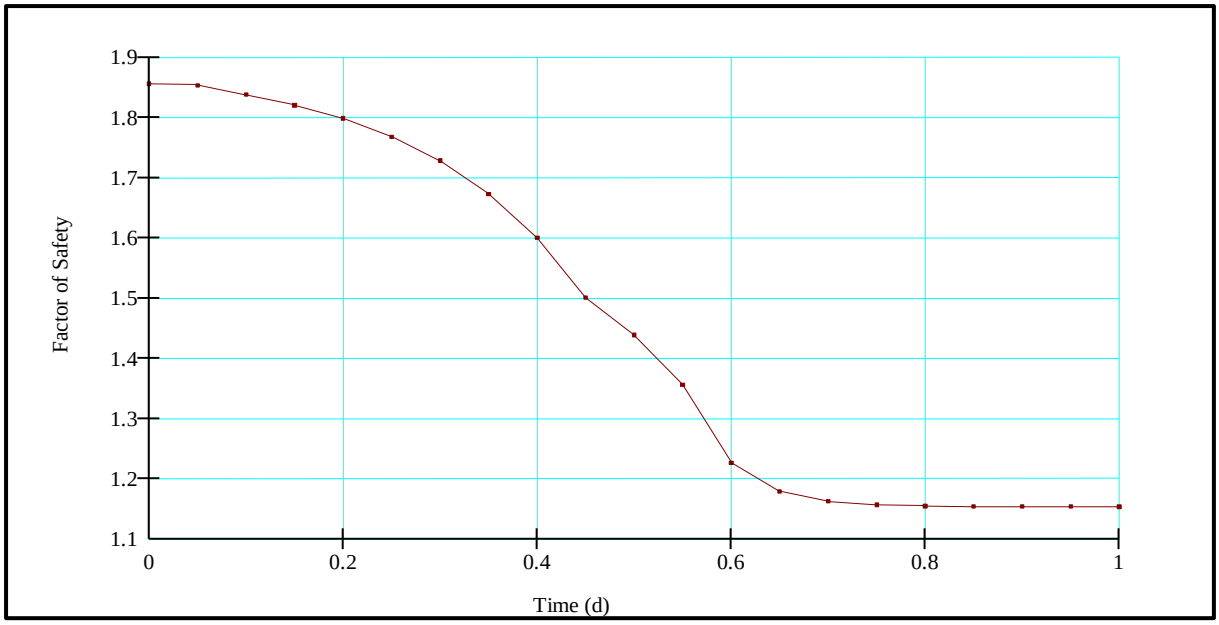

Fig. 6.33: Variation of FOS of slope with time during high intensity rainfall event

6.4.5 Chareel (S_5)

The soil from this location has been identified as low compressible silt with clay (CL-ML). The height and width of slope are 98 m and 298 m respectively. For the development of initial condition of pore water pressure, an input of rainfall influx of 2.54×10^{-8} $m^3/sec/m^2$ was made in steady seepage analysis. Maximum negative and positive pore water pressure within the soil after steady seepage analysis are -450 kPa and 450 kPa. The safety factor after steady seepage analysis is 2.290. The high FOS may be attributed to the high cohesive strength due to high clay fraction 13.15%. The pore water pressure variation within the slope at different duration during rainfall event is shown in Fig. 6.34. At the beginning of rainfall both negative and positive pore water exists within the slope but with the increase in the duration of rainfall, the slope gets saturated and pore water pressure becomes positive throughout the slope reducing the shear strength of soil. After transient analysis, stability analysis is carried out and FOS obtained is 1.557. Fig. 6.35, shows the variation of FOS over the entire duration of rainfall event, the FOS reduces steeply first 10 hours due to dissipation of matric suction and subsequent saturation of slope.

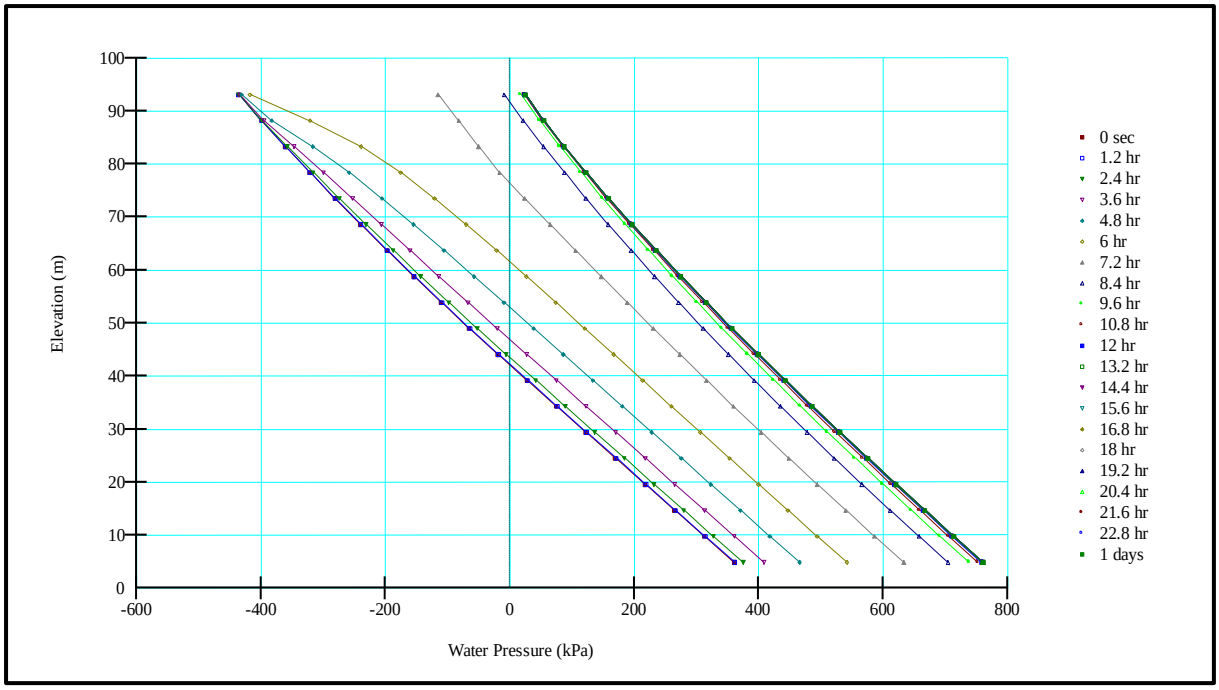

Fig. 6.34: Variation of pore water pressure along the depth of slope with time during high intensity rainfall event

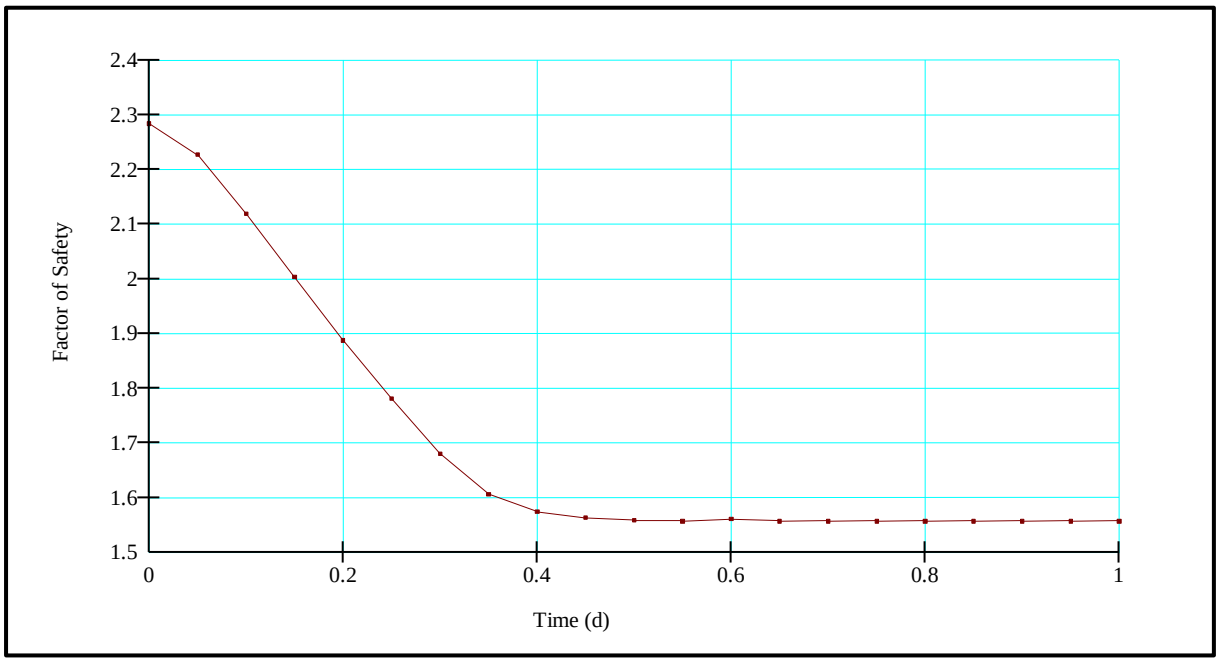

Fig. 6.35: Variation of FOS of slope with time during high intensity rainfall event

Chapter 7
Conclusion and Future Scope

7.1 Conclusions

For this study, the stability of slopes under normal weather conditions and the impact of high rainfall event on the stability of slope was examined by numerical analysis. The study was carried out in a phased manner. In first phase, geotechnical characterisation of soil samples collected from the selected location was carried out. In second phase, rainfall data was extracted and analysed from 2011-2021, to get annual average daily rainfall and maximum daily rainfall data. In the final phase, numerical simulation was carried out in GeoStudio 2018 R2 software, to analyse the stability of slope under normal conditions and high rainfall event. Following conclusion were drawn from the study undertaken:

- Locations S3, S4, and S5 have a high proportion of silt fraction (> 60 percent), whereas locations S1 and S2 have both a high percentage of sand and silt. The plasticity of soil sample was evaluated to be between low and medium. Significant cohesion values are attributable to the presence of medium-plastic silt. It was also observed that the cohesiveness of soil samples with a high proportion of silt was significantly altered by inundation. The impact of inundation was minimal on the S1 soil sample, which contained the lowest percentage of clay, 1.07 percent.
- The analysis of rainfall data showed that 2015 was the year with maximum annual rainfall with almost 40% excess rainfall in comparison to the normal average annual rainfall. The analysis further revealed the that most of the high intensity rainfall events were of short duration i.e, lasting for 1 day. Various researchers have concluded from their studies that with the increase in global warming, the probability of high intensity short duration rainfall will increase. Thus, it becomes necessary to analyse the stability of slopes under such high intensity short duration rainfall events.
- The pore water distribution inside slopes indicated positive pore water pressures below the ground water table and negative pore water pressure above it, as determined by the SEEP/W module's steady state seepage analysis. This suggests that under normal conditions, when there is no precipitation, slopes are unsaturated. By creating apparent cohesiveness between soil particles, the existence of negative/matric suction promotes further stability in slopes. After performing transient analysis for a substantial rainfall event, negative pore water pressure dissipation due to the saturation of slope and subsequent rise of the ground water table was observed in all slopes under consideration.
- The stability analysis performed by the SLOPE/W module indicated that, under normal or no rainfall conditions, all slopes are stable (FOS > 1) with the exception of S1, which has a FOS of 0.542. The instability of S1 was ascribed to the slope's steepness and height. Under the effect of heavy precipitation, the FOS of S2 decreased from 2.086 to 1.228, the FOS of S3 decreased from

3.416 to 2.1, the FOS of S4 decreased from 1.708 to 1.154, and the FOS of S5 decreased from 2.290 to 1.550. The decrease in FOS indicates that short duration, intense rainfall has a significant impact on all slopes. FOS greater than 1 does not guarantee slope stability during heavy precipitation events. Presence of any surface discontinuity may result in localised high water pressure zones leading to localised shallow slope failures.

- Of the five selected places, only two slopes are stable, two are slightly stable, and one is extremely unstable. This implies that slope stabilisation is required along the selected stretch due to the high likelihood of landslide incidents. All of this is only achievable after identifying landslide hotspots along NH-44. After identifying the slope, sensors can be placed at various positions along the slope to generate alerts in the event of a landslide. Various slope stabilisation measures, such as the construction of retaining walls, soil nailing, usage of geo fabrics and geogrids, etc., can be employed to mitigate the hazard of landslides.

7.2 Scope for future work

The various aspects that can be researched as an extension of this work are discussed below:

- The present study has been carried out considering the effect of precipitation only. Further analysis can be carried out considering the effect of seismic effects and traffic loads also.
- In the present study the FOS of slope has been computed using limit equilibrium method. Numerical analysis for computation of deformation and FOS using finite element method can be carried out as an extension to the present study.
- This study has been carried out in 2D plain strain condition. Further extension can be carried out by carrying out 3D analysis of present work.
- In the present study, homogeneous slope has been considered. Further extension can be carried out with consideration of stratification in slopes.
- The effect of various stabilisation techniques on the stability of slopes can be studied in future.

References

1. Kanungo, D.P., Pain, A., and Sharma, S. (2013). Stability Assessment of a Potential Debris Slide in Garhwal Himalayas, India. *Indian Landslides*, 6(2):9-20
2. Abramson, L.W., Lee, T.S., Sharma, S., and Boyce, G.M. (2002). *Slope stability and stabilization methods*, 2nd Edition, Wiley, New York
3. Griffths, D.V. and Lane, P.A. (1999). Slope stability analysis by finite elements. *Géotechnique* ,49(3): 387-403
4. Patel, S.K., Nanda, A., Singh, G., and Patel, S. (2020). A review of disasters in Jammu and Kashmir, and Ladakh region in India. *International Journal of Population Studies,* 6(1):69-81.
5. Singh, Y, Haq, A.U., Bhat, G.M., Pandita, S.K., Singh, A., Sangra, R., Hussain, G., and Kotwal, S.S., (2018). Rainfall-induced landslide in the active frontal fold–thrust belt of Northwestern Himalaya, Jammu: dynamics inferred by geological evidences and Ground Penetrating Radar. *Environmental Earth Sciences.* 77(16):592-609
6. Pandey, V.K., (2018). Geological and geotechnical challenges in road widening, national highway-44: Jammu- Udhampur- Banihal- Qazigund, J&K, India. *International Research Journal of earth Sciences,* 6(12): 22-28
7. Duncan, J.M.(1996). State of the art: limit equilibrium and finite-element analysis of slopes. *Journal of Geotechnical Engineering*, 122(7) : 577-596
8. Dawson, E. M., Roth, W. H. and Drescher, A. (1999). Slope stability analysis by strength reduction. *Géotechnique* , **49**(6): 835-840
9. Hammah, R.E., Curran, J.H., Yacoub, T.E., and Corkum, B., (2004). Stability analysis of rock slopes using the finite element method. *In Proceedings of the ISRM Regional Symposium EUROCK 2004 and the 53rd Geomechanics Colloquy*, Salzburg, Austria
10. Hammah, R.E., Yacoub, T.E., Corkum, B., and Curran, J.H.,(2005). A comparison of finite element slope stability analysis with conventional limit-equilibrium investigation. *Proceedings of the 58th Canadian Geotechnical and 6th Joint IAH-CNC and CGS Groundwater Specialty*: Saskatoon, Saskatchewan, Canada
11. Huat, B.B.K., Ali, F.H., and Raju, R.K.S., (2006). Stabilty analysis and stability chart for unsaturated residual soil slopes. *American Journal of Environmental Sciences*, 2(4):154-160
12. Rahardjo, H., Ong, T. H., Rezaur, R. B., and Leong, E.C., (2007). Factors controlling instability of homogeneous soil slopes under rainfall. *Journal of Geotechnical and Geoenvironmental Engineering, ASCE*, 133 (12):1532-1543
13. Hammouri, N.A., Malkawi, A.I.H., and Yamin, M.M.A.,(2008). Stability analysis of slopes using the finite element method and limiting equilibrium approach. *Bulletin of Engineering Geology and the Environment*, 67(4):471-478

14. Kanungo,D.P., Pain,A., and Sharma, S.(2013). Finite element modeling approach to assess the stability of debris and rock slopes: a case study from the Indian Himalayas. *Journal of the International Society for the Prevention and Mitigation of Natural Hazards* ,69(1):1-24
15. Chandrasekaran,S.S., Owaise,R.S., Ashwin,S., Jain,R.M., Prasanth,S., and Venugopalan, R.B.,(2013). Investigation on infrastructural damages by rainfall-induced landslides during November 2009 in Nilgiris, India. *Natural Hazards*, 65: 1535–1557
16. Fawaz, A., Farah, E., and, Hagechehade, F., (2014). Slope Stability Analysis Using Numerical Modelling. *American Journal of Civil Engineering*, 2(3): 60-67
17. Raj, M., and Sengupta, A., (2014). Rain-triggered slope failure of the railway embankment at Malda, India. *Acta Geotechnica*, 9:789–798
18. Tang, D., LI, D. Q., and Cao, Z.J., (2016). Slope stability analysis in the Three Gorges Reservoir Area considering effect of antecedent rainfall. *Georisk Assessment and Management of Risk for Engineered Systems and Geohazards*, 11(2):1-12
19. Kristo, C., Rahardjo, M., and Satyanaga, A., (2017). Effect of variations in rainfall intensity on slope stability in Singapore. *International Soil and Water Conservation Research*, 5: 258–264
20. Singh,A.K., Kundu,J., and Sarkar,K., (2018). Stability analysis of a recurring soil slope failure along NH-5, Himachal Himalaya, India. *Natural Hazards*, 90(2):863–885
21. Dey, N., and Sengupta, A., (2018). Effect of rainfall on the triggering of the devastating slope failure at Malin, India. *Natural Hazards*, 94:1391-1413
22. Hussain,G., Singh,Y., Bhat,G.M., Sharma,S., Sangra,R. and Singh,A.(2019). Geotechnical Characterisation and Finite Element Analysis of Two Landslides along the National Highway 1-A (Ladakh Region, Jammu and Kashmir). *Journal Geological Society of India*, 94:93-99
23. Sarma, C.P., Dey, A., and Krishna, A.M., (2020). Investigation of rainfall-induced landslides at the hillslopes of Guwahati region, Assam. *Geotechnics for Natural Disaster Mitigation and Management*,(7): 75-87
24. Mohsin, F., and Khader. S.A., (2020). Identifying the parameters responsible for Landslides on NH-44 Jammu Srinagar National Highway for Early Warning System. *Disaster Advances*, 13 (2): 32-42
25. Bashir, S., and Ramkumar, T.,(2021). A multi-temporal landslide inventory and hazard zonation using relative effect method along the Mughal Road Shopian, India. *Disaster Advances*, 14 (7): 42-51
26. Dhanai, P., Singh, V.P., Soni, P., (2022). Rainfall triggered slope instability analysis with changing climate. *Indian Geotech J*, 52(2):477–492
27. Duncan, J.M., Wright, S. G., and Brandon, T.L., (2014). *Soil Strength and Slope Stability*. Second Edition, Wiley, New Jersey
28. IS - 2720 Part 4 (1985) (Reaffirmed 2006): Indian Standard Method of test for soils, Grain size analysis, Bureau of Indian Standards, New Delhi.

29. IS - 2720 Part 5 (1985) (Reaffirmed 1995): Indian Standard Method of test for soils, Determination of Liquid and Plastic Limit, Bureau of Indian Standards, New Delhi.
30. Ranjan, R. and Rao, A.S.R.,(1991). *Basic And Applied Soil Mechanics*, Third Edition, New Age International, New Delhi
31. IS 2720-29 (1975) (Reaffirmed 2006): Methods of Test for Soils, Determination of Dry Density of Soils In-place by the Core-cutter Method, Bureau of Indian Standards, New Delhi.
32. IS 2720-2 (1973) (Reaffirmed 2010): Methods of test for soils, Determination of water content, Bureau of Indian Standards, New Delhi.
33. IS – 2720 Part 15 (1965) (Reaffirmed 2002): Methods of Test for Soils: Determination of Consolidation Properties, Bureau of Indian Standards, New Delhi.
34. Crozier, M.J. (1986) *Landslides: Causes, Consequences & Environment*. Taylor & Francis, London.
35. IS 2720-3-1 (1980) (Reaffirmed 2002): Methods of test for soils: Determination of specific gravity, Section 1: Fine grained soils, Bureau of Indian Standards, New Delhi.
36. IS - 2720 Part 13 (1986) (Reaffirmed 2002): Indian Standard Method of test for soils: Determination of Direct Shear Test, Bureau of Indian Standards, New Delhi.
37. Mokwa, R. L. (1999). *Investigation of the Resistance of Pile Caps to Lateral Loading*. PhD thesis, Virginia Polytechnic Institute and State University, Blacksburg, Virginia
38. Pandit, K., Singh, M., Sharma, S., Sandhu, H. A. S., and Sahoo, J. P., (2021). Back-Analysis of a debris slope through numerical methods and field observations of slope displacements. *Indian Geotechnical Journal*, 51(2)
39. Fellenius, W., (1936). Calculation of the Stability of Earth Dams Transactions, *2nd Congress on Large Dams*, 4: 445
40. Zolkepli, M. F., Ishak, M. F., and, Zaini, M. S. I., (2019). Slope stability analysis using modified Fellenius's and Bishop's method. *IOP Conf. Ser.: Mater. Sci. Eng.* 527